Flame and Acoustic Waves Interactions and Flame Control

A thesis submitted to the University of Manchester for the degree of Doctor of Philosophy in the Faculty of Engineering and Physical Sciences

2011

Huimin Guo

School of Mechanical, Aerospace and Civil Engineering

List of Contents

The final word count is 36,411

List of Figures

List of Tables

Nomenclature

Symbol	Description	Unit
A	Pipe cross-sectional area	m^2
c	Speed of sound in air	m/s
d	Diameter of the resonance tube	m
D	Hydraulic diameter of the pipe	m
f	Frequency	Hz
f_a	Acoustic excitation frequencies	Hz
f_d	Dominant frequencies	Hz
H	Transfer function of the system	---
K_P	Parameter for proportional component	---
K_I	Parameter for integral component	---
K_D	Parameter for derivative component	---
l	Length of the tube	m
L	Distance, traveled length of fluid	m
p	Ration of brighter area to whole flame area	---
p'	Pressure fluctuation	Pa
q'	Heat release fluctuation	kJ/s
Q	Volumetric flow rate	m^3/s
R_e	Reynolds number	---
U	Input	---
V	Mean fluid velocity	m/s
Y	Output	---
ρ	Density of the fluid	kg/m^3
μ	Dynamic viscosity of the fluid	$kg/m \cdot s$
v	Kinematic viscosity	m^2/s
θ	Angle of incidence	degree
θ'	Angle of reflection	degree

Abbreviation Description

A/D	Analogue to Digital
AIC	Active Instability Control
AoF	Area of Flame
B/W	Black and White
C2	Hydrocarbon Oxidation
CH	Hydro Carbon Species
CH^*	Transient combustion species, CH
CO	Carbon Mono Oxide
CO_2	Carbon Dioxide
CoF	Centre of Flame
CTA	Constant Temperature Anemometer
D/A	Digital to Analogue
DAQ	Date Acquisition
dB	Decibel
DFT	Discrete Fourier Transform
DPC	Dynamic Phase Converter
FFT	Fast Fourier Transform
FT	Fourier Transform
GND	Signal Ground
Hz	Hertz
IAS	Instantaneous Angular Speed
I/O	Input and Output Channels
LCD	Liquid Crystal Display
OH	Hydroxyl Species
PC	Personal Computer
PIC	Passive Instability Control
PID	Proportional-Integral-Derivative
PMG	Power Amplifier Gain

PMT	Photomultiplier
PSD	Power Spectral Density
RGB	Red, green and blue
RXD	Received Data to Instrument
SD	Standard Deviation
TXD	Transmitted Data from Instrument
1D	One Dimension
2D	Two Dimensions
3D	Three Dimensions

Abstract

In this PhD project, the investigation of the stability of a laminar diffusion flame and the interaction of the flame with acoustic waves inside an acoustically excited cylindrical tube is presented. Interesting phenomena have been observed by studying both the infrasound and sound effect on the flame structure and dynamics.

When a cylindrical tube burner is acoustically excited at one end, a standing wave will be produced along the tube burner. By applying a programming controlled signal from a signal generator, the loudspeaker generates acoustic waves with different frequencies and intensities to excite the flame, which can make the flame relatively stable or unstable, even blow out. Different methods in both frequency domain and time domain have been applied to analyze the flame stability affected by acoustic waves.

Both infrasound and sound are tested in this research. Infrasound is the acoustic wave with a frequency too low to be heard by human ear covering sounds beneath the lowest limits of human hearing (20Hz) down to 0.001Hz. It is found that infrasound is able to take over buoyancy-driven flame flickering and make the flame flicker at the same frequency as the forcing infrasound. For some infrasound, half excited frequency has been detected clearly in the power spectrum of CH^* chemiluminescence signals acquired by a photomultiplier.

On the other hand, some higher frequency acoustic wave can have observable effect on flame flickering but the buoyancy-driven flickering is still the dominant oscillating mode; some other higher frequency acoustic wave can make the flame very stable, such as the acoustic wave at 140Hz. Image processing technique has shown that the influence of acoustic waves on the laminar diffusion flame varies spatially.

It is also observed that a diffusion flame may oscillate at different frequency spatially. Taking the flame without acoustic excitation as an example, the inner most area of the flame oscillates at the typical flickering frequency, but the most outer areas of the flame oscillate at the second-harmonic of the typical flickering frequency.

Finally, some control strategies are developed for the laboratory tube burner based on the gained physical insights in this research.

Declaration

No portion of the work referred to in the thesis has been submitted in support of an application for another degree or qualification of this or any other university or other institute of learning.

Copyright

Acknowledgements

First of all, I would like to express my sincere gratitude to my supervisor, Professor Yang Zhang, whose most creative and original thinking have been a great source of inspiration for me. I admire his distinctive and penetrating views on so many areas of combustion stability research. I feel particularly indebted to him for accepting me join in his research group when my first supervisor left the University of Manchester in 2007, sharing his thoughts and at the same time allowing me considerable freedom to pursue my own ideas to arrive at this final work. It will be never enough just to say thanks to him for his guidance, encouragement and advice throughout the course of the studies and his painstaking efforts for checking the entire manuscript.

This work has been financially supported by the University of Manchester under a scholarship scheme, which is gratefully acknowledged.

I would like to thank Dr Rong Wang for her kindly assistance on both my experiments and life in Manchester. The present thesis has also benefited in part from the useful discussions with many of my colleagues, in particular Dr Sarmad Yaqub, Dr Jizhao Li for which I am truly grateful.

I want to thank Professor Andrew Ball and Dr Fengshou Gu, for their encouragement, patience and invaluable advice during my first two years study.

Last, but not least, I would like to thank my husband, Yifan, for his unfailing and unreserved love and support, never-ending patience and for believing in me. I feel deeply indebted to my dearest parents, for their continuing great support for my life and looking after my baby. Finally, I wish to thank my lovely baby boy, Ziyu, for his love and understanding.

Chapter 1

Introduction

This part briefly addresses three topics: background and motivation, research objectives and organization of the thesis.

1.1 Background and Motivation

The phenomenon of detrimental instabilities inherent to industrial combustors has been emerged as a well known and highly investigated issue in recent years. As a result of unstable combustion, the amplitude of the oscillations induced inside the combustion chamber can reach high values to endanger the safe operation of the combustion system. The high amplitude instability-induced pressure oscillations and instability-induced heat release oscillations reduce the efficient operability of the combustor and can result in failure of the whole system. Combustion instabilities are harmful, undesirable and dangerous. They have represented as one of the major problems encountered while designing rocket motors, jet engine afterburners and industrial furnaces. Therefore, it is very important and necessary to understand how to avoid, control and eliminate the combustion instabilities.

According to the phenomenological description given by Lord Rayleigh [71], the phase or the time delay between heat release signal and pressure signal plays a very important role in the determination of a combustion system's stability. Thermoacoustic instability happens if the pressure and heat release are in phase,

which is the most common problem for a practical industrial combustor. Thermoacoustic instability also is a self-sustained instability in combustion system referred as natural instability of the system, resulting from an unstable coupling among an excitation, acoustic pressure, and the corresponding response of the system heat release. However, it has been reported that these parameters are very difficult to be measured or predicted in experimental studies and in practical situations [20]. Therefore some other ways need to be investigated to monitor the combustion process, for example, by monitoring the change of characteristics of heat release and flame profile etc.

Once the existence of unstable combustion process has been determined, two tasks are opened for researchers: one is how to control or prevent the onset or generation of combustion instabilities; the other is how to minimize the detrimental effects if the onset of combustion instabilities can not be eliminated. For both tasks, a complete understanding of the mechanisms responsible for initiating and sustaining combustion instabilities is essential. The studies of different combustion parameters including heat release, pressure oscillations, the acoustic response and fuel flow rate variations, can help understand the nature of flame structure and dynamics.

Applications of mathematical method and signal processing technique can aid determine the characteristics of observations of flames. Effectiveness of internal or external parameters which control or affect the peak dominant frequency of heat release or flame oscillation is an area that has attracted more and more investigations. Detail of the implement of active or passive control techniques to eliminate or control unstable combustion strongly depends on some combustion parameters that is able to affect basic combustion characteristics. Determination of any such parameters is extremely helpful in understanding the nature of unstable combustion. And potentially, they can serve as an input for achieving more efficient active control strategies for combustion instabilities. The extensive experimental work conducted has indicated that there are some operational parameters that can affect the flame dynamics, such as: fuel type, fuel flow rate,

flame inlet location, external acoustic frequency and acoustic intensity etc.

In order to investigate the flame structure and dynamics in spatial and temporal domains, the high speed image processing techniques have been applied in this research. The advantages of a digital camera, such as higher shutter speeds, shorter exposure times, larger storage capacities, better spatial resolution supported by sophisticated image processing software, has enabled this technique to be widely used for studying and investigating the flame structure and dynamics. A comparative study of different flame observations, combining with high speed imaging of the flames supported by suitable image processing techniques offers a broad area of research that has not been investigated so far. For example, the local oscillation of flame can be easily demonstrated by utilizing high speed image processing techniques, which provides more detailed information of the flame than other methods to help learn the flame structure and associate dynamics. A few image processing algorithms have been well developed recently and have been commonly employed by lots of applications. However, it is always difficult to apply them in a completely new application, because some unknown noise during image acquisition and unsuitable setting of parameters, such as the sampling frame rate, image resolution and the number of gray levels etc, can be obstacles to achieve designed results.

This research has introduced some new image processing algorithms to the field of combustion instability control. It has been well known that the acoustic wave has strong effects on flame structure and dynamics. The investigation of the interaction between acoustic wave and flame dynamics is therefore the crucial step for understanding, monitoring, avoiding and eliminating thermoacoustic instability. By combining these new image processing algorithms with the extensive experimental and theoretical work conducted during last two years, the interaction between acoustic wave and flame structure and dynamics have been well studied and some encouraging results have been achieved. A loudspeaker was used as the external acoustic driver to provide the required acoustic power. The frequencies and intensities of the loudspeaker can be controlled by a

computer. It is worthy to point out that all experimental works on the investigation of flame dynamics and instabilities have been conducted on laboratory scale burners. The behaviors of full scale industrial combustion chamber need further attention and research.

1.2 Research Objectives

In terms of the background information and research motivation raised in previous section, the main objectives of this research are summarized as following:

- Set up an experimental system that can deliver computer-controlled acoustic excitation for the burner. It includes designing a program that can control the signal generator power the loudspeaker, a hardware module and associated program that are able to acquire the signals of heat release fluctuation, hot wire and microphone by multi-channels.
- Investigate the interactions between flame structure and associate dynamics and acoustic waves inside a laboratory cylindrical tube burner, within a frequency band from infrasound to an acoustic excitation frequency below 300Hz.
- Study the local oscillation characteristics of the flame under different acoustic excitation using the newly presented high speed image processing techniques.
- Explore flame parameters from flame observations that can determine the degree of the combustion stability, which can then be used as inputs of the control strategies of combustion instability.
- Investigate active control strategies for monitoring the combustion process of a laboratory burner, and set up a closed-loop feedback controller for combustion instability.

1.3 Organization of the Thesis

This thesis contains seven chapters. It begins with the introduction for the research in Chapter 1. The significance of investigation of combustion instabilities has been highlighted and the objectives of this research work have been listed.

Chapter 2 reviews monitoring and instability control of combustion process, with focus on the interaction between acoustic wave and flame dynamics in a cylindrical tube, the combustion instability and corresponding control methods, and the monitoring methods for combustion process.

Chapter 3 presents the description of experimental setup and details of corresponding data acquisition. Measurement of uncertainties is also analyzed at the end of this chapter.

Chapter 4 investigates the interaction of acoustic wave and flame dynamics by analyzing the CH^* chemiluminescence signal, collected by photomultiplier, in both time domain and frequency domain.

Chapter 5 discusses the results of investigation of combustion instability by using some newly presented high speed image processing techniques.

Chapter 6 focuses on the discussion of control strategy for the laboratory burner based on the gained physical insights.

Finally, the conclusions of the research are given in Chapter 7, which also provides some suggestions on potential direction for future research.

Chapter 2

Review of Monitoring and Instability Control of Combustion Process

---

This chapter introduces the acoustic wave propagation inside a cylindrical tube and the interaction between acoustic wave and a diffusion flame. Different types of combustion instability are reviewed. The control background and methods of combustion thermoacoustic instability are presented. Finally, monitoring and control methods of combustion process are brought in.

2.1 Introduction

Combustion process is a very complicated chemical process. It is usually classified as premixed and diffusion or non-premixed, which depends on whether the fuel and oxidizer are well mixed initially or are supplied from different origins. For premixed flames, the reagents are well mixed or completely mixed before entering the flame. The best example of this type of flame is the well known Bunsen flame, where the premixed gases flow up a burner tube at a specific rate. When the rate exceeds the normal burning velocity of the mixture, a flame is maintained above the burner top. The premixed flames are very common used in people's living, particularly in domestic heating, and gas fires for cooking. On the contrast, for diffusion flames, fuel and air are not fully mixed or are not

mixed at all before combustion occurs. Candle flame is a typical example of this type of flame. Obviously, mixing of the reactants and combustion are concurrent (moving upwards) for diffusion flame. It is very important to note here that although the classification for premixed flames and diffusion flames is not difficult, the criteria of the classification can't be conducted too rigidly. For example, for a diffusion flame, the flame may lift off the burner if fuel and air were not mixed enough near by the burner rim, which result in the flame propagate back against the gas stream and maintain the flame. Because the pressure is reduced, the region of premixing near by the base of a diffusion flame becomes larger until the whole flame becomes indistinguishable from a premixed flame. Similarly, for rich premixed flames of the Bunsen type, although given clear inner cone, are dependent on the outer cone or outer diffusion flame.

Furthermore, there is another way to classify the combustion process: laminar or turbulent, which is dependent on the flow is "smooth" or "rough". No matter for premixed or diffusion flames, the flow can be laminar or turbulent. The threshold to distinguish laminar and turbulent is called Reynolds number (R_e), which can be defined as:

$$R_e = \frac{\rho V L}{\mu} \quad \textbf{(2-1)}$$

where:

V denotes mean fluid velocity (m/s)

L denotes distance, traveled length of fluid (m)

ρ denotes density of the fluid (kg/m^3)

μ denotes dynamic viscosity of the fluid ($kg/m \cdot s$)

For flow in a pipe or tube, the Reynolds number is generally defined as:

$$R_e = \frac{\rho V D}{\mu} = \frac{V D}{v} = \frac{Q D}{v A} \quad \textbf{(2-2)}$$

where:

D denotes hydraulic diameter of the pipe (m)

v denotes kinematic viscosity (m^2/s)

Q denotes volumetric flow rate (m^3/s)

A denotes pipe cross-sectional area (m^2)

Values of R_e in flames between 10^3 and 10^4 signal the transition from laminar to turbulent flow.

Normally, a steadily burning laminar flame makes practically no noise, whereas flame becomes noisy when they are turbulent. Most of time, the flame noise is associated with pressure pulses, which is due to irregularities in direction and speed of movement of the flame front.

Besides flame noise, the combustion chamber also has noises or oscillations. It is well known that periodic vibrations in combustion systems are harmful, undesirable and dangerous, because it causes intense sound, loss of flame stability and destruction of metal parts. Usually, an enclosed combustion chamber has its own characteristic acoustic frequencies, which are determined by its dimensions and the velocity of sound through the burning gases, known as acoustic resonance frequency (see the next part for detailed information). Furthermore, acoustic vibrations in combustion chamber may couple with or be driven by varying heat release rate that can deduce thermoacoustic instability (detailed introduction is presented in the next section). This would happen if the combustion processes are affected by the periodic changes in pressure or gas velocity, and the changes in the combustion process have an associated time factor that can resonate with the acoustic frequency. There are some potential factors that may cause variation in heat release rate:

- Direct effect of pressure on heat release;

  For premixed gases, the burning velocity usually does not vary rapidly with pressure so that the heat release rate tends to be proportional to overall pressure.

- Variation of flame area;

  This may be caused by varying supply rate of the combustion mixture under the influence of the pressure fluctuations or by flame movement relative to the tube walls.

- Variation of fuel/air ratio;

Pressure fluctuations may affect the supply rate of fuel and air differently. Fluctuation in air flow rate pasting a spray injector may alter the droplet concentration in the mixture.

- Variation in mixing rate;

  Increased turbulence due to gas motion may improve mixing. In some cases variation of angle of attack of a gas flow may alter vortex shedding from the rim of a flame holder and affect the mixing processes.

Therefore, in order to minimize the flame noise and eliminate chamber oscillation, it is very important to monitor the combustion process. Moreover the complication of combustion process makes the condition monitoring very necessary. The early detection of the combustion instability can avoid different levels damage to the whole combustion system.

It is well known that thermoacoustic instability is one of the most commonly occurred problems for industrial combustor, and the investigation of the interaction between acoustic wave and flame dynamics is the key step for avoiding and eliminating thermoacoustic instability.

Firstly, based on the equipment condition of the University of Manchester combustion laboratory, this chapter introduces the propagation of acoustic wave inside a cylindrical tube chamber and the corresponding interaction between acoustic wave and flame dynamics. Different types of combustion instability, active and passive control background and methods of controlling combustion thermoacoustic instability are then reviewed. Finally, monitoring and controlling methods for combustion process are discussed in the last part of this chapter.

2.2 Interaction between Acoustic Wave and Tube Flame

It is well known that acoustic waves have capabilities to affect the flame dynamics. The interaction between acoustic wave and flame has been well documented theoretically and experimentally. The acoustic excitation induces flame instability and variations of the flame shape [27][67][79]. Zhang [67]

presented some interesting results by studying the flame dynamics in a cylindrical tube burner with the excitation of acoustic wave under laboratory conditions. It was observed that the diffusion flame was severely, especially affected in the frequency range between 200Hz and 300Hz, where the strongest oscillation occurred at the second harmonic of the test rig. Very complicated and interesting flame patterns caused by different acoustic excitation frequencies were reported. They explained that the acoustic wave affects the characteristics of flame by changing the pressure and the mixture of fuel and air. It has been reported that by utilizing the influence of acoustic wave on the flame there is a possibility to improve the performance of combustion control of many phenomena, such as high-load combustion [90], soot suppression [74], NO_x reduction [69] and noise control.

It has been found that acoustic waves interact with flames both in direct and indirect ways. The direct interaction between the acoustic waves and flames occurs in the flame zone. The wave incident upon the flame zone is scattered and potentially amplified because of the steep gradients in gas properties at the flame front and the response of the flame to the perturbations. The effect of this interaction has been examined both for premixed and diffusion flames (Welle et al.[87]; Lieuwen [55]; Pun et al.[69];). The indirect interaction, on the other hand, occurs in the flow field substantially regardless of the flame characteristics (diffusion flame or premixed flame). It has been found that the acoustic forcing on a non-reacting jet or flow induces velocity fluctuations (Lebedev et al.[53]; Krasheninnikov et al.[51]), sinuous oscillations (Nolle [64]), or steady streaming (Chu [15]). Suzuki et al.[79] investigated the behavior and structure of internal fuel-jet in diffusion flame under transverse acoustic excitation. They found that the meandering behavior is synchronous with the acoustic wave and its periodicity corresponds to the acoustic wave frequency. It is possible that this effectiveness plays a noteworthy part in the excited behavior of jet diffusion flames under acoustic forcing, which has been shown in previous studies of Hertzberg [33]; Saito et al.[74]; Yoshida et al.[90]; Lee et al.[54].

The interaction mechanisms between flame and acoustic wave have been reviewed in very detail by Lieuwen [55] in 2003. He noted that acoustic disturbances on the flame can be classified into different categories (see Figure 2-1) depending on whether they modify the local internal structure of the flame (such as the local burning rate) or its global geometry (such as its length, or its area). The former and latter categories are often associated with pressure and velocity coupled mechanisms, respectively.

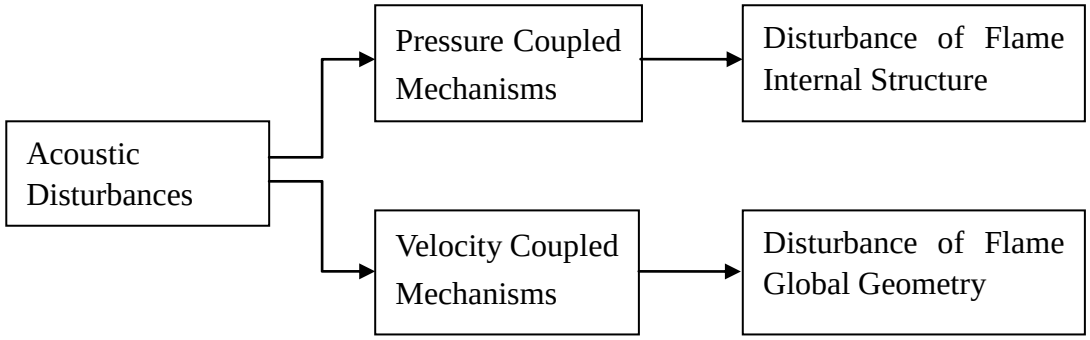

Figure 2-1: Acoustic disturbances classification

2.2.1 Acoustic Wave Propagation in Tube

It is well known that resonant acoustic fields can be easily excited when acoustic wave propagates in a tube of finite length. In some cases, notably in some musical instruments, excitation and amplification of acoustic waves are desirable. But in other cases, like in combustion chambers, most of time excitation and amplification of acoustic waves by the interaction between external acoustic wave and flame dynamics are detrimental, which makes the combustion unstable. The acoustic resonance needs to be avoided and dissipated. The elimination is usually accomplished either by decoupling the system from the source, or by damping the waves that exist in the system. This research aims to analyze and present the acoustic wave influence of flame stability inside a cylindrical tube burner. It is therefore very important to understand how acoustic propagates in the cylindrical tube and how the acoustic resonance is generated. Some fundamental but very important concepts about acoustic wave propagation in

tube and acoustic resonance are introduced in the following part.

Standing wave

Consider an acoustic source, e.g. a loudspeaker, placed near one of the ends of a cylindrical tube. A part of the acoustic energy produced by the loudspeaker enters into the tube in the form of a ‘travelling acoustic wave’. When it reaches the other end of the tube, a part of the energy reflects back into the tube, again in the form of a “travelling acoustic wave”. The rest of the energy transmits through the open tube boundary and comes out of the tube. The reflection of acoustic wave follows the law of "angle of incidence equals angle of reflection" (see Figure 2-2, where $\theta = \theta'$), called the law of reflection. When $\theta = 0$, the reflected wave follows the incident wave exactly, but the propagation direction is changed. The reflected waves can interfere with incident waves, producing patterns of constructive and destructive interference (can lead to resonances, see the next part). Hence, in the presence of the loudspeaker, the acoustic wave that reflects from the other end of the tube interacts with the oncoming travelling wave to produce what is termed as a standing wave or a stationary wave. It also means that the acoustic wave intensity near a surface is enhanced because the reflected wave adds to the incident wave, giving pressure amplitude that is twice as great in a thin "pressure zone" near the surface.

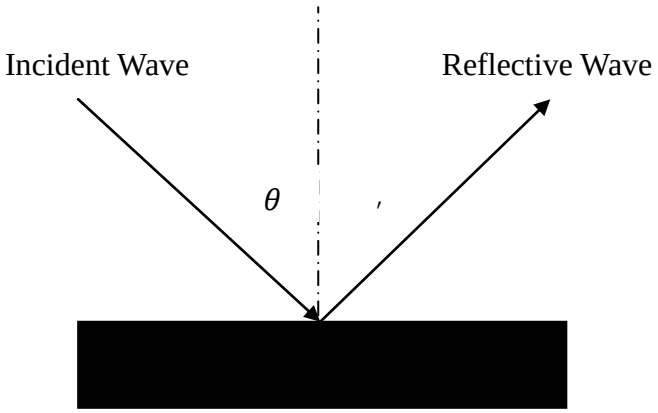

Figure 2-2: Law of reflection

Take the string as an example to illustrate the generation of standing wave. For a

string held at both ends, forcing zero movement at the ends, the ends become zeroes or nodes of the wave, and the reflective wave has the same amplitude and frequency as the incoming wave. Let the incoming wave (acoustic wave from the loudspeaker) y_1 and the reflective wave y_2 be represented by the equations below:

$$y_1 = Asin\,(kx - \omega t) \tag{2-3}$$

$$y_2 = A\sin\,(kx + \omega t) \tag{2-4}$$

where A denotes the amplitude of the wave, k denotes wave number ($\frac{2\pi}{\lambda}$) and ω denotes angular frequency ($\frac{2\pi}{f}$). So the resultant wave y equals to the sum of y_1 and y_2:

$$y = A\sin(kx - \omega t) + A\sin\,(kx + \omega t) \tag{2-5}$$

Using a trigonometric identity to simplify the above equation, the standing wave is described by:

$$y = 2Asin(kx)\cos\,(\omega t) \tag{2-6}$$

This describes a wave that oscillates in time, but has a spatial dependence that is stationary: $\sin\,(kx)$. At locations of $x = 0, \lambda/2, \lambda, 3\lambda/2$... called the nodes, whose amplitude is always zero, whereas at locations of $x = \lambda/4, 3\lambda/4, 5\lambda/4$, ... called the anti-nodes, the amplitude is maximum.

Acoustic resonance

Acoustic resonance is the tendency of an acoustic system to absorb more energy when it is forced or driven at a frequency that matches one of its own natural frequencies of vibration (its resonance frequency) than it does at other frequencies. The resonance of a tube of air is related to the length and the geometry of the tube, whether it is closed or open at two ends. By convention a rigid cylindrical tube open at both ends is referred to as an "open" cylinder (Figure 2-3(a)); whereas, a rigid cylinder open at one end and has a rigid surface at the other end is referred to as a "closed" cylinder (Figure 2-3(b)).

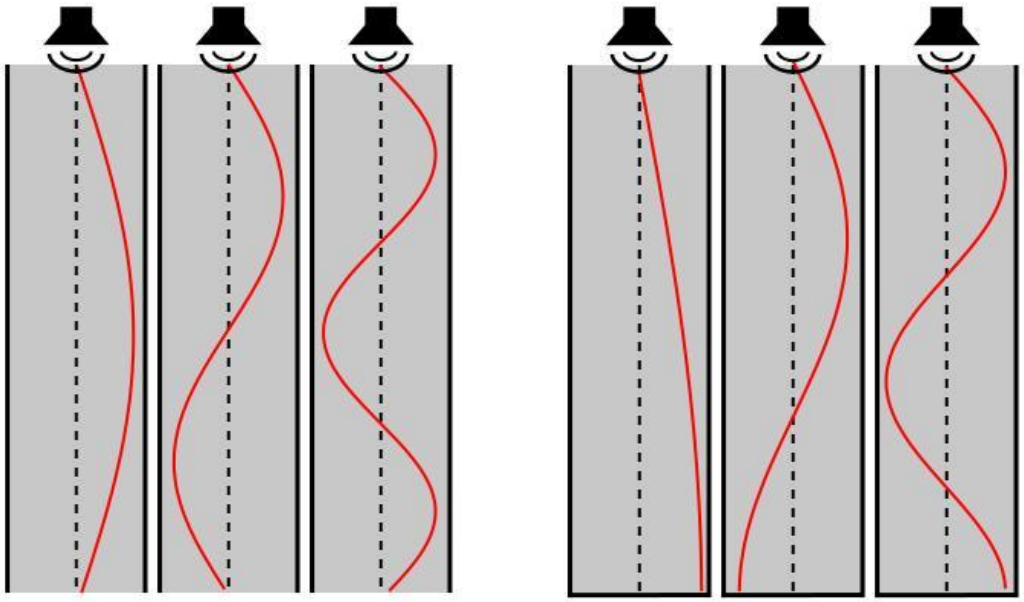

(a) (b)

Figure 2-3: The first three resonances in a cylindrical tube. (a) Open cylindrical tube. (b) Close cylindrical tube

Open cylindrical tube

For a cylindrical tube with both ends open, each end of the column must be a node for the acoustic wave, since the ends are open to the atmosphere and cannot produce significant pressure changes. For the fundamental mode, there is one antinode at the center. Open cylindrical tubes resonate at the approximate frequencies

$$f = \frac{nc}{2l} \quad \textbf{(2-7)}$$

where n is a positive integer (1, 2, 3...) representing the resonance node (the fundamental frequency $\frac{c}{2l}$ is obtained when $n = 1$), l denotes the length of the tube and c denotes the speed of sound in air (which is approximately 343 meters per second at 20 ℃ and at sea level).

A more accurate equation considering an end correction is given below:

$$f = \frac{nc}{2(l+0.8d)} \quad \textbf{(2-8)}$$

where d denotes the diameter of the resonance tube. This equation compensates for the fact that the exact point where a acoustic wave is reflecting at an open end

is not perfectly at the end section of the tube, but a small distance outside the tube (see Figure 2-3(a)).

Closed cylindrical tube

A closed cylindrical tube produces resonant standing waves at a fundamental frequency at odd harmonics. The closed end is constrained to be an antinode of the wave and the open end is of course a node. This makes the fundamental wavelength is four times the length of the air column. A closed cylinder has approximate resonances of

$$f = \frac{nc}{4l} \quad \textbf{(2-9)}$$

where n is an odd number (1, 3, 5...), and the fundamental frequency for closed cylindrical tube is denoted by $\frac{c}{4l}$. This type of tube can produce odd harmonics only and has a fundamental frequency lower than that of an open cylinder (that is, half the frequency) (see Figure 2-3(b)).

A more accurate equation is given below:

$$f = \frac{nc}{4(l+0.4d)} \quad \textbf{(2-10)}$$

2.2.2 Effect of Acoustic Wave on the Flame

Acoustic waves always have an influence on flame dynamics. It can be represented in many different aspects and the impacts can be very different for the premixed flame and the diffusion flame. Hence, in the following sections, the influence of external acoustic source on the premixed flame and diffusion flame are discussed respectively.

Influence on premixed flame

The most fundamental interference of an acoustic wave on a flame is simply causing a fluctuation in the mass flow rate of reactive mixture into the flame. This mass flow fluctuation is due to both the velocity oscillations, which carry the mixture toward the flame, and density oscillations, which affect the mass of

reactive mixture per unit volume. Furthermore, because the position and orientation of the flame depend on the local burning rate and flow characteristics, and velocity perturbations cause wrinkling and movement of the flame front. In turn, it modifies its local position and curvature, as well as its overall area or volume. These velocity disturbances can be acoustic or vortical in nature and, thus, propagate at the acoustic wave or flow speeds, respectively. Normally the distortion of the flame front results in heat release oscillations. The heat release oscillations are generally attributed to the variation in flame surface area.

Besides the influence on the fuel flow rate or heat release, the external acoustic source also has an impact on the burning velocity. The premixed flame's burning velocity is the velocity with which a plane flame front moves normal to its surface through the adjacent unburnt gas. It is also sensitive to the perturbations in pressure which directly accompany the acoustic wave. The local rate of heat release per unit area of flame or volume of reactor oscillates in time, even if the total surface area or volume of the combustion process remains fixed. Besides the direct effect of an acoustic oscillation on the burning rate and flame position, acoustic pressure and velocity oscillations can also exert indirect effects. For example, disturbances in the premixing section of the combustor generate oscillations in the fuel/air ratio of the reactive mixture. This fuel/air ratio disturbance can be generated either by a fluctuating fuel flow rate (such as by fluctuating the pressure drop across the fuel nozzle) or the fluctuating air flow rate due to acoustic velocity perturbations.[56]

Influence on diffusion flame

Diffusion flames emanating from small burners are sensitive to acoustic wave. And the influence of the acoustic wave on diffusion flame dynamics is very dependent on the frequency and intensity of acoustic wave.

A laminar diffusion flame with certain height is generated with the supply of coal-gas through a burner. With the increment of fuel flow rate, the flame becomes longer and sensitive. If acoustic wave is applied at certain fuel flow rate,

the flame seems to become prematurely turbulent and shorter or relative stable depends on the acoustic wave frequency and amplitude applied. It is found in this study that a flame is not sensitive to all acoustic wave frequencies. It is only sensitive to a few frequencies within a limited range. Furthermore, some frequencies make the flame turbulent; others make the flame relatively stable. Besides the acoustic wave frequency, the flame sensitivity varies with the direction from which the acoustic wave comes and the distance between the sound source and the fuel nozzle. The flames show different characters when the sound source is moved around the flame or the position of the nozzle relative to sound source is changed. The frequencies to which a flame is sensitive are dependent of fuel flow rate, the size and shape of the burner and the type of fuel. The phenomenon of sensitive flames appears to be closely associated with the flame flicker (discuss in the next section). Hence it is expected that a flame sensitive to acoustic wave at a specific frequency affects the rate of vortex shedding. And this inspires us to investigate use the acoustic wave influence on flame characteristics to monitor and control the combustion instability.

Brown [9] found that the flame sensitivity to acoustic wave can be affected by the jet of gas. He used a stroboscope coupled with the acoustic wave frequency to view the smoke jets. He observed waves travelling up the gas stream and found that at certain point the jet forked. Near the frequencies of maximum sensitivity the amplitude of the waves increased and the forking point moved down towards the burner orifice. The observations also showed that jets were already turbulent did not develop the wavy structure, whereas sensitive laminar jets, although near the point of turbulence, did develop distinct periodic sinuosity. It is known that the jets of air, made visible with smoke, have different characteristics according to whether the orifice is circular or rectangular. The rectangular jet tends to develop cylindrical vortexes, whereas the circular jet gives ring-shaped vortices. Brown measured the angular velocity of vortices, ω, caused by acoustic wave frequency f, and found that:

$$\omega = \pi f \qquad \textbf{(2-11)}$$

which means that the frequency of rotation of the vortices is the same as the acoustic wave frequency, indicating that the vortices are triggered by the acoustic wave impinging on the base of the jet. The fact that only certain acoustic wave frequencies can produce vortex means that only vortex with certain angular velocities is physically possible. [64]

2.2.3 Effect of Heat Release on Acoustic Oscillation

Previous section introduced the acoustic wave effects on the flame dynamics. In order to completely show the interaction between the acoustic wave and the flame, this part will present how the heat release generates and influences the acoustic wave.

It has been well known that oscillation in heat release can generate a acoustic wave. Historically, the "singing flame" was discovered by Higgins in 1777 [84] . This phenomenon caught the interest of many researchers and they found that high levels of sound can be produced by placing a flame, anchored on a small diameter fuel supply tube in a large diameter tube [18] [24]. The flame was found to excite the fundamental mode or one of the harmonics of the large tube. The effect occurs for both diffusion flames and premixed flames, and appears to be associated with resonance between some vibrations of the flame on its burner with that of a surrounding shield or enclosure. The amplitude of a acoustic wave is proportional to the pressure variation ΔP (the difference between pressure of the initial unburnt gas inside the flame cone and pressure in the final condition), and the acoustic wave intensity I, measured as the energy flux, is given by:

$$I = \Delta P^2 / \rho c \qquad \textbf{(2-12)}$$

where c denotes the velocity of sound and ρ denotes the density. Considering a flame, the expansion of the gas as a result of the heat release during combustion tends to produce a rise in pressure around the flame and an outward flow, but fluctuations in pressure only occur when the rate of combustion changes, i.e. when there is some changes in the flame.

The "dancing flame" was discovered later by Conte [18] where a flame pulses in synchronous with the audible beats of music. Rijke [72] showed that a sound can be generated in a vertical tube open at both ends by placing a heated metal gauze inside the tube. The sound was heard only when the heating element was placed in the lower half of the tube, specifically at a distance of a quarter the tube length from the bottom. These phenomena occur for both diffusion and premixed flames, and appear to be associated with resonance between some vibrations of the flame on its burner with those of a surrounding shield or enclosure.

2.3 Combustion Instability

Combustion instabilities appear in different forms and at different scales. They represent one of the major problems encountered while designing rocket motors, jet engine afterburners and industrial furnaces. On the one hand, when combustion instabilities occur in practical systems, these instabilities can be detrimental, for example, they can create conditions that may cause damage and mechanical failure to the combustion device, and they can induce large mechanical vibrations and enhanced heat transfer rates at the combustor walls, which in extreme cases can lead to the total loss of the system. On the other hand, in some situations, combustion instabilities may be favorable for enhancing mixing and increasing burning rates [61]. The following sections introduce some typical instabilities for a combustion system, which include thermoacoustic instability, buoyancy-driven instability and Kelvin-Helmholtz instability etc.

2.3.1 Thermoacoustic Instability

Dynamic instability occurs in combustion process due to the feedback coupling between two dominant processes, acoustic and heat release, shown in Figure 2-4, and it is referred to as thermoacoustic instability. The phenomenon of self-sustained thermoacoustic instabilities in combustion system also referred to as natural instabilities of the system, results from an unstable coupling between

an excitation, acoustic source, and the corresponding response of the system, heat release. As discussed in above sections, the heat release from the combustion of reactants affects the acoustics, and the acoustic perturbations alter the heat release dynamics, closing the positive loop in Figure 2-4. It can be physically realized as fluctuations in the heat release of combustion excite acoustic motions which in turn cause new fluctuations of heat release simultaneously.

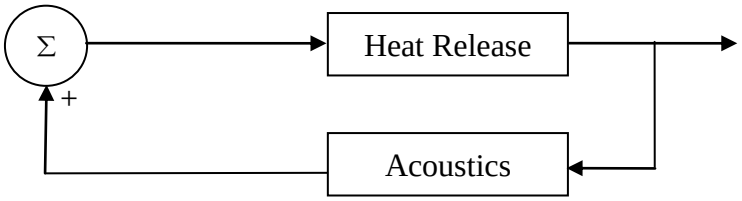

Figure 2-4: Thermoacoustic instability in a combustion system

Rayleigh [71] is the first researcher who hypothesized the onset of this instability, and defined a criterion for positive coupling based on a phenomenological, heuristic, description of the instability. The criterion was defined as follows:

Rayleigh's Criterion

"If heat be periodically communicated to, and abstracted from, a mass of air vibrating in a cylinder bounded by a piston, the effect produced will depend upon the phase of the vibration at which the transfer of heat takes place. If heat be given to the air at the moment of greatest condensation or to be taken from it at the moment of greatest rarefaction, the vibration is encouraged. On the other hand, if heat be given at the moment of greatest rarefaction, or abstracted at the moment of greatest condensation, the vibration is discouraged"

The Rayleigh criterion can be described by the following inequation:

$$\int_0^\tau \int_0^V p'(x,t)q'(x,t)dvdt > \int_0^\tau \int_0^V \emptyset(x,t)dvdt \qquad \textbf{(2-13)}$$

where p' and q' denote unsteady pressure and heat release rate, respectively, τ denotes the period of oscillation, V denotes the combustion volume (control volume) and $\emptyset$ denotes the wave energy dissipation.

Thermoacoustic instability occurs when the inequality in equation (2-13) is

satisfied. The LHS and RHS of the inequality describe the total mechanical energy added to the oscillations by the heat addition process per cycle and the total energy dissipated by the oscillation per cycle, respectively. Normally, the acoustic dissipation in combustors can be assumed very small (RHS ≈ 0). Therefore, the Rayleigh criterion commonly used in thermoacoustic instability research can be simplified from inequation (2-13) to the flowing inequation:

$$\int_0^\tau \int_0^V p'(x,t)q'(x,t)dvdt > 0 \qquad \textbf{(2-14)}$$

The inequation (2-14) indicates that there is a specific relationship between p' and q' to satisfy the Rayleigh criterion. If p' and q' are in phase, the effect will be a stable status, if p' and q' are out of phase, the effect will be an instability status. It has been noted that the integrals are also spatial, which means that both effects can occur at different locations of the burner, and at different times.

2.3.2 Buoyancy-Driven Instability

The influence of buoyancy on flame behaviour is of practical importance to combustion research. In most practical combustion systems, buoyancy has substantial impacts on pollutant emissions, burning rate and flame stabilization limits such as the time and the condition of flame flash back and blow-off. Regarding flame instability issues such as flame oscillation, buoyancy causes flame front to regularly oscillate at a low frequency, typically ranging from 10Hz to 20Hz for propane jets burning in air and around 18Hz for city gas (containing 40% of primary air) in air [61], known as flame flickering frequency. This frequency is relatively independent of the fuel type, nozzle size, and jet exit velocity. The flame flickering phenomenon plays a very important role for the studying of the stability of flame. It is therefore introduced in detail in the following section.

Flame flickering phenomenon

As can be observed by the human eye, a diffusion flame in an industrial combustor always pulsates randomly and irregularly with some low frequencies, typically within the 10-20Hz range, in addition to emitting steady light. The oscillation of a flame referred to as “flicker” that reflects the geometrical pulsation of the flame, the oscillation of the heat radiation and pressure and other characteristics, plays an very important role in flame dynamic property, radiation field and energy efficiency. Flame flickering of jet diffusion flames also indicates the instability of hot gases ascending column. Its frequency can be taken as a criterion of flame stabilities or a variable to be controlled for the monitoring of the status of the combustion system.

This phenomenon of flame flickering has interested many researchers for a long time. It has been found that, if the average flame height exceeds a certain value and if inertial effects are not dominant, natural convection can lead to low frequency vertical oscillation in the flame height and width. This motion is caused by the formation of shear instability in the burnt mixture originating at a height of a few centimetres and which, in the case of axially symmetrical flames, generates vortex at regular intervals. These vortexes, created in the burnt chemical mixture, arise along the reaction zone under the action of natural convection. The thickness of the layer of burnt gas is modified due to the regular passage of these vortexes ahead of the front cyclically and the oxygen supply is altered as well. Therefore, the flame surface adapts and deforms in relation to the oxygen flux locally involved in combustion process. It has been observed that there were two kinds of vortexes (see Figure 2-5) that located at inner and outer sides of a luminous flame, and that the scale of the inner vortex (roll up vortex) was smaller compared with that of the outer vortex (toroidal vortex). The smaller vortexes (inner vortex or roll up vortex) were initiated by Kelvin-Helmholtz instabilities (see the next part for Kelvin-Helmholtz instabilities). The larger vortexes (outer vortex or toroidal vortex) were assumed to be combustion buoyancy driven instabilities due to acoustic resonance of the nozzle, and the reacting interfaces were attributed to this high frequency vortex system. The

frequency of the outer vortex (the high frequency or toroidal vortex) driven by the buoyant force was equivalent to the flame flickering frequency [12][22]. Take the picture taken by Chen [12] as an example for vortex visualization, shown in Figure 2-5, two outer vortexes, some inner vortexes and an flame bulge (near point A) were detected. They speculated that the flame bulge was probably formed due to the rotational flow inside the outer vortices; the toroidal vortex below the flame bulge moves the flame surface radially outward while the one above the bulge drags the flame surface inward. Inside the luminous flame, well defined roll-up vortices first appeared at some distance for the burner, and then the inner vortices grew rapidly until certain point was reached. Beyond this point, the size of the inner vortices remained relatively constant before Point B was reached. Downstream of Point B, inner vortices seemed to be stretched before vortex pairing was observed near the flame bulge.

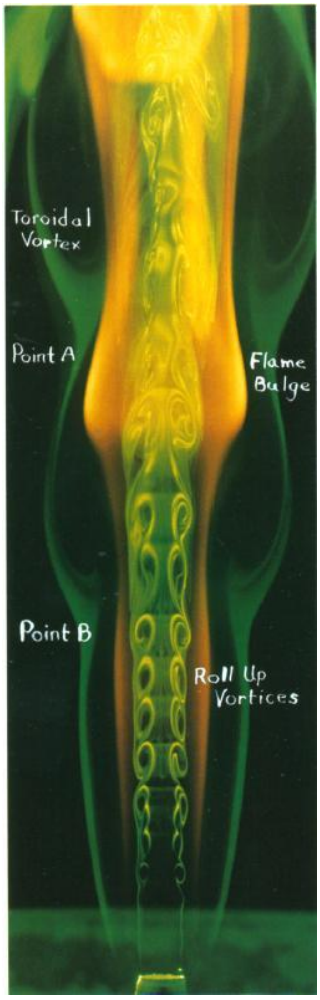

Figure 2-5: Vortex visualization of a methane jet diffusion flame [12]

The flame flicker phenomenon also is closely associated with combustion process efficiency and pollutant emissions. As the essential attribute of flame dynamics, in this research, the flame flickering frequency is used as an indication parameter of investigating the flame stability. Lots of researches have been reported about the flame flickering phenomenon and the calculation for the flame flickering frequency has attracted more and more attentions. Durox et al. [21] used two types of burner to determine the flickering frequency. A photomultiplier was adjusted to aim at a point on the screen equivalent to the area over with the flame front passed during its oscillatory motion. The experimental results were in agreement with the works of Lingens et al. [57][58], who noted only a weak influence of the fuel velocity upon the flickering frequency of diffusion flames at small jet velocities. The experimental works of Cetegen and Dong [11] on large

scale dynamic behaviour diffusion flames have found that buoyant diffusion flames originating from circular nozzles exhibit two different modes (sinuous and varicose) of flame instabilities. The experiments point towards the feasibility of altering buoyant flame behaviour under earth gravity. Experiments of predicting buoyancy-induced flame flickering frequency were carried out under the swirling flow conditions produced by a rotating Bunsen burner. Four discrete peaks were reported on the frequency spectrum for the flame flickering with U=0.6 m/s and N=1200 rpm. The observed harmonic frequencies indicated that the flame flickering frequency had a clearly defined periodicity [31]. Huang et al. [45] introduced a parameter of "flicker" of flame, which was defined in terms of weighted spectral components over the entire frequency range in the frequency domain and the signal was obtained by processing the radiation intensity of individual pixels within the luminous region of a flame image. They observed that this parameter is an important physical parameter associated with the characteristics of a combustion process. They reported that the flicker of a diffusion flame depends predominantly on the burner diameter, and the flicker of a premixed flame varies with the equivalence ratio and a peak flicker exists for a given air flow rate. Flame stability under various gravity fields was also investigated to clarify the buoyancy effects on combustion phenomena. Katta et al. [49] investigated the growth behaviour of two instability waves which consisted of inner and outer vortices in a jet diffusion flame. They showed that the flickering frequency decreased in weak gravity fields, which was due to the reduction of the velocity gradient in the shear layer of the jet. The experiments carried out by Sato et al. [75][76] were under wide conditions regarding the Reynolds number and gravity levels. It has been found that there were two different flickering modes (tip flickering and bulk flickering), which were characterized by the Froude number coupling with the buoyant force. They suggested that flickering phenomena due to forced convection, for which frequency is affected by the velocity, would be observed at relatively low velocity conditions. Arai et al. [3] investigated effects of artificial gravity level

on the flame stability and flickering motion by using the spin tester for the propane jet diffusion flames. They found that the flame lifting phenomenon and the blow-off limit depended strongly on the gravity level and the dependence of the transition from the stable flame to the flickering flame on the gravity level was not so stronger than that of the blow-off limit. And the magnitude of its dependence was almost the same as the Reynolds number.

2.3.3 Kelvin-Helmholtz instability

It is known that jets above a certain Reynolds number exhibit the shear-driven hydrodynamic instability, known as the Kelvin-Helmholtz instability. For example, vortex rings appear in the flow and then subjected to some wavy instability that brings to their breakdown. An example of this phenomenon is shown in Figure 2-6 for a round jet at a Reynolds number of about 13000. On the left image of Figure 2-6, the round jet is not excited acoustically; on the right one, its instability is forced by means of weak periodic acoustic waves introduced through a loudspeaker near the jet at its natural frequency. The forced acoustic waves reduce the length of the laminar boundary layer on the periphery of the jet and cause more regular formation of vortex rings than under the non-excitation condition (Photographs by R. Wille and A. Michalke taken from [85]).

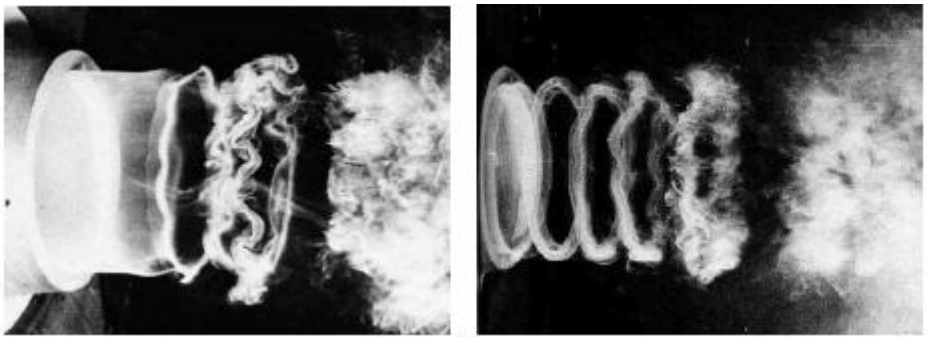

Figure 2-6: Smoke visualization of a jet flame [85]

Kelvin-Helmholtz instability has important implications in numerous applications involving non-reacting as well as reacting mixing layers. Normally,

Kelvin–Helmholtz instability occurs when velocity shear is present within a continuous fluid or, when there is sufficient velocity difference across the interface between two fluids. [30]

2.3.4 Other Instability

Besides thermoacoustic instability, buoyancy-driven instability and Kelvin-Helmholtz instability, there are some other types of instability that occur in both premixed and diffusion flame combustion systems. For premixed flames, the hydrodynamic instability resulting from thermal expansion plays a central role and is particularly dominant in large-scale flames. It is responsible for the formation of sharp folds and creases in the flame front and for the wrinkling observed over the surface of expanding flames. In contrast, instabilities in diffusion flames are mainly driven by diffusive-thermal effects, induced by the disparities between mass and thermal diffusivities of the combustible mixture, with thermal expansion playing a secondary role. [61][91]

Hydrodynamic Instability

Hydrodynamic instability was first identified by Darrieus (1938) and Landau (1944) [48][91], who treated the flame as an interface with a constant propagation speed, and showed that the flame is intrinsically unstable to perturbations of any wavelength. However, this result is in contradiction to some phenomena, because in normal laboratory conditions smooth and stable flames often can be observed in tubes. Markstein (1964) [48][91] reconciled the difference by taking into account the flame structure, which has a finite thickness due to molecular diffusion. Laudau and Darrieus's approach is appropriate only if wavelengths of disturbances are sufficiently long compared to a preheat zone thickness of the flame. Subsequently, the hydrodynamic flame stability taking account of the preheat zone (finite characteristic length) was investigated by several other researchers (Frankel and Sivashinsky, 1982; Peke and Clavin, 1982; Matalon and Matkowsky, 1982; Kadowakiand Tsuge, 1985) [48][91]. They

obtained the dispersion relation asymptotic to the Darrieus-Landau solution in sufficiently small wave numbers, revealing the existence of a stable region for wave numbers larger than the critical wave number.

Diffusive-thermal Instability

The onset of cells on spherically expanding flames more clearly illustrates the distinction between the diffusive-thermal and hydrodynamic instabilities. Diffusive-thermal instability was first theoretically investigated by Barenblatt (1962) and then rigorously analyzed by Sivashinsky (1977), Joulin and Clavin (1979) for adiabatic and non-adiabatic flames, respectively, based on the assumption of constant density. The dispersion relation obtained from the linear stability analysis shows that cellular instability of premixed flames occurs when the Lewis numbers (L_e) of the mixture is smaller than a critical value. L_e is defined as the thermal diffusivity divided by the diffusion coefficient, which is slightly less than unity, while pulsating instability occurs when L_e is larger than a critical value, which satisfies the criterion $Z_e(L_e - 1) > 4 \times (1 + \sqrt{3}) \approx 10.9$ for the adiabatic flame, where $Z_e = \frac{E(T_b - T_u)}{{T_b}^2}$ is the Zeldovich number. This criterion was extended by Joulin and Clavin (1979), who showed that heat loss can significantly reduce the critical value. Furthermore, numerical simulation with constant density showed that Sivashinsky's criterion under predicts the onset of pulsation as L_e increases or $Z_e$decreases, which is reasonable.[91]

Shock wave Instability

Shockwave is a thin transitive area propagating with supersonic speed in which there is a sharp increase in density, pressure and speed of substances. Shockwave is formed due to extreme pressure distribution. In certain combustion systems with very high heat release rates, fluctuations in the combustion rate can result in the formation of shockwaves, which may produce concentrated heat pulses and result in a self-sustained oscillation. Shockwave instabilities have been observed in rocket motors such as ramjet where the combustion heat release rates are

particularly intense. The interaction of shockwaves with fluid non-uniformities modifies the geometry and amplitude of wave fronts by reflection, refraction, diffraction and scattering, and modifies the morphology of the inhomogeneities by fluid deformation, vorticity and entropy production and transport. The interactions between shockwave and flame were reviewed by Oppenheim [66].
In this research, only the flames under atmospheric pressure and low fuel flow rates are investigated. Therefore shockwave is not studied due to absence.

Instability of Cylindrical Flames

The stability of cylindrical flame was analyzed by Sivashinsky (1979) and Matkowsky, Putnick, and Sivashinsky (1980) using the diffusive-thermal flame model [91]. It was reported that the cylindrical flames are stable compared to the plane flames, and that the cylindrical flames become unconditionally stable when the radius of the flame front is smaller than a critical value. Kadowaki et al. [48] compared the stability between plane flame and cylindrical flame. They observed growth rates of disturbances of cylindrical flames depending on wave numbers. Their results showed that the growth rates in the cylindrical flames are consistent with those in the plane flames for the case where the Lewis number is unity, which means that the hydrodynamic effect on the flame instability is independent of the mean curvature of the front. But when the Lewis number is smaller/larger than unity, the growth rates in the cylindrical flames are lower/higher than those in the plane flames. It presumes that the instabilizing/stabilizing influence of the diffusive-thermal effect is less in the cylindrical flames than in the plane flames, because the mean curvature of the front is finite.

2.4 Background and Methods of Controlling Combustion Thermoacoustic Instability

This research aims to monitor the combustion process under the excitation of external acoustic source and control the flame stability by means of the

interaction between the flame and the acoustic wave. Above sections have introduced the interaction between acoustic wave and the flame along with the different types of combustion instability, this part reviews some different methods that have been studied for controlling the combustion instability. Before introducing the control strategies of combustion instability, general ideas of process monitoring and control methodology in industry process are presented.

2.4.1 Theoretical Background of Industrial Process Monitoring and Control

The applications of condition monitoring or fault diagnosis have been necessitated by the demand for improving performance from expensive industrial plants and minimizing unscheduled shutdown costs. The early detection of the occurrence of faults is critical for avoiding product deterioration, performance degradation or major damage to the machinery and/or operators, especially for faulty combustion system, whose damage may be very dangerous.

Economy and every-day life depend on the function of manufacturing systems, including industrial production facilities (gas turbines, power plants, chemical plants, oil refineries, steel mills, paper mills, etc.), transportation systems (trains, ships, airplanes, automobiles, etc.) and household appliances (heating/air conditioning equipments, refrigerators, washing machines, etc.), consist of many different machine tools, robots and control systems. Faults in a single component have a major effect on the availability and performance of the system as a whole. Every component has been designed to provide a certain function and the overall system works satisfactorily only if all components provide the service by which they are designed for, and all of which have to correctly satisfy their purpose in order to ensure an efficient and high-quality production.

In the general sense, a fault is something that changes the behavior of a technological system such that the system does no longer satisfy its destined functionality. It may be an internal event in the system, which stops the power

supply, breaks an information link, or creates a leakage in pipe. It may be a change in the environmental conditions that causes a temperature increase that eventually stops a reaction or even destroys the reactor. It may be a wrong control action given by the human operator that brings the systems out of the required operation point. Or it may be an error in the design of the system, which remained undetected until the system comes into a certain operation point where this error reduces the performance considerably. In any case, the fault is the primary cause of changes in the system structure or parameters that eventually leads to a degraded system performance or even the loss of the system function. Therefore even a fault in a single component it could change the performance of the overall system. In order to avoid production deteriorations or damage to machines and humans, faults have to be found and located as quickly as possible and decisions that stop the propagation of their effects have to be made [34]. Hence the process monitoring has become very necessary.

The goal of process monitoring is to ensure the success of the planned operations by recognizing anomalies of the behavior. The information not only keeps the plant operator and maintenance personnel better informed of the status of the process, but also assists them to make appropriate remedial actions to remove the abnormal behavior from the process. As a result of proper process monitoring, downtime is minimized, safety of plant operations is improved, and manufacturing costs are reduced.

The four procedures associated with process monitoring are: fault detection, fault identification, fault diagnosis and process recovery.

1. Fault detection

   This procedure is to determine whether a fault has occurred or not. Early detection may provide invaluable warning on emerging problems, with appropriate actions taken to avoid serious process upsets. For combustion process, whether instability happens or not needs to be found out in this procedure because the combustion instability can be a potential factor to induce a fault, for example, change of pressure and fuel flow rate etc.

2. Fault identification

   This step is to identify the observation variables most relevant to diagnose the fault. The purpose of this procedure is to focus the plant operator's and/or engineer's attention on the subsystems, so that the effect of the fault can be eliminated in a more efficient manner. For this research, the flame flicker frequency is observed as the key variable for the fault identification.

3. Fault diagnosis

   This procedure is to determine which fault occurred, in other words, determining the cause of the observed out-of-control status. The fault diagnosis procedure is essential to the counteraction or elimination of the fault.

4. Process recovery

   This procedure, also called intervention, is to remove the effect of the fault, and it is the procedure needed to close the process monitoring loop (see Figure 2-7). It is an important and necessary component of the processing monitoring loop. This research is achieved by the external acoustic excitation based on the interaction between acoustic wave and the flame.

Whenever a fault is detected, the four procedures are employed in the respective sequence; otherwise, only the fault detection procedure is repeated [13].

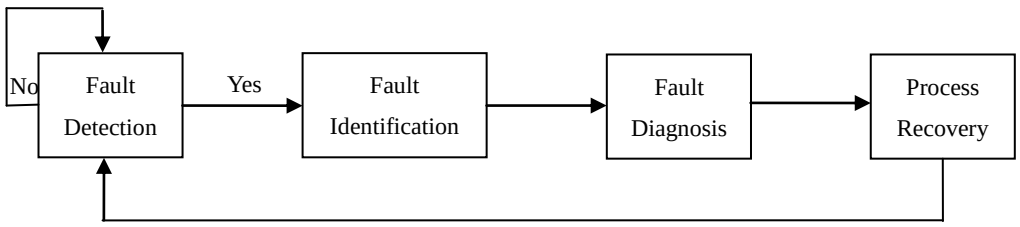

Figure 2-7: Schematic diagram of the process monitoring loop

There are many different ways to classify the condition monitoring techniques. In one aspect, the methods of fault detection and diagnosis can be classified into two major groups. One utilizes the mathematical model of the plant, model-based

methods, and the other is the model-free methods. In modern industrial, the model-free methods are applied more widely than model-based methods, because the mathematical model is uniquely determined from a given set of experimental data for model-based methods. Otherwise, conclusions based on the mathematical model can be very misleading. Model-free methods normally utilise some sensors to do online measurement and provide feedback to monitor the system. This part introduces some popular methods and techniques for both model-free methods and model-based methods along with the corresponding related knowledge.

2.4.1.1 The Model-Free Method

As implied by its name, model-free method is a method that is not based on the system mathematical model. Normally, model-free methods range from physical redundancy, limit-checking through spectrum analysis to logical reasoning [46]. Most of time, they are not used separately, always in crossed application.

Physical Redundancy

In this approach, a set of the same sensors are required to be installed to measure the same physical quantity. Any serious discrepancy between the measurements indicates a sensor fault. It there are only two parallel sensors, it is obviously not possible to isolate the fault. If there are three sensors, a voting scheme can be formed that isolates the faulty sensor. This kind of method involves extra hardware cost and extra weight, the latter representing a serious concern in practical applications, such as aerospace application. Therefore, with the development of the control techniques, this method is not an ideal choice for monitoring of the process condition.

Limit checking

This method compares the online measurements with present limits. Limit checking raises an alarm when observations cross predefined thresholds.

Exceeding the threshold indicates a fault occurrence. In many systems, there are two levels of limits (see Figure 2-8), the first of which serves for pre-warning while the second of which triggers an emergency reaction. Limit checking has been applied traditionally because it is easy to implement and may be extended to monitor the time-trend of selected variables.

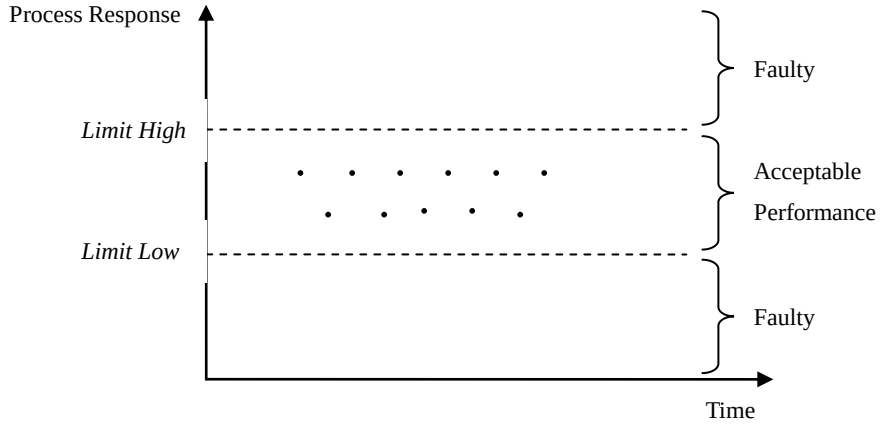

Figure 2-8: Method of limit checking

Spectrum analysis

Most variables exhibit a typical frequency spectrum under a healthy condition. Sometimes a distinct frequency or different peak frequency appears in frequency spectrum in faulty condition. Any deviation from the healthy spectrum is a potential indication of fault. Different patterns of spectrum allow to diagnose different types of faults and to quantify fault severity.

For monitoring of combustion condition, pressure oscillation is of most significance. In many applications, the pressure oscillations are undesirable since they result in excessive vibration, causing high levels of acoustic noise and mechanical failure. Spectrum analysis is very powerful to this kind of problem. In the frequency domain, the pressure is characterized by dominant peaks at discrete frequencies which correspond to the acoustic modes of the combustion chamber. When some unusual frequencies appear in the pressure spectrum, there must be some failure happened in the system or there will be some faults happened very soon.

Logic reasoning

Like fuzzy logic control methods, the simplest techniques consist of trees of logical rules of the

IF symptom1

AND symptom2

THEN conclusion

Each conclusion can, in turn, serve as a symptom in the next rule, until the final conclusion is reached. The system may process the information presented by the detection hardware/software or may interact with a human operator, inquiring from the operator about particular symptoms and guiding him through the entire logical process.

2.4.1.2 Model-Based Methods

For the purpose of engineering analysis and design, some physical systems are usually represented in some mathematical forms, which is also called the model of the system. The properties of the model reflect the nature of the system, though in many cases the model may just be an approximation of the true system behavior. Dynamic systems can always be characterized by continuous-time operation or equivalent transformed representations. However, the monitoring computers operate in a sampled fashion, using sampled data. Therefore it is practical to describe the monitored systems in discrete time, in the form of difference equations or their transformed equivalents.

Model-based fault detection along with associated diagnosis method is the method that utilizes the mathematical model of the monitored plant. For fault detection purposes, the model of the system can be used to calculate model outputs for the measured inputs. The traditional mode-based fault detection and diagnosis methods are introduced in this part, which are the discrepancy detection method, the fault tolerant controller method and the parameter estimation approach.

Discrepancy Detection

Discrepancy detection raises an alarm by comparing simulated values based on the mathematical model of the system to actual observed values. It is very similar to the limit checking method introduced in the previous part. It highly depends on the model accuracy, but model inaccuracies are unavoidable in practice. So, it may lack robustness and is difficult to distinguish genuine faults from errors in the model. This method normally is just applied in the small or very simple plant system instead of the large or complicated system.

Fault Tolerant Controller

In most plant systems, the effects of a fault in a single component may be of minor importance of this component. However, due to the propagation of the fault effects throughout the overall system, the fault may eventually initiate the safety system to shut off the whole system that causes a system failure. Basically, there are two ways to stop the propagation of the fault. Either the fault propagation is stopped inside the affected component by making the component fault-tolerant or the propagation of the fault among the components has to be stopped. The propagation of the fault effects through the overall system usually takes time. The time gives the fault-tolerant controller of the affected component the chance to adjust its behavior to the faulty situation and, hence, to keep the overall system in operation.

The first task of fault-tolerant control concerns the detection and identification of existing faults. Take an example of a dynamical system with input u and output y is subjected to some faults F. The diagnostic system obtains the I/O pair (U, Y), which consists of the sequences:

$$U = (u(0), u(1), \dots, u(k_h)) \quad \textbf{(2-15)}$$

$$Y = (y(0), y(1), \dots, y(k_h)) \quad \textbf{(2-16)}$$

of input and output values measured at discrete time points k within a given time horizon k_h. Fault detection has to solve the following problem:

For a given I/O pair(U, Y), find the fault F.

In order to be able to detect a fault, the measurement information (U, Y) alone is

not sufficient, but a reference, which describes the nominal plant behavior, is necessary. This reference is given by an explicit mathematical model of the plant, which describes the relationship between the possible input sequences and output sequences. This model is a representation of the plant healthy behavior β. Assume that the current I/O pair (U,Y) is represented by a point, say point A in Figure 2-9 . If the system is faultless, then A lies in the set β. However, if the system is faulty, it generates a different output $\hat{Y}$ instead of Y for the given input U. If the new I/O pair $(U,\hat{Y})$ is represented by point C, which is outside of β, then the fault is detectable.

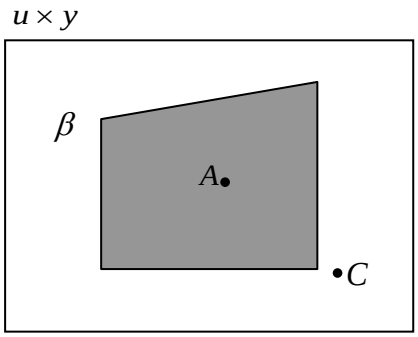

Figure 2-9: Graphical illustration of the system behavior

The above idea can be described as consistency-based diagnosis. It does not depend on the kind of the model used, and just concerns the comparison of the measured I/O pair with a plant model. But it also has some drawbacks:

1. Fault detection is not possible without any information about the behavior of the faulty plant.
2. Fault isolation and identification is not feasible without information about the faults.
3. The way in which the faults affect the system can't prove that a certain fault is present, which need further investigation.

For the fault tolerant controller, continuous-based diagnosis concerns the comparison of the measured I/O pair with a plant model; the comparison of discrete-based diagnosis is done in a direct way. For continuous systems, the usual way of comparison consists in using residuals. And most of model-based

detection and diagnosis methods rely on the concept of analytical redundancy. In contrast to physical redundancy discussed in last part, the sensor measurements are compared to analytically computed values of the respective variable instead of straightly comparing to each other. The result differences, called residuals, are indicative of the presence of faults in the system (See Figure 2-10). The generation of residuals needs to be followed by residual evaluation, in order to arrive at detection and isolation decisions. Because of the presence of noise and model errors, even if in healthy condition, the residuals are never zero (in theory, the residual vanishes or is close to zero in the healthy case. A non-vanishing residual indicates the deviation between measured and set point values.). Therefore, the detection decision requires testing the residuals against thresholds, obtained empirically or by theoretical considerations [8].

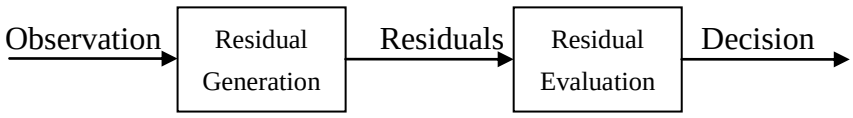

Figure 2-10: Stages of model-based fault detection and diagnosis

Parameter Estimation

Parameter estimation, depicted in Figure 2-11, is a natural approach for the detection and diagnosis of parametric faults, which could be caused by any fault of the system. Initially, a reference model is obtained by identifying the system in the healthy situation. The parameters are then repeatedly identified. Deviations from the reference model parameters serve as a basis for fault detection [86].

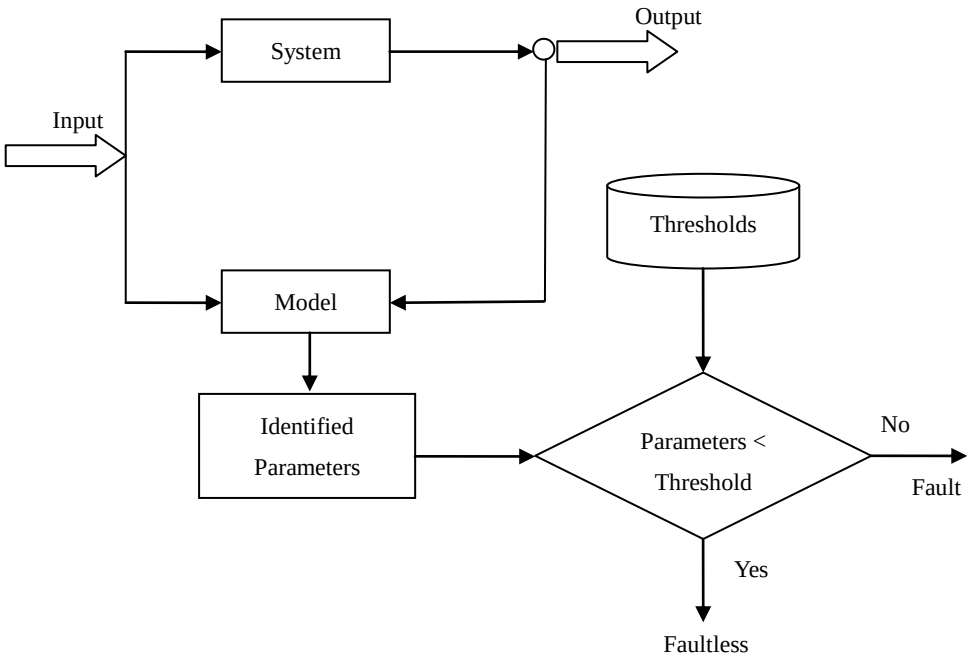

Figure 2-11: Schematic diagram of fault detection using parameter estimation approach

The general procedure to detect faults follows the steps below [23]:

1. Construct of the mathematical model of the system's normal behavior, $y(t) = f(u(t), \theta)$, where $y(t)$ represents the output vector of the system, $u(t)$ denotes the input vector, θ denotes the non-measurable parameters which are likely to change on the occurrence of a fault.
2. Determine the relationship between the model parameters θ_i and the physical system parameters p_j.
3. Estimate the model parameters θ_i from measurements of $y(t)$, $u(t)$ by a suitable estimation procedure:

$$\widehat{\boldsymbol{\theta}}(\boldsymbol{t}) = \boldsymbol{g}(\boldsymbol{y}(\mathbf{1}), \boldsymbol{y}(\mathbf{2}), \ldots, \boldsymbol{y}(\boldsymbol{t}), \boldsymbol{u}(\mathbf{1}), \boldsymbol{u}(\mathbf{2}), \ldots, \boldsymbol{u}(\boldsymbol{t})) \quad (2\text{-}17)$$

   And then calculate parameters of the physical system, via the inverse relationship:

$$\hat{p}(t) = f^{-1}(\hat{\theta}(t)) \quad \textbf{(2-18)}$$

4. The decision on whether a fault has occurred in terms of either on the changes Δp_j or on the changes $\Delta\theta_i$ and tolerances limits. If the decision is made based on the $\Delta\theta_i$, the affected p_i can be easily determined from

the step 2. This may be achieved with the aid of a fault catalogue where the relationship between process faults and changes in the coefficients Δp_j has been established. Decision can be made either by simply checking against the predetermined threshold levels, or by using more sophisticated methods from the field of statistical decision theory.

2.4.1.3 Review of Different Sensors

For detection and diagnosis in an industrial plant, no matter using the model-free method or the model-based method, it is necessary to collect online data correctly and promptly. Hence, sensors are very necessarily and importantly to be installed explicitly. They could be limit sensors, e.g., temperature sensor, flowing sensor or pressure sensor, which performs limit checking in hardware. Other special sensors may measure some fault-indicating physical value, such as sound, vibration, speed and load, etc. Based on several physical characteristics, like particle contamination of fluid, temperature of the operation situation, flow of a fluid system, angular speed of the rotary machine and vibration, some special sensors will be introduced in the following sections.

Temperature Measurement Sensor

Temperature measurement is the simplest and lowest cost form of monitoring. It is desirable to keep the operating temperature of the system within a specified working range and closed-loop temperature control may be achieved with a degree of success using either a water cooler or fan-driven cooler. From a condition monitoring point of view changes in temperature, for example in a pump case drain line, may indicate a change in leakage flow rate and hence wear of a component within the pump. The change in temperature differential across a component may also indicate component deterioration, but this and most other applications require the measurement of small temperature differential changes. There are lots of different types of temperature sensors, such as thermocouple sensors, resistance temperature detectors and thermistor etc.

Take the temperature probes as an example, which are widely used in science and industry. They may easily be fitted into components, and they utilize the thermocouple principle of combining dissimilar metals which generates an electromotive force change with temperature change at the junction [86]. A temperature probe from OPENXTRA is shown in Figure 2-12.

Figure 2-12: Temperature probe [44]

Flow Measurement Sensor

The performance of a fluid power system may be assessed by placing flow meters at strategies points in a circuit. By comparing the measured flow rates with the ideal values, a fault in the fluid power system could be detected. But this method needs to be executed at the same working temperature and pressure which is very difficulty achieved for the actual working situation. A typical turbine-type flow meter from NIXON is illustrated in Figure 2-13. [43]

Figure 2-13: Turbine-type flow meter [43]

A popular method of determine air flow velocity is using hot-wire anemometer in fluid mechanics. It has been used extensively for many years as a research tool. Figure 2-14 shows a hot-wire anemometer probe [41]. Typical dimensions of the

wire sensor are 0.00015 inches to 0.0002 inches (0.0038mm to 0.005 mm) in diameter and 0.040 to 0.080 inches (1.0 to 2.0mm) long, which is very weak and fragile. This is the type of hot wire that has been used for such measurements as flow patterns around models, turbulence levels in wind tunnels, and blade wakes in radial compressors. Besides the hot wire, there is another type of sensor, hot film, which is much stronger than hot wire. The film type of sensor is shown in Figure 2-15. The hot film is used in regions where a hot wire probe would quickly break such as in water flow measurements.

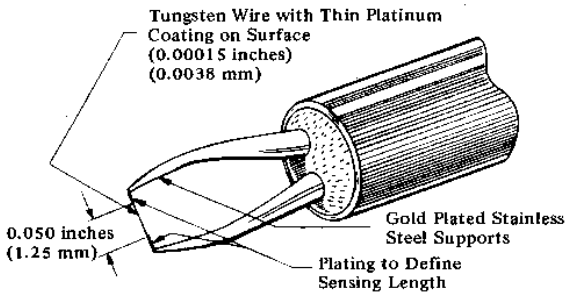

Figure 2-14: Tungsten hot wire sensor and support needles-0.00015” Dia. (0.0038mm) [41]

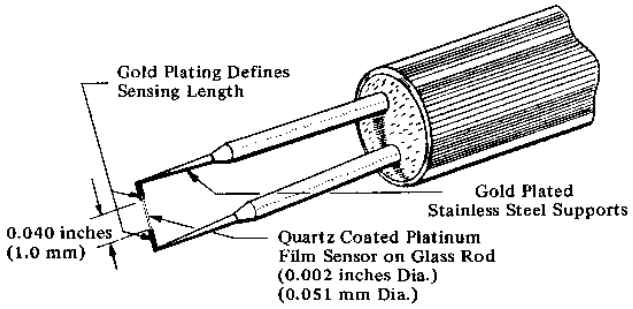

Figure 2-15: Cylindrical hot film sensor and support needles-0.002” Dia. (0.051mm) [41]

Acoustic Measurement Sensor

Microphone is a typical sensor for acoustic measurement. Microphone serves two principal purposes. Converting sounds into electrical signals and measuring parameters. The latter purpose is to determine the sound pressure or the particle velocity. For different applications, a variety of microphones have been developed, and two main types of which are pressure microphone and pressure-gradient microphone. Pressure microphone is the most widely used in

laboratory acoustic measurement, which uses a diaphragm between a fixed internal volume of air and the environment, and responds uniformly to pressure from all directions, so it is said to be omnidirectional. Because a pressure-gradient microphone uses a diaphragm that is at least partially open on both sides, the pressure difference between the two sides produces its directional characteristics [37]. A pure pressure-gradient microphone is equally sensitive to sounds arriving from front or back, but insensitive to sounds arriving from the side because sound arriving at the front and back at the same time creates no gradient between the two sides.

Particle contamination sensor

Particle contamination of fluid is a major cause of failure in fluid power systems and the early detection of such a problem is essential.

Take the ferrography as an example. This is a technique for magnetically precipitating wear debris and contamination and then using electromagnetic characteristics or light blockage to establish a particle count. A relatively low cost portable unit is the Particle Quantifier which falls into the ferrography category. This unit assesses the quantity of magnetic particles with a specific sample in terms of their magnetic density. This is achieved by measuring the change in the magnetic force field of a sample placed within the field compared to a null measurement made when it is removed from the field. The numerical value is called the PQ index.

Alternative forms of particle counting are available. The simplest and most time consuming is to use an optical microscope to examine a fixed volume of oil filtered through a membrane. Particles are manually counted and compared with a reference slide to determine the cleanliness.

Most of these techniques are off-line in that a sample of fluid must be drawn from a carefully selected point in the system. The sample container must not be contaminated with particles either at the sampling stage or during subsequent analysis. Such problems can be minimized if on-line techniques are used and this

requires insertion of sensors or bypassing fluid permanently through and appropriate analyzer [86]. Figure 2-16 shows a Ferrous Debris Sensor [42].

Figure 2-16: Ferrous debris sensor [42]

Vibration Measurement Sensor

Using the vibration signal to detect and diagnosis faults is a very popular approach in mechanical field in recent years. When an instrument has a local fault, such as a motor or a gearbox, the vibration signal may contain amplitude and phase modulations that are periodic with the rotation frequency of the shaft or the gear. Many researchers have been investigated on this subject.

Critical to vibration monitoring and analysis is the machine mounted sensor. There are three parameters representing motion detected by vibration monitors. They are displacement, velocity and acceleration. These parameters are mathematically related and can be derived from a variety of motion sensors. Selection of a sensor proportional to displacement, velocity or acceleration depends on the frequencies of interest and the signal levels involved. Sensor selection and installation is often the determining factor in accurate diagnoses of machinery condition.

Displacement sensors are used to measure shaft motion and internal clearances. Monitors have used non-contact proximity sensors such as eddy probes to sense shaft vibration relative to bearings or some other support structure. These sensors are best suited for measuring low frequency and low amplitude displacements typically found in sleeve bearing machine designs.

Velocity sensors are used for low to medium frequency measurements. They are useful for vibration monitoring and balancing operations on rotating machinery.

As compared to accelerometers, velocity sensors have lower sensitivity to high frequency vibrations. Thus, they are less susceptible to amplifier overloads. Overloads can compromise the fidelity of low amplitude, low frequency signals. Traditional velocity sensors use an electromagnetic (coil and magnet) system to generate the velocity signal. Now, hardier piezoelectric velocity sensors (internally integrated accelerometers) are gaining in popularity due to their improved capabilities.

Accelerometers are the preferred motion sensors for most vibration monitoring applications. They are useful for measuring low to very high frequencies and are available in a wide variety of general purpose and applicable to specific designs.

Recently, a new developed sensor has improved the measurement for vibration signal, piezoelectric sensor. They overcome problems associated with mounting non-contact probes, and are more suitable for rolling element bearing machine designs. Piezoelectric sensors yield an output proportional to the absolute motion of a structure, rather than relative motion between the proximity sensor mounting point and target surface, such as a shaft. The piezoelectric sensors are versatile, reliable and the most popular vibration sensor for machinery monitoring. They get a rugged, solid-state construction which enables them to operate under the harshest environmental conditions. They are unaffected by dirt, oil, and most chemical atmospheres. Most piezoelectric sensors used in vibration monitoring contain internal amplifiers. The piezoelectric element in the sensor produces a signal proportional to acceleration. This small acceleration signal can be amplified for acceleration measurements or converted (electronically integrated) within the sensor into a velocity or displacement signal. The piezoelectric velocity sensor is more rugged than a coil and magnet sensor, and has a wider frequency range, and also can perform accurate phase measurements.

2.4.2 Control Methods of Combustion Instability

There is a substantial effort has been expanded to the control of combustion

thermoacoustic instability. Generally speaking, control strategies that can be employed to solve the combustion thermoacoustic instability problem can be classified as Passive Instability Control (PIC) and Active Instability Control (AIC).

2.4.2.1 PIC of Combustion Oscillations

For many years, PIC techniques have been widely used in industrial burners in most practical combustors. PIC techniques generally involve modifications to the fuel injector or combustor hardware to eliminate the source of the variation in heat release or to increase the acoustic damping in the system and thereby reduce the amplitude of any pressure oscillations. Typically passive measures are detuning a system by changing the flame anchoring point, the burning mechanism and the acoustic boundary conditions, and modifying its burners or the acoustics of its combustion chamber, by disturbing the propagation of acoustic waves via resonators and baffles.

Compared to active control solutions, passive methods have the advantage of being more reliable and independent of an external source of energy and thus raising less problems. But on the other hand, due to acoustic properties of the combustor depend on its physical dimensions and the operating conditions; it is a very difficult task to use hardware to disturb the sound propagation. Also it is difficult to optimize performance using PIC means alone by means of changing the dynamic properties with the operating point. Furthermore, the effectiveness of passive measures taken for one instability mode may be offset by a loss of stability of another mode. In contrast, by interfering with the feedback mechanism, AIC can not only damp the oscillation system but also suppress the other instability mode.

2.4.2.2 AIC of Combustion Oscillations

AIC is the term that is widely used to describe the situation where control is

affected by adding energy to the system via the use of actuators in a way that counteracts the oscillation.

For many years, attention has been paid to the possibility of using active control techniques for stabilizing self-sustained oscillations, which began with the early work of Tsien [83], Crocco [19] and Marble [60]. Several previous studies have shown that active control techniques introducing an additional coupling with controllers lead to a stabilization of the system. This feature has been demonstrated in many different situations, such as combustion instabilities, flow-excited cavity oscillations, and compressor surge. In this part, the method using AIC to suppress the combustion instabilities is introduced.

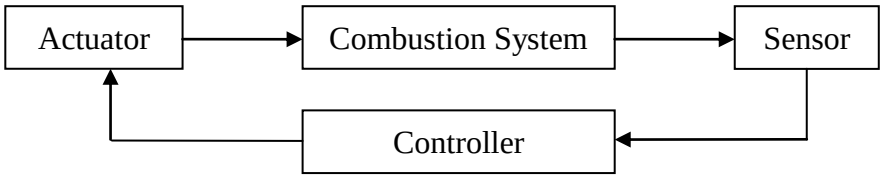

Figure 2-17: Feedback control mechanism of AIC

Figure 2-17 shows the feedback control mechanism of AIC. Sensor in the diagram can be a temperature sensor, microphone, pressure sensor, photomultiplier, hot wire anemometry or high speed camera etc. Based on the control techniques of the controller, AIC can be classified as robust control AIC, adaptive control AIC, neural networks control AIC and phase-shifter AIC etc. According to the different types of actuator applied, AIC includes secondary fuel injector AIC and external acoustic excitation AIC etc.

Adaptive Control AIC

Billoud et al. [6] presented an adaptive controller for the active control of flow instability. Figure 2-18 shows the typical AIC setup with adaptive controller. The photomultiplier is used to detect the global emission from CH^* radicals related to heat release in the combustor, which serves as the input to the adaptive controller, whose output is then fed into an actuator. The global response is collected by a microphone and is used to update the controller's coefficients.

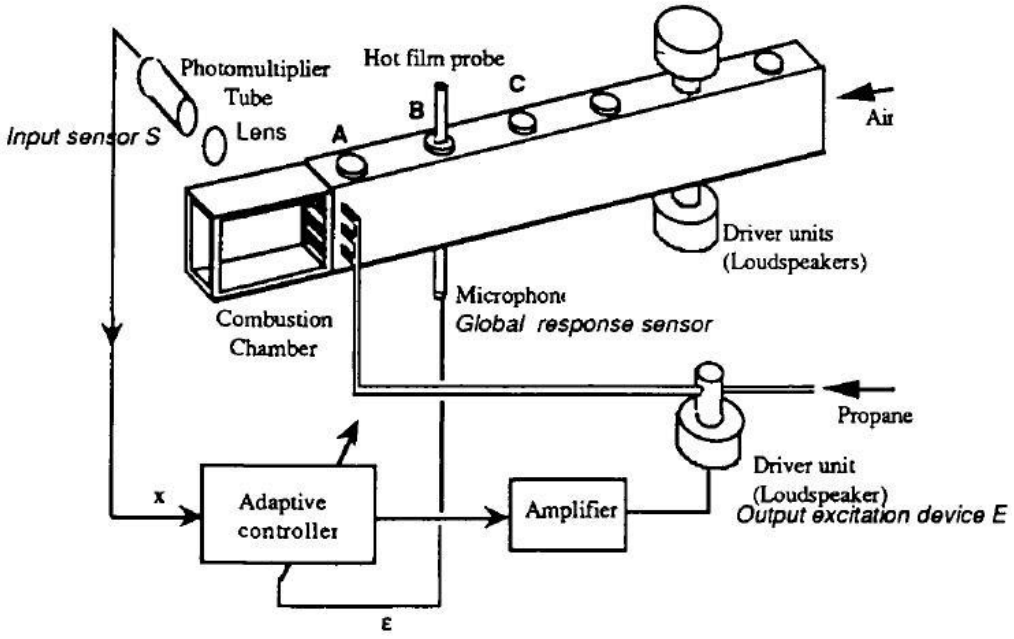

Figure 2-18: Schematic diagram of a closed-loop control system for combustion instabilities [6]

Neural Network Control AIC

Liu et al. [59] (1999) presented a control strategy for the active stabilization of combustion system based on neural network. The control algorithm is comprised of three parts: an output model, an output predictor and a feedback controller. The output model is established using neural networks, which is used to predict the output in order to overcome the time delay of the system. The feedback controller uses the output of the predictor to suppress instability in the combustion process.

Phase-shifter/converter AIC

A prevalent approach in experimental investigations of active combustion control is the use of a phase-shift/converter controller where the strategy for suppressing the pressure oscillations is to measure the pressure, add an appropriate phase, and generate a signal that is equal and opposite to the actual pressure. The phase-shift control strategy, which is sometimes referred to as a phase-delay or a time delay strategy, has been used extensively in active combustion control. Since the undesirable pressure oscillations often occur at a few, not a single frequency, the phase shift controller includes a filter in addition to the actual phase-shift action

and some amplification, as shown in Figure 2-19.

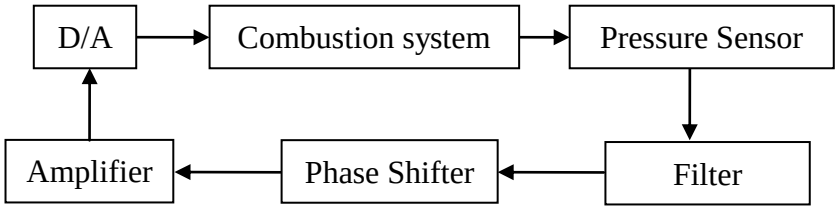

Figure 2-19: Schematic diagram of a phase-shifter AIC

Noiray et al. [63] suppressed the onset of oscillations over a broad range of frequencies by inserting a dynamic phase converter (DPC) in a burner comprising a large number of injection channels. The DPC system was imposed an out of phase motion of perturbed individual flames, yielding opposite heat release fluctuations which compensate each other and yield a steady global response to incoming perturbations.

Secondary Fuel Injector AIC

AIC by secondary fuel injection has been observed to have a high impact on the combustion instability, feeding only a small fraction of the fuel anti-cyclical to the heat release oscillation. With this method, the instabilities can be suppressed by measuring the phase and amplitude of the pressure or heat release in the combustor, suitably phase shifting or amplifying the measured signal, and then driving a secondary fuel injector with this signal. Figure 2-20 shows a sketch of a secondary fuel injector by Auer et al. [4]. AIC modulates secondary fuel that is injected into the combustion system to destroy the thermoacoustic feedback cycle to suppress the instability.

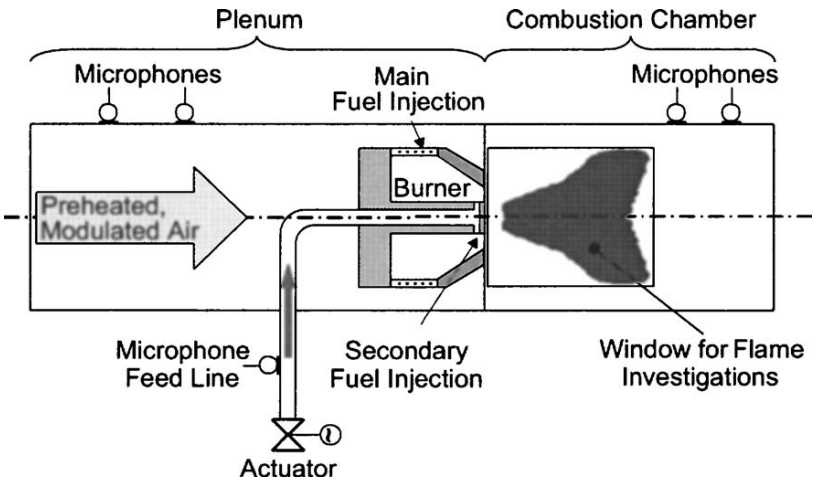

Figure 2-20: Sketch of a secondary fuel injector [4]

Conrad et al. [17] proved it is possible for applying an ‘‘intermittent’’ active control approach for suppressing combustion instabilities in liquid fueled combustors. A ‘‘smart’’ fuel injector that can modify the spray properties in response to changes in combustor operating conditions was applied, which weakens or breaks up the coupling between the combustion process and combustor acoustic modes oscillations, thus preventing the excitation of large amplitude instabilities. This strategy required only ‘‘intermittent’’ modification of the combustion process by a single control action which was opposed to the continuous action required by most other active control methods.

External Acoustic Excitation AIC

Experimental researches of combustion thermoacoustic instability are often based on external excitation methods. The external excitation can both trigger and suppress flame instability. Lang et al. [52] used external acoustic excitation by a loudspeaker to suppress the oscillation of a flame. The excitation signal is provided by a microphone located upstream of the flame. This signal is filtered, processed, amplified, and then sent to the loudspeaker. The experimental results showed that this method can suppress all unstable modes of the burner and the locations of microphone and loudspeaker also had influence of the performance.

AIC based on the model of combustion system

Hong et al. [35] developed a robust feedback controller for suppressing

combustion instabilities, based on the known model of the combustion system. Normally, the robustness in a model-based control system is traditionally predicted in terms of phase and gain margins. But when the combined uncertainties in both phase and gain simultaneously take into effect, a very small uncertainty may drive the system into instability. Instead, the robustness of a control system could be judged by the size of μ or H_∞ norm to guarantee a trade-off relationship between stability and performance in the presence of uncertainties and exogenous inputs.

2.5 Monitoring Methods of Combustion Process

Combustion is a complicated process, and it is difficult to give this phenomenon a precise meaning. Although a few flames, such as that of hydrogen burning with clean dust-free air, may be practically non-luminous, people generally associate the emission of light with flames. It should be bear in mind that both the quantity and quality of this light may differ remarkably from that of mere hot gases, and the causes of this will form a part of the examination of the nature of flame. The emission of radiation by the hot flame gases offers several possible methods of measuring the gas temperature, studying the state of equilibrium in the reacting gases. The light of the flame is also very useful in locating the position and form of the flame front. Both of them are very important for the analyzing of flame dynamics.

2.5.1 Combustion Process Monitoring Based on Radiation Emissions

When a chemical reaction leads directly to the formation of an atom or a molecule in an electronically excited state, from which radiation may occur. And then there may is a light emission out of all proportion to that to be expected from thermal emission. This phenomenon is usually referred to as

chemiluminescence. Common chemiluminescence species in hydrocarbon-air flames are CH^*, OH^* and C^*_2. Figure 2-21 shows an example of transient combustion chemiluminescence species. Chemiluminescence can potentially provide information about reaction zone conditions that relate to combustor performance, pollutant formation and combustor health.

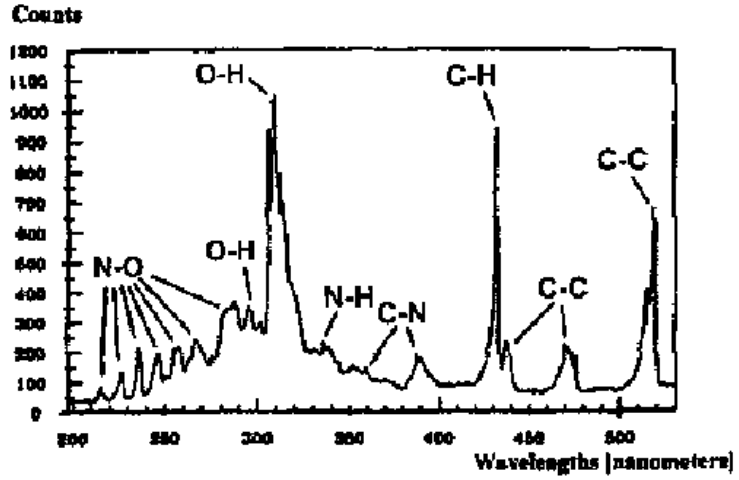

Figure 2-21: An Example of transient combustion chemiluminescence species [73]

As shown in Figure 2-21, CH^* has peak intensity in the emission spectrum. The CH^* comes only from the reaction zone; thus the total light intensity for CH^* should be proportional to the factual surface area of the flame front. So CH^* chemiluminescence is often employed in combustion diagnostics, for example as a measurement of heat release rate. The primary CH^* emission in the ultraviolet and visible region of the spectrum is due to the $A^2\Delta \rightarrow X^2II$(431nm) transitions. The main reaction of CH^* formation is [65]:

$$C_2 + OH \rightarrow CH^* + CO \quad \textbf{(2-19)}$$

There is also some other process responsible for CH^* excitation which is not dependent on C_2. The possible reactions are:

$$C_2H + O_2 = CO_2 + CH(A^2\Delta) \quad \textbf{(2-20)}$$

$$C_2H_2 + OH = H_2 + CO + CH(X^2II) \quad \textbf{(2-21)}$$

which could be followed by

$$CH + OH + H = CH^* + H_2O \quad \textbf{(2-22)}$$

2.5.2 Combustion Process Analyzing Based on Flame Photograph

Measurements and analyzes of flame shape are usually made from its photographs. For hydrocarbons the inner flame is usually sufficiently bright to enable photographs to be taken with exposures of less than one second. The method for analyzing the flame photographs taken by a high speed camera is the image processing method, which is any form of signal processing method whose input is an image or a series of images, such as photographs or frames of video. The output of image processing method can be an image, a group of images, or a set of characteristics or parameters related to the input image or images. Most image-processing techniques involve treating the image as a two-dimensional signal and applying standard signal-processing techniques. It has been widely applied in many fields. And it has been proved that it is an effective way to solve many problems.

2.5.3 Schlieren photography

Schlieren photography maps the variations of density in fluids. Schlieren can easily be observed when salts are dissolved in water or when hot air rises above a hot body. Generally schlieren are any things which cause irregular deflection of light from a relatively small area. They may be caused either by change in refractive index or by change in the thickness of a transparent body such as a glass plate which then behaves like a lens. Schlieren photography of flame has several advantages over normal flame photography. One of the greatest advantages is the exposure time. Usually it is not possible to take an instantaneous photography of a flame because the light is not sufficiently bright. For schlieren photography, photographs can be taken usually in 0.001second, and with spark sources down to 10^{-5} or even 10^{-6} seconds. Schlieren photography has been extensively used in aerodynamics for the location of shock fronts and the study of the onset of non-stability. For flame studies the large

temperature jump at the flame front produces strong schlieren and the flames are often smaller than aerodynamic flow regions, so that the large expensive mirrors used in aerodynamic work are not often needed for flame study.

2.6 Summary

Combustion instabilities constitute a serious problems in a wide range of industrial applications, because they enhance noise levels, induce structural vibrations, intensify heat fluxes to the boundaries and in extreme cases lead to damage and even destruction of the system. Thermoacoustic instability is the most common instability that happens during industrial combustion, which is an unstable coupling between an excitation, acoustic source, and the corresponding response of the system, heat release. Acoustic wave has capabilities to influence flames. It interacts with flames both in direct and indirect ways. It can change the flame shape, make combustion unstable and sometimes can improve the combustion stability. By reviewing different methods for combustion instability control, PIC and AIC are two mains control methods, but nowadays, AIC is a more popular method than PIC due to its flexibility, low cost and good performance. Some common methods for system fault detection and diagnosis were also been reviewed and compared.

In the first two years PhD study in the Condition Monitoring Lab of the University of Manchester, main jobs were focused on the condition monitoring and fault detection for motoring system. But for some uncontrollable reasons, concentration of the research has to be moved to the study of the research of combustion dynamics and corresponding control in the last two years.

Chapter 3

Experimental Apparatus and Setup

This chapter introduces the experimental apparatus and corresponding setup of this research. Five main units, workstation unit, acoustic wave generating unit, burner unit, measurement unit and data acquisition unit, have been elaborated. The details of the instruments used to measure and observe different combustion parameters have been given. At the end of this chapter, the uncertainties for measurements have been discussed, which demonstrate difficulties encountered in this research.

3.1 Introduction

This research analyzes the interaction between acoustic wave and flame dynamics in a cylindrical tube burner by monitoring the flame CH^* chemiluminescence signal, 2D images of the flame and the air flow velocity around the flame nozzle. As an important part of this research, the details of the experimental apparatuses applied are introduced in this chapter and the uncertainties of measurement during the experiments are also discussed to reduce the influence of noise during experiments.

3.2 Experimental Rig

The experimental apparatuses used in this research can be illustrated by in Figure

3-1. This system has five units: workstation unit, acoustic wave generating unit, burner unit, measurement unit and data acquisition unit that build up a closed-loop system, as show in Figure 3-2. Based on the measured data, the workstation sends a series of control commands to acoustic wave generating unit to produce the designed external acoustic wave for the burner unit. Four main units except the workstation are briefly introduced as follow.

1. Acoustic wave generating unit;
   This unit is composed of a PC, a loudspeaker, a power amplifier, and a controllable frequency signal generator;
2. Burner unit;
   It consists of a fuel supply sub-system and a transparent cylindrical tube burner (combustion chamber), which is located on a three-ways traverse system.
3. Measurement unit;
   This unit includes a high speed digital camera, a photomultiplier, a microphone and a hot-wire anemometry;
4. Data acquisition unit;
   This unit includes a 16-channel data acquisition card PCI1711 that receives the signals from the photomultiplier, the microphone and the hot-wire anemometry.

Details of assembly and important components of these units are discussed in the following parts.

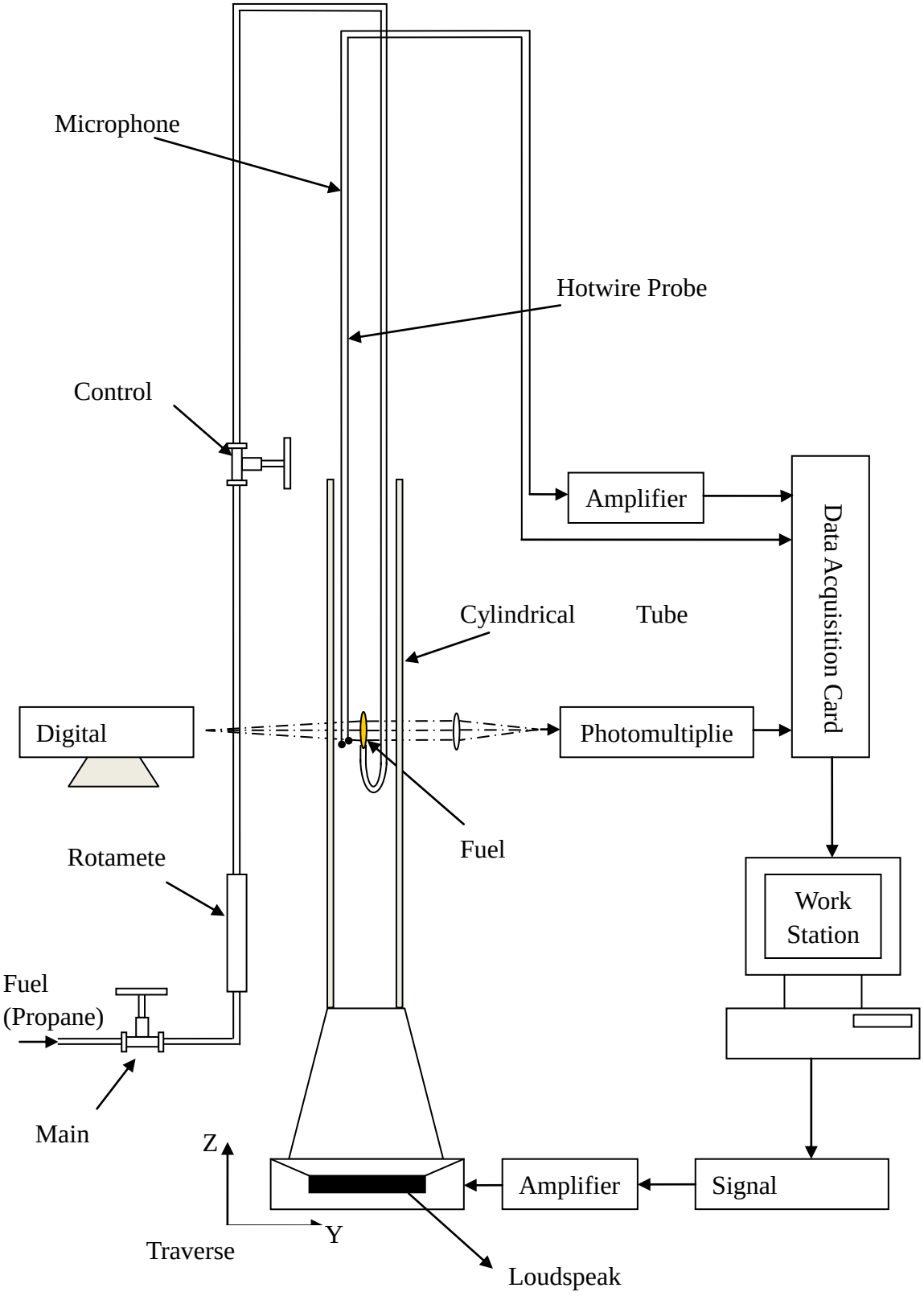

Figure 3-1: Experimental setup

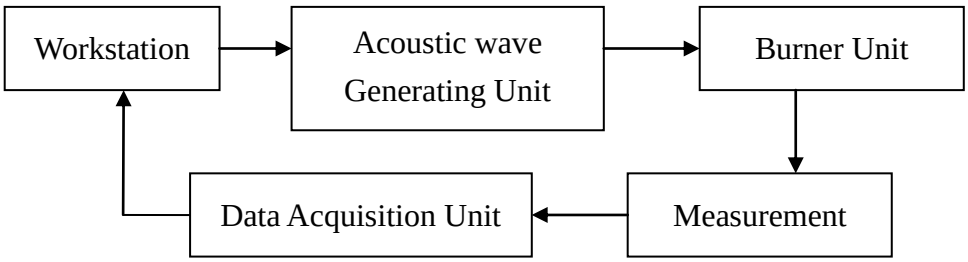

Figure 3-2: Main four units of the experimental setup

3.2.1 Acoustic Wave Generating Unit

This research aims to investigate the interaction between acoustic waves and flame dynamics and establish a control strategy that allows the acoustic waves control the flame dynamics reach the designed observation. Therefore, it is necessary to build an external acoustic source that is able to generate an arbitrary frequency acoustic wave in a limited range. In this experiment, a loudspeaker (shown in Figure 3-1) is mounted under the cylindrical tube to produce the external acoustic excitation for the system. To produce electric sine-wave signal with different frequencies for the loudspeaker, a PC is used as the host to control a controllable signal generator. Before transmitting to the loudspeaker, the signal has to be processed, filtered and amplified by a power amplifier to drive the loudspeaker, as shown in Figure 3-3.

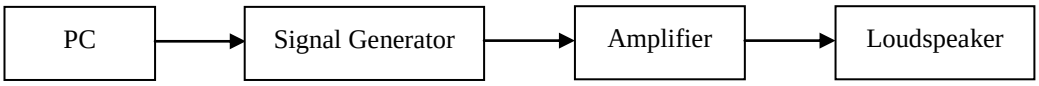

Figure 3-3: Scheme of Acoustic signal generation

3.2.1.1 Loudspeaker

Loudspeaker is an electromagnetic transducer for converting electrical signals into sounds. To adequately reproduce a wide range of frequencies, most loudspeaker systems require more than one driver, particularly for high sound pressure level or high accuracy. Individual drivers are used to reproduce different frequency ranges. The drivers are named subwoofers (very low frequencies, typically below 120Hz), woofers (low frequencies), mid-range speakers (middle

frequencies), tweeters (high frequencies) and sometimes super tweeters optimized for the highest audible frequencies. Besides the drivers, the production of a good high-fidelity loudspeaker also requires that the loudspeaker be enclosed. A loudspeaker enclosure is a cabinet designed to transmit sound to the listener via mounted loudspeaker drive units. The major role of the enclosure is to prevent the out-of-phase acoustic waves from the rear of the speaker combining with the in-phase acoustic waves from the front of the speaker. Such mixing results in interference patterns and cancellation, causing the efficiency of the speaker to be reduced, particularly in the low frequencies where the wavelengths are large enough that interference will affect the entire listening area. There are many ways to enclose a loudspeaker, such as Flat Enclosure (Figure 3-4 (a)), Open-Back Enclosure (Figure 3-4 (b)), Closed Enclosure (Figure 3-4 (c)), Bass-Reflex enclosure (Figure 3-4 (d)) and Drone-Cone enclosure (Figure 3-4 (e)).[40]

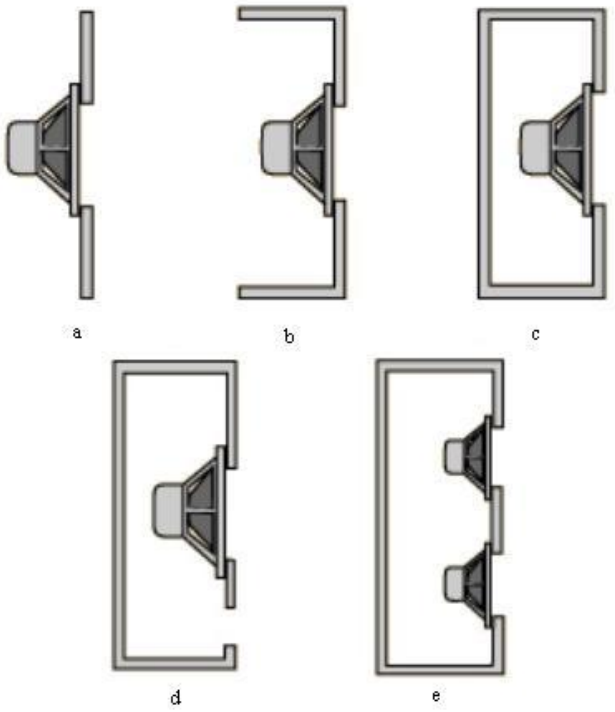

Figure 3-4: Different types of loudspeaker enclosures. (a) Flat Enclosure. (b) Open-Back Enclosure. (c) Closed Enclosure. (d) Bass-Reflex enclosure. (e) Drone-Cone enclosure [40]

The loudspeaker employed in this research adopts the closed enclosure method to enclose the sound. It (Bumper model) has a maximum power of 350Watt, and a frequency range up to 4000Hz. Detail of its specification is given in the Table 3-1. Since the loudspeaker has a larger diameter than the tube, a cone tube (cowl) is used to connect the loudspeaker and the tube. The rear side of the loudspeaker diaphragm is enclosed by a closed-box (21cm (width) × 21cm (length) × 16cm (height)). It is worthy to be pointed out that the connection between the loudspeaker and the tube is only "acoustically" sealed and it is not air tight, so that fresh air is allowed to flow in from the bottom part of the cylindrical tube to sustain the combustion and ensure that the internal and external pressures can slowly equalize over time.

Table 3-1: Loudspeaker specifications

Parameter	Value
Advertised Diameter	8-in (0.2m)
Loudspeaker Resistance R_e	4Ω
Effective Diaphragm Radius	0.0875m
Effective Diaphragm Area	0.02405 m^2
Voice Coil Length	3.4m

3.2.1.2 Controllable Frequency Signal Generator

In order to study the influences of different acoustic waves on flame dynamics, it is very important and essential to produce an accurate and variable acoustic wave frequency as requested during experiments. To help solve this problem, TGA1244 40 MHz Arbitrary Waveform Generator (as shown in Figure 3-5), a programmable and controllable signal generator, is employed in this research.

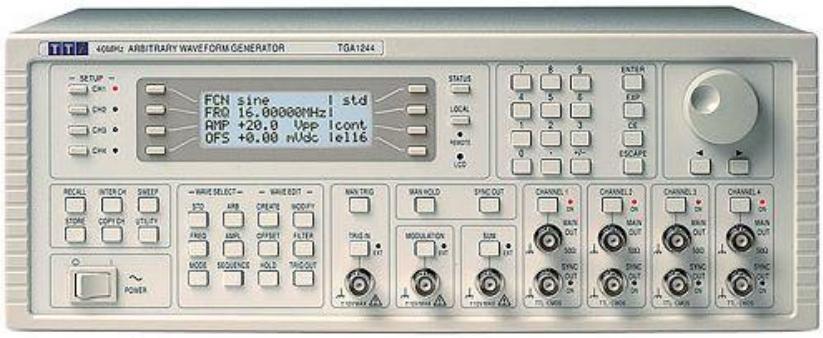

Figure 3-5: TGA1244 40 MHz arbitrary waveform generator

This instrument can generate a wide variety of waveforms between 0.0001Hz and 16 MHz with high resolution and accuracy. A number of standard waveforms are available including sine, square, triangle, ramp and pulse. Amplitude modulation is available for all kinds of waveforms and is controlled from the previous channel or from an external generator via the MODULATION input socket. The generator parameters are clearly displayed on a backlit LCD with 4 rows of 20 characters. All parameters can be entered directly from the numeric keypad. Alternatively most parameters can be incremented or decremented using the rotary control on the top right of the panel. The generator has a RS232 and a GPIB interface as standard which can be used for remote control of all of the instrument functions or for the downloading of arbitrary waveforms. As well as operating in conventional RS232 mode the serial interface can also be used in addressable mode whereby up to 32 instruments can be linked to a single PC serial port.

The generator uses 9−pin D−connector compatible with addressable RS232. The description of pin connections is shown below in Table 3-2.

Table 3-2: Pin connections of RS232

Pin	Name	Description
1	-	No internal Connection
2	TXD	Transmitted data from instrument
3	RXD	Received data to instrument
4	-	No internal connection
5	GND	Signal ground
6	-	No internal connection
7	RXD2	Secondary received data
8	TXD2	Secondary transmitted data
9	GND	Signal ground

When power is on, the instrument will be in the local state with the REMOTE lamp off. In this state all keyboard operations are possible. When the instrument is addressed to listen and a command is received, the remote state will be entered and the REMOTE lamp will be turned on. In this state the keyboard is locked out and only remote commands will be processed. The instrument may be returned to the local state by pressing the LOCAL key. However, the effect of this action will remain only till the instrument is addressed again or receives another character from the interface, when the remote state will once again be entered.

By connecting the PC through RS232 with a single instrument, the generator generates variable frequency, waveforms and amplitudes signal as the control command sent from PC. Figure 3-6 shows the single instrument’s RS232 connection with a PC, where only pins 2, 3 and 5 are connected to the PC in this application.

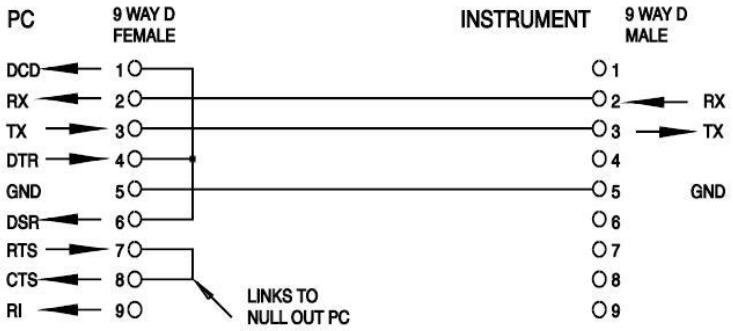

Figure 3-6: Single instrument RS232's connection with PC

Serial input to the instrument is buffered in a 256 byte input queue that is filled, under interrupt, in a manner transparent to all other instrument operations. The instrument will send XOFF when approximately 200 characters are in the queue. XON will be sent when approximately 100 free spaces become available in the queue after XOFF was sent. This queue contains raw data that is taken, by the parser, as required. Commands (and queries) are executed in order and the parser will not start a new command until any previous command or query is completed. In non–addressable RS232 mode responses to commands or queries are sent out immediately, which means that there is no output queue. In addressable mode the response formatter will wait indefinitely if necessary, until the instrument is addressed to talk and the complete response message has been sent, before the parser is allowed to start the next command in the input queue.

Commands must be sent as specified in the commands list and must be terminated with the command terminator code 0AH (Line Feed, LF). Commands may be sent in groups with individual commands separated from each other by the code 3BH (;). The group must be terminated with command terminator 0AH (Line Feed, LF).

Responses from the instrument to the controller are sent as specified in the commands list. Each response is terminated by 0DH (Carriage Return, CR) followed by 0AH (Line Feed, LF).

Table 3-3 lists some remote control commands which have been used in this research.

Table 3-3: Remote command list

Function	Command	Description
Channel	SETUPCH <nrf>	Select channel <nrf> as the destination for subsequent commands. <nrf> may take the range 1 to maximum channel number in the instrument.
Frequency	WAVFREQ <nrf>	Set the waveform frequency to <nrf> Hz.
Period	WAVPER <nrf>	Set the waveform period to <nrf> sec.
Amplitude	AMPL <nrf>	Set the amplitude to <nrf> in the units as specified by the AMPUNIT command.
Amplitude Unit	AMPUNIT <cpd>	Set the amplitude units to <VPP>, <VRMS> or <DBM>.
Waveform	WAVE <cpd>	Select the output waveform as <SINE>, <SQUARE>, <TRIANG>, <DC>, <POSRMP>, <NEGRMP>, <COSINE>, <HAVSIN>, <HAVCOS>, <SINC>, <PULSE>, <PULSTRN>, <ARB> or <SEQ>.
Phase	PHASE <nrf>	Set the generator phase to <nrf> degrees

3.2.1.3 Platform Design to Control Signal Generator

Besides the study of the interaction of the acoustic waves and flame dynamics, monitoring the combustion status to avoid the flame becoming unstable is another main objective for this research. If the flame is detected as unstable, the frequency of the excitation sound is required to be adjusted automatically with a fast response until a stable flame is observed. Obviously, it is not feasible to set the acoustic wave frequency manually. Hence, a software platform is developed using C++ language to deliver the designed frequency calculated by the proposed control strategy to the signal generator TGA1244.

As discussed in previous part, TGA1244 provides a RS232 interface to connect with computer or other devices. The communication protocol can be summarized in Figure 3-6. This platform was developed based on Microsoft Visual C++ 6.0 (VC++), which has friendly and visual interface and strong function library as a program tool. There are three kinds of method to conduct communication based on RS232 in VC++: Win32 API Function, MSComm Control and CSerialPort Class. MSComm Control was employed in this paper because of its simplicity and reliability. VC++ has an ActiveX component named Microsoft Communications Control, which can send and receive data through serial port

and provide serial communication for application. The scheme of the whole procedure and corresponding code can be summarized as in the following steps:

1. Select the port of the PC to connect with signal generator.

   Example: SetCommPort(1); // Select port

2. Set input and output buffer size.

   Example: SetInBufferSize(1024);
   SetOutBufferSize(1024);

3. Open the port.

   Example: SetPortOpen(TRUE);

4. Set transfer mode.

   Example: SetInputMode(1); //Data is retrieved through the input property as binary.

5. Set some key parameters, such as Baud rate etc.

   Example: SetSettings("9600,n,8,1"); // Baud rate: 9600 Hz, No Parity, 8: Data Bits, 1: Stop Bit;

6. Set the number of characters to receive before setting the CommEvent property to comEvReceive and generating the OnComm event;

   Example: SetRThreshold(1);

7. Set the number of characters of the Input property allowed to be read from the receive buffer.

   Example SetInputLen(0);

8. Read buffer and clean out residual data.

   Example: GetInput();

9. Send data out.

   Example: SetOutput(COleVariant("TEST"));

The designed frequency sent to the signal generator was achieved from the analyzed software for stability detection of flame. Assume the first channel of TGA1244 is required to generate a set of SINE signal with the designed frequency $10Hz$ and amplitude $\pm 5V$, the code can be written as:

CMSComm m_com;

```
m_com.SetCommPort(1);
m_com.SetOutBufferSize(512);
if(!m_com.GetPortOpen())
    m_com.SetPortOpen(TRUE);
m_com.SetInputMode(1);
m_com.SetSettings("9600, n, 8, 1");
m_com.SetRThreshold(1);
m_com.SetInputLen(0);
m_com.GetInput();
m_com.SetOutput(COleVariant("SETUPCH <1>"));
m_com.SetOutput(COleVariant("WAVE <SINE>"));
m_com.SetOutput(COleVariant("AMPL <5>"));
m_com.SetOutput(COleVariant("WAVFREQ <10>"));
m_com.SetOutput(COleVariant(0x0AH)); //send the command terminator code
```

3.2.2 Burner Unit

As illustrated in Figure 3-1, the burner system consists of a fuel supply sub-system and a transparent cylindrical tube (combustion chamber). The cylindrical tube has a length of 0.755m and an inner diameter of 0.125m. The chamber is made of transparent material with a wall thickness of 2.5mm. It is supported by a thin sheet steel cowl with a height of 37.5cm. The diffusion jet flame has a negligible effect on the chamber wall because of the relatively large cross-section of the chamber. Propane fuel (C_3H_8) is supplied from a compressed gas cylinder at initial flow rates of 40 ml/min which is measured by a rotameter and regulated by a control valve. The burner is a single copper pipe with an inner diameter of 5mm. There is an orifice at the end of the pipe, which reduces the overall inner diameter to 1.8mm. The Reynolds number is 160 based on the fuel flow rate and pipe diameter. Therefore the fuel jet is laminar in nature without disturbance. The burner fuel nozzle position relative to the cylindrical tube can

be adjusted automatically by using a computer controllable traverse system as shown in Figure 3-1. The traversing speed can be varied from 1mm/s to 15mm/s along the tube. The system can make movement in three dimensional ways, X, Y and Z. But in current study, only Z direction (up and down direction) is used to change the relative height between the nozzle and the bottom of the cylindrical tube. It has been arranged in such a way, that the fuel nozzle is fixed and the cylindrical tube can be moved relative to the fuel nozzle by moving the traverse system in Z direction. Therefore, the relative height of the nozzle and the bottom of the tube can be changed, in other words, the distance of the flame to the acoustic source is changeable, and the results based on different heights can be achieved and compared. Because the nozzle and measurement probe is relatively stable, the disturbance to the nozzle and the measurement probes is reduced.

As discussed in previous section, a loudspeaker, driven by a signal generator that produced an electric periodic sine wave with adjustable frequency, amplitude, and phase, was mounted under the cylindrical tube to serve as the external acoustic source to produce the external acoustic excitation for the tube burner. A PC was used to send control commands for the signal generator. The signal is amplified by a power amplifier firstly and then transmitted to the loudspeaker finally. As shown in Figure 3-1, a photomultiplier was applied to collect the CH^* chemiluminescence signal of the diffusion flame; A high-speed digital camera was used to acquire the high-speed sequence of 2D images of the flame; A hot wire anemometer adhered to the nozzle was applied for the velocity fluctuation measurement; A microphone attached to the nozzle was used to collect the acoustic signal around the flame nozzle in the cylindrical tube burner.

It is very important to learn knowledge of acoustic properties of the tube burner for studying the influence of acoustic waves on diffusion flames. By use the equations (equation (2-7) to (2-10)) introduced in the section 2.2.1, the acoustic resonance frequency of the cylindrical tube can then be calculated. There are two typical types of tubes, one of which is the open tube and the other is the closed tube. The cylindrical tube applied in this study is one end open and the other end

"acoustically" seal but air tight. So, this cylindrical tube can't be taken as an open tube or closed tube just from its appearance.

If the tube is considered as an open tube, then the tube resonance frequency should be calculated as:

$$f = \frac{n\times 343}{2\times\left((0.755+0.375)+0.8*0.125\right)} = n \times 139.43(Hz) \quad \textbf{(3-1)}$$

$$(n = 1,2, \dots \dots . N)$$

But if the tube is reckoned as a closed tube, then the tube resonance frequency should be calculated by:

$$f = \frac{n\times 343}{4\left((0.755+0.375)+0.4*0.125\right)} = n \times 72.67(Hz) \quad \textbf{(3-2)}$$

$$(n = 1,3,5, \dots \dots .2N - 1)$$

Farhat [25] proved that the resonance frequency of the tube is 75Hz by lots of experiments. Therefore, it is deduced that the tube burner in this experiments is more like a closed tube, even though the steel cowl is just "acoustically" sealed with transparent cylindrical tube.

3.2.3 Measurement Unit

In this research, there are four methods of measurement applied in the experiments. They are chemiluminescence emission measurement that measures the CH^* chemiluminescence signal of the diffusion flame using the optical system and photomultiplier; hot-wire anemometry unit that measures the air flow velocity around the flame, high-speed digital camera that takes high-speed sequence of 2D images of the flame and microphone that measures the acoustic signal in the tube.

3.2.3.1 Chemiluminescence Emission Measurement

The bifurcated fiber optical system used for the simultaneous measurement of chemical species can be illustrated by Figure 3-7, which consists of focusing lens, fiber optic cables, monochromatic filters and photomultiplier tubes (PMTs), for

the sensing of light emissions at two chosen wavelengths simultaneously. It can collect an integrated light signal originating from all of the flame. The intensity of the light is converted into voltage signals. Outputs from the photomultipliers were displayed and stored in the work station. An A/D card named PCI1711, a software developed based on VC++, Matlab and the Origin 6.0 were employed for data acquisition, monitoring and analyses.

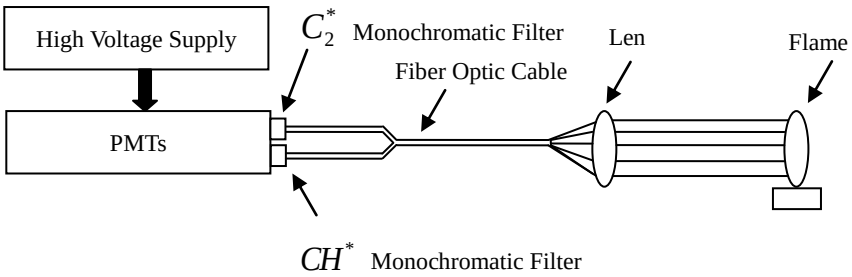

Figure 3-7: Schematic diagram of the optical system

Flame emissions from excited species need to be collected, transferred, filtered and then measured. A lens system is used to collect the chemiluminescence by imaging the flame onto a fiber optic cable, which transmits the light signals. Two equal channels of light signals of the same intensity from the same image volume are guided to two photomultiplier tubes that measure the intensity of chemiluminescence. The filtering of the light collected from the flame is performed using CH^* and C_2^* monochromatic interference filters. A fiber optic cable is used for the transmission of the light signal. This setup can measure the summation of the soot light and chemiluminescence emissions of CH^* and C_2^* at the two chosen wavelengths for a diffusion jet flame. Some key components of this measurement are discussed as follow.

1. Focusing Lens

   A focusing lens is an optical device with axial symmetry which transmits and refracts light. By using a converging lens, the flame is focused to an image at the focal point where the optical fibre is positioned.

2. Monochromatic Filters

   The monochromatic filters only allow a narrow range of wavelengths to

pass. Two narrow band interference filters, CH^* at wavelength of 430±5nm and C_2^* at wavelength of 516±2.5nm were used in the experiments (as shown in Figure 3-8). The chemiluminescence emissions of two active radicals (CH^* and C_2^*) of a diffusion flame can be measured using monochromatic filters together with photomultiplier-tubes and data acquisition system. These measurements can provide spatial information of flame intensity.

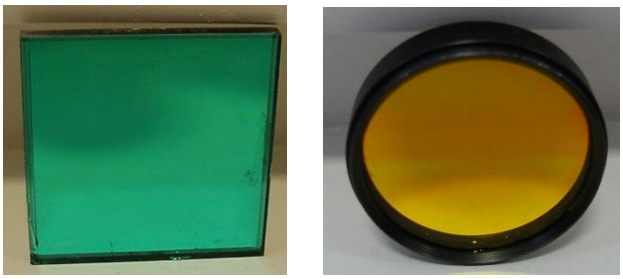

Figure 3-8: Monochromatic filters

3. PMTs

PMTs, which convert incident light flux to a linearly proportional current, are extremely sensitive detectors of light in the ultraviolet, visible and near infrared region. They are constructed from a glass vacuum tube, which houses a photocathode, several dynodes, and an anode (as shown in Figure 3-9) [38]. The photocathode of PMTs collects incoming photons and emits electrons in direct proportion to the incoming light flux. The emitted electrons impact the first dynode stage, with the dynode acting as an electron multiplier to emit multiple electrons for each incident electron. After several dynode stages, the electron flux can then be amplified to the extent so that a current can be measured. These detectors multiply the signal produced by incident light by as much as 10^8, from which single photons can be resolved.

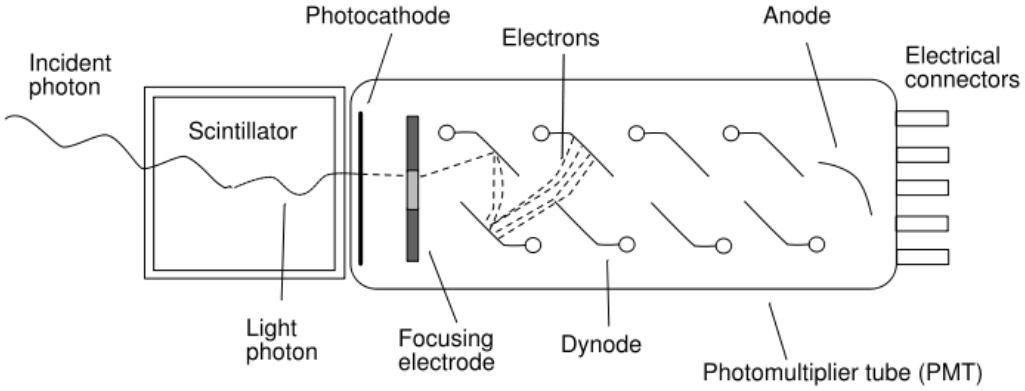

Figure 3-9: Schematic of a photomultiplier tube coupled to a scintillator [38]

Two PMTs (ORIEL model 70704) with two monochromatic filters (CH^* and C_2^*) placed in front of each tube were used in this study, but only CH^*signal is collected. A voltage supply of 0-2000volts ensured the proper operation of PMTs. The PMTs are however plagued by 'dark-noise', which results from the spontaneous emission of electrons by the photocathode or any of the dynode stages. Dark-noise is a strong function of the excitation voltage used in the PMT. The higher the applied voltage, the more sensitive the PMT, but also the more dark-noise is observed in the resulting current signal.

Care is required to be taken to make sure that the PMTs are working in the linear region of signal outputs versus the applied high voltage. While powered, photomultipliers were shielded from ambient light to prevent their destruction through over-excitation.

Output from the PMTs, which is the voltage signals converted from the intensity of the flame, were displaced and stored in a PC.

3.2.3.2 Air Flow Measurement

In this study in order to measure the velocity of the air around the flame, the hot-wire anemometry will refer to the use of a small, electrically heated element exposed to the air. Since the air fluid velocity is sensitive to heat transfer between the element and its environment, changes of temperature and

composition can also be sensed. In the experimental setup of this research, Constant Temperature Anemometer (CTA) is applied, as shown in Figure 3-10. It works based on the fact that the probe's resistance is proportional to the temperature of the hot wire, maintaining a constant resistance R of the probe means that its temperature is also kept constant.

By modifying the adjustable resistor, the bridge is essentially balanced at a certain condition. It is necessary to balance the bridge before operation, also for very start up of the bridge. Due to an increase in heat transfer causing a fall in temperature, it can be seen that a reduction in the resistance of the probe will cause the bridge to become unbalanced. This change will introduce a positive error voltage at the input of the servo amplifier. After considerable amplification, the signal from the amplifier increases the bridge voltage and also the current through the sensor, so that the sensor is heated and the bridge balance is restored. In this way the probe temperature is kept essentially constant and the effect of the thermal inertia of the probe is minimized. Since the amplifier has a very high gain and the probe is very small, the anemometer is able to respond to very rapid fluctuations in fluid velocity. And the faster the fluid flows, the higher the bridge voltage is.

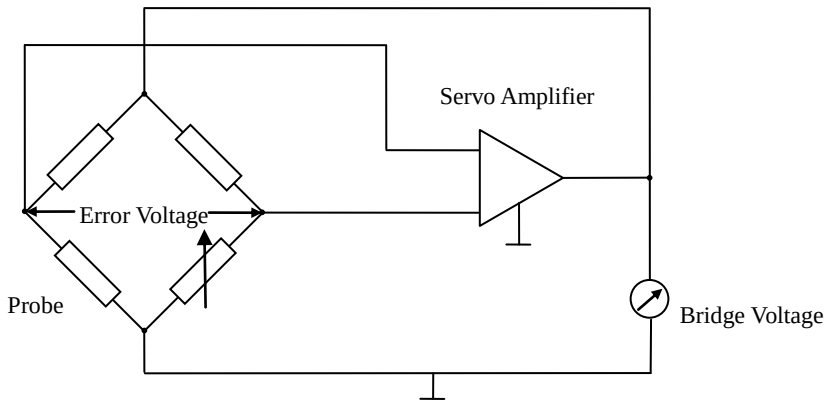

Figure 3-10: Basic bridge circuit for CTA

As shown in Figure 3-1, the hot-wire probe is stuck to the nozzle of the cylindrical tube to measure the fluctuation of the fluid velocity when using different frequency acoustic excites the combustion chamber.

3.2.3.3 High Speed Imaging Setup

In order to obtain flame dynamics, a high-speed digital camera, FASTCAM-Ultima APX, was applied to obtain 2D images of the visible flame. The camera operates at up to 2000 frames per second with full resolution. The APX system consists of a processor, camera head, remote-control keypad and control software. Table 3-4 briefly lists the specification of the camera.

Table 3-4: FASTCAM-Ultima APX high speed camera specifications

Imaging Sensor	C-MOS Imaging Sensor
Sensor Resolution	1024×1024 Pixels
Frame Rates	Up to 2000 FPS, full resolution
Shutter Speed	1/250,000 to 1/60 seconds
Lens Mount	F Mount; C Mount; Hi-G Mount
Shutter	Electronic Shutter
Recording Media	IC Memory
Memory Capacity	2.6GB Standard
Image Output Customization	Built-in Customizable LUT
Trigger Signal Input	TTL, Contact
External Controls	Remote Keypad, RS422 External control Interface

3.2.3.4 Acoustic Measurement

Microphone is a most popular instrument for acoustic measurement. It is an acoustic-to-electric transducer or sensor that converts sound into an electrical signal. Most microphones use electromagnetic induction (dynamic microphone), capacitance change (condenser microphone), piezoelectric generation, or light modulation to produce an electrical voltage signal from mechanical vibration. As shown in Figure 3-1, the microphone is adhered to the nozzle to sensor the acoustic signal. The collected acoustic signal is sent to the power amplifier to

make it strong enough to be collected by the data acquisition card and the work station then compares it with the generated acoustic signal frequency to generate the control command.

3.2.4 Data Acquisition Unit

A data acquisition system was applied to record the CH^* chemiluminescence emissions, acoustic pressure, and hot-wire signal. The system is based on a personal computer Pentium III and a National Instrument DAQ card (PCI1711, Figure 3-11) and a software developed in Visual C++ have been applied for data acquisition, monitoring and analyses. The specifications of the DAQ card are shown in Table 3-5.

Figure 3-11: PCI1711 data acquisition card

Table 3-5: Specifications of PCI1711

A/D Channels Input	16 Single-Ended	
A/D Resolution Input	12-bit	
Sampling Rate of A/D Input	100 KS/s max	
Input Rages	Software Programmable： $\pm 10V$, $\pm 5V$, $\pm 2.5V$, $\pm 1.25V$, $\pm 0.625V$	
D/A Channels Output	2	
D/A Resolution Output	12-bit	
Sampling Rage of D/A Output	38 KS/s min	
Output Range	Internal Reference	0 ~ +5 V, 0 ~ +10 V
	External Reference	0 ~ +x V @ -x V (-10 ≤ x ≤ 10)
Application Software Support	VC++, VB, C++ Builder and Delphi.	

3.3 Uncertainties of Measurement

Chemiluminescence Emissions Measurements

The chemiluminescence emission measurements carried out in this experimental investigation have been supported by the idea of observing the heat release variations in the combustion chamber. The chemiluminescence signal from the photomultipliers is a global estimate of CH^*. The light emissions from the burner are focused on a single point of the fibre optic cable by the help of suitable lens. In this way, the measurement setup yields only the overall measure of chemiluminescence emissions from combustion zone and no local area analyses are available.

High speed imaging

The high speed imaging technique also involves approximation. The images of

the flame are actually the optical integration of a 3D flame into a two dimensional image sensor. For this reason the data from captured by the high speed camera has not been referred to as quantitative. In fact the term semi-quantitative has been used, as the database still provides good spatial and temporal resolutions to observe combustion phenomena. If the volume of the combustion zone is taken into account then the instantaneous light intensity from the combustion zone can be expressed as:

$$I_{vis} = \varepsilon \int \int \int \int I(x,y,z)dxdydzdT \quad (3\text{-}3)$$

where I_{vis} denotes the visible light intensity, ε denotes the efficiency of the optical system of the high speed camera, I denotes the light intensity; x, y and z denote the flame physical position, V denotes the three dimensional space for flame and T denotes the exposure or gating time.

When viewed in form of an image or two-dimensional array of pixels, this visible light can be described as:

$$I_{vis} = \varepsilon \int \int \int I(x,y)dxdydT \quad (3\text{-}4)$$

Assume A denotes the two dimensional area of flame. In order to obtain a single value of light intensity, the intensities of all pixels in A (x and y directions) are further added by using Equation (3-4). In this way the sequence of images captured over a span of time shapes up in the form of a discrete signal which possesses a discrete value of overall luminosity or mean pixel intensity for a discrete value of time.

Besides the approximation in capturing light intensity, there are some other uncertainties involved in data acquisition using a digital camera.

For example, aberrations in the lens can curve a perfect line in real world on the four corners of the image, and meanwhile the speed of shutter can dramatically affect the profile of the flame. The image captured in a camera can be viewed as an overlay during the opening time of the shutter, which is the reason why a slow shutter speed can make the flame size bigger, especially for an unstable flame. However, if the shutter speed is too fast, the exposure time could be not long enough to form a clear picture, which calls underexposure. The errors generated

by exposure are inevitable, as there is always a trade off between image brightness and sharpness. It often needs lots of test and rich experience to achieve the best observations. There are some other factors that are out of control, such as dithering of the camera, calibration of colour and veracity of focus etc.

3.4 Summary

The experimental setup and corresponding measurement techniques provide an opportunity to conduct qualitative and quantitative measurements of flame parameters. The measurement of CH^* chemiluminescence signal and the 2D flame images taken by the high speed digital camera provide useful information for analysing the flame dynamics and flame spatial characterises. In order to provide accurate measurement, the data acquisition system based on personal computer Pentium III and a National Instrument DAQ card is employed, and a programme developed in VC++ has been used for online collecting data.

By applying different frequency and intensity acoustic excitation to the jet diffusion flame, some interesting phenomena have been observed. In next two chapters, by applying mathematical methods and image processing techniques, the collected data are analysed and some encouraging results are discussed.

Chapter 4

Investigation of Flame Dynamics in Frequency Domain

This chapter presents results of the influence of the external acoustic excitation on the flame dynamics. By using different processing methods, some interesting results are revealed.

4.1 Introduction

Low frequency flame oscillations, known as the flame flicker, have been well observed in real life and experiments. The flicker frequency observed in diffusion flames and partially premixed flames is typically in the range from 10 to 20Hz. As discussed in Chapter 2, two different vortices have been identified in jet diffusion flames: small roll-up vortices inside the luminous flame and large toroidal vortices outside the luminous flame. The small vortices are due to Kelvin-Helmholtz instability of the jet, and the toroidal vortices outside the luminous flame are caused by the buoyancy driven instability.

Besides Kelvin-Helmholtz instabilities and buoyancy driven instabilities, thermoacoustic instability phenomenon also exists due to the interaction between the self-excited acoustic pressure and heat release rate in the combustor. The interaction between acoustic waves and diffusion flames has attracted more and

more investigations in past years because it may damage combustors especially for an advanced low emission combustor. Thermoacoustic instability establishes when the acoustics of the system generates a feedback mechanism between fluctuations of pressure and heat release rate. The acoustic signal generated in the combustion chamber modulates fuel feeding and changes local fuel-air ratio, thus making heat release unsteady, which are the disadvantages of the interaction between acoustic waves and diffusion flames. On the other hand, the interaction between acoustic waves and diffusion flames can be used as a method to monitor the combustion process and control the combustion instability. It has been found that the flame's dynamics can be changed when using an external acoustic source to disturb the flame. The flame is only sensitive to a few frequencies within a limited range, instead of all acoustic wave frequencies. Some acoustic excitation has a very strong impact on the flame flickering frequency. At some excitation frequencies, the flame flickering frequency disappears, which means the flame is relatively stable in this situation; at some excitation frequencies, the flame becomes very unstable and even blows out; and at some other excitation frequencies, no significant change of the flame behavior has been observed. Therefore, the external acoustic excitation can change the dominant combustion instability mode. In some cases, the thermoacoustic instability takes over the buoyancy-driven instability, and in other cases, the thermoacoustic instability surpasses the buoyancy-driven instability.

Moreover, there are many other kinds of instability occur in the combustion process. But in this research, only three instabilities, as shown in Figure 4-1 were studied. All of them are dependent on each other. The thermoacoustic instability is a not a self-excited instability but generated by an external acoustic source.

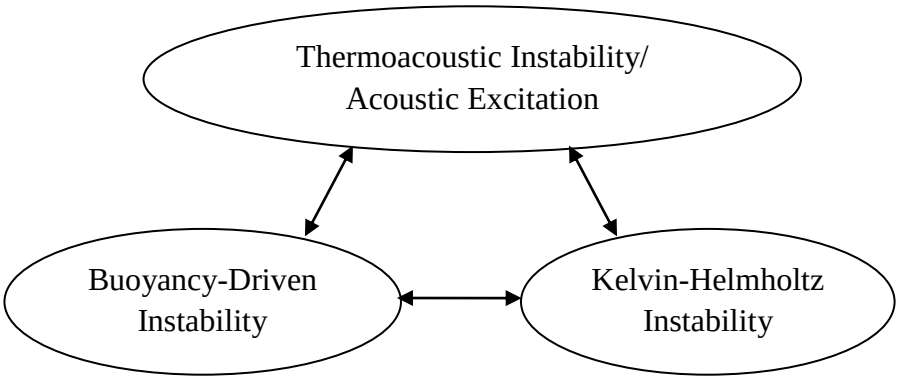

Figure 4-1: Three instabilities in the tube burner

A loudspeaker described in the experimental setup, as described in Chapter 3, was employed as the external acoustic source for the cylindrical tube burner. By applying programming controlled signal from a controllable signal generator, the loudspeaker generates different frequency acoustic waves to excite the flame. Sound can be classified as infrasound, sound that can be heard by human ear and ultrasound. Infrasound is a kind of sound with a frequency too low to be heard by human ear covering sounds beneath the lowest limits of human hearing (20Hz) down to 0.001Hz. The effects of both infrasound and sound on the flame dynamics are investigated in this chapter. This chapter also provides a detailed analysis of the frequency domain characteristics of the measured signal for different combustion observables: CH^* chemiluminescence signal and hot-wire anemometry data, and some interesting results have been achieved.

4.2 FFT Methods

In mathematics, the Fourier Transform (FT) is an operation that transforms one complex-valued function of a real variable into another function. In signal processing, the original mathematical function is typically in time domain and the new mathematical function is in frequency domain. Hence FT is often called the frequency domain representation of the original function. There are several conventions for defining the FT of an integral function $f: R \to C$ (Kaiser, Gerald (1994),). This research uses the definition of:

$$\hat{f}(v) = \int_{-\infty}^{\infty} f(t) e^{-2\pi i t v} dt, \text{ for every real number } v \quad \textbf{(4-1)}$$

where $f(t)$ is the original function in time domain and $\hat{f}(v)$ is the new function in frequency domain. The independent variable t represents time and the transform variable v represents frequency. The inverse transform form can be expressed as the equation:

$$f(t) = \int_{-\infty}^{\infty} \hat{f}(v) e^{2\pi i t v} dv, \text{ for every real number } t \quad \textbf{(4-2)}$$

Now consider generalization to the case of a discrete function, $f(t) \to f(t_k)$ by letting $f_k \equiv f(t_k)$, where $t_k \equiv k\Delta$, with $k = 0, \ldots, N-1$. The Discrete Fourier transform (DFT) can be represented by the equation:

$$F_n = \sum_{k=0}^{N-1} f_k e^{-2\pi i n k/N} \quad \textbf{(4-3)}$$

The inverse transform then can be written as the equation:

$$f_k = \frac{1}{N} \sum_{n=0}^{N-1} F_n e^{2\pi i k n/N} \quad \textbf{(4-4)}$$

DFT is extremely useful because they reveal periodicities in input data as well as the relative strengths of any periodic component.

However, as we can notice from the above equations, DFT is very time consuming. To compute a DFT of N points, it has to take $O(N^2)$ arithmetical operations, which often leads to unfeasible for a large value of N. Hence to solve this problem, a Fast Fourier Transform (FFT) algorithm was developed to compute the DFT and its inverse transform, which can produce exactly the same results but much faster speed: only $O(N \log N)$ operations for N points. [36]

FFT was first discussed by Cooley and Tukey (1965). The basic idea is to break up a transform of length N into two transforms of length $N/2$ using the identity equation of:

$$F_n = \sum_{k=0}^{N-1} f_k e^{-\frac{2\pi i n k}{N}} = \sum_{k=0}^{\frac{N}{2}-1} f_{2k} e^{-2\pi i (2k) n/N} + \sum_{k=0}^{\frac{N}{2}-1} f_{2k+1} e^{-2\pi i (2k+1) n/N} \quad \textbf{(4-5)}$$

In practice, there are two basic problems: one fact is that we can only measure the signal for a limited time; and the other fact is that the FFT only calculates

results for certain discrete frequency values, 2^N. If the number of the sampled data is not exactly 2^N, the data in the data set are necessary to be added or deleted to be 2^N. Traditionally, a window is always employed to pre-process the original function. There are many kinds of windows that are commonly used, such as Rectangular, Triangular, Hanning, Hamming, Poisson, Cauchy, Guassian, Kaiser-Bessel, Parzen, Welch and Sine etc. The choice of window type can be variable in terms of different applications. Next part introduces some popular windows for mechanical researches.

In signal processing, in order to smooth or shape the resulting spectrum and reduce spectral leakage, a window function that is multiplied by the signal (data segment) is mainly used before computing the FFT spectrum of the signal. The window function is a function that is zero-valued outside of the chosen interval. For instance, a rectangular window function is a function that is constant inside the interval and zero elsewhere, which is describe by the shape of its graphical representation. When another function or a signal (data) is multiplied by the rectangular window function, the product is also zero-valued outside the interval. A more general definition of window functions does not require them to be identically zero outside an interval, as long as the product of the window times its argument is square integral, which means that the function goes sufficiently rapidly toward zero. In mechanical research, rectangular window, Hanning window and Hamming window are three most popular windows, which are introduced in the following part.

Assume N represents the width, in samples, of a discrete-time window function. Three types of window can be represented by the following equations.

1. Rectangular Window

$$w(k) = 1, for\ k = 0,1, \ldots\ldots, N-1 \qquad \textbf{(4-6)}$$

2. Hanning Window

$$w(k) = \frac{1}{2}\left(1 - \cos\left(\frac{2\pi k}{N-1}\right)\right), for\ k = 0,1, \ldots\ldots, N-1 \qquad \textbf{(4-7)}$$

3. Hamming Window

$$w(k) = 0.54 - 0.46\cos\left(\frac{2\pi k}{N-1}\right), for\ k = 0,1,\ldots\ldots,N-1 \qquad \textbf{(4-8)}$$

4.3 Results and Discussion based on CH^* Chemiluminescence Data

Chemiluminescence is the generation of electromagnetic radiation as light by the release of energy from a chemical reaction. The radiation can, in principle, be emitted in the ultraviolet, visible or infrared region. Those emitting visible lights are the most commonly observed. They are very useful information for combustion instability analysis.

Chapter 2 has presented the idea of using chemiluminescence in flame dynamic measurements and analysis, which was explored since early 70s last century. A quantitative measurement of dynamic heat-release rate is important in combustion instability research. The optical system, described in the experimental setup (as introduced in Chapter 3), detected, collected, transported, filtered and then measured light emitted from the diffusion jet flame. In this research, for measurements of the heat-release rate oscillation, light at wavelength of 430 ± 5 nm, which is called CH^*, was studied. The radiation of the CH^* comes only from the reaction zone. And it is assumed that, for a mixture of fixed composition of the total light intensity for CH^* is proportional to the actual surface area of the flame front and heat release rate. The frequency of CH^* radiations can be taken as the heat-release oscillation frequency and the flame oscillation frequency, flickering frequency, as well. It should be pointed out that the CH^* signal is polluted by the soot broadband emission but this does not affect the analysis in this investigation because only the dynamics of the signal is of interest.

Figure 4-2 and Figure 4-3 demonstrate the time series and corresponding Power Spectral Density (PSD) distribution of the flame signal in normal condition collected by the photomultiplier, at the experimental condition that the fuel

nozzle at the height of 13.5cm from the tube bottom and the fuel flow rate at 40ml/min. The PSD distribution of CH^* clearly shows that the flame flicker frequency is 12.45Hz. The harmonic frequencies of the flame flickering were also observed at the frequency of 24.89Hz and 37.05Hz. This observation indicates that the flame flickering has a clearly defined periodicity, and the flame flickering frequency can be quantitatively determined as the first peak in the PSD, which is 12.45Hz. But the flame flickering frequency of the flame can change dramatically when an external acoustic excitation is applied in the experiment. The level of interference is significantly related to the excitation frequency that is demonstrated by following observations..

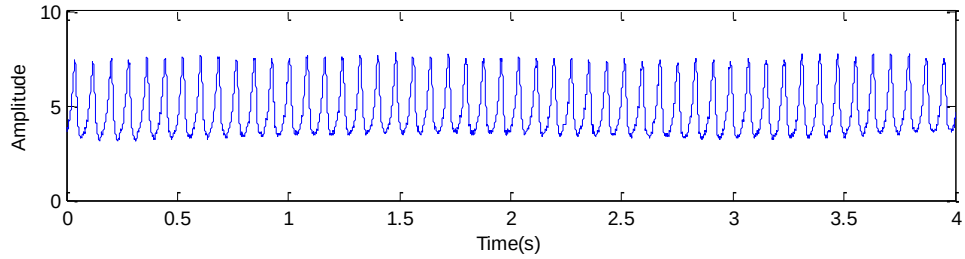

Figure 4-2: Time series of $\boldsymbol{CH^*}$ chemiluminescence without acoustic excitation

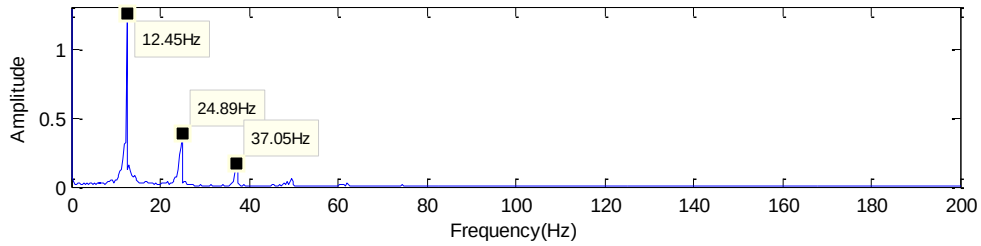

Figure 4-3: PSD of $\boldsymbol{CH^*}$ chemiluminescence without acoustic excitation

It was found that variation in the flame shape was observed when the fuel gas flow rate is gradually increased. When fuel gas discharges at velocities below a critical value from the nozzle into stagnant air surroundings, the flow of gas is laminar and the mixing of gas and air occurs by molecular diffusion in the flame surface. As the nozzle velocity increases, the length of flame increases until a critical velocity is reached and the tip of the flame becomes unsteady and begins to flutter. Following further increment of the flow rate, the unsteadiness develops into a noisy turbulent brush of flame starting at a definite point along the flame

where breakdown of laminar flow occurs and a turbulent jet develops. Furthermore the flame breakpoint moves toward the nozzle, which results in a reduced flame length. When the breakpoint approaches very close to the nozzle, the fully developed turbulent flame condition is reached. Further increment of the fuel flow rate has practically no effect on flame length, but flame noise continues to increase and flame luminosity continues to decrease. The flame finally blows off the nozzle at a certain velocity [5]. Since this research aims to study the influence of external acoustic excitation on the flame, all experiments were carried out with the fuel flow rate maintained at a constant value of 40ml/min by re-adjusting the fuel control valve.

By changing the power amplifier gain (PMG), the flame experiences different acoustic intensities. It was observed that the intensity of acoustic wave has strong influence on the flame dynamics. For high intensity acoustic wave at a low frequency, it is difficult to establish a flame. In order to study the acoustic effects at a wider frequency band, two test cases were conducted. Test Case 1 aims to investigate the influence of acoustic wave at a low frequency (<80Hz), especially the effects of infrasound on flame dynamics. Test Case 2 examines the acoustic effects on the flame dynamics at a frequency higher than 100Hz but lower than 300Hz.

4.3.1 Test Case One

In this test case, the nozzle height was at 13.5cm from the tube bottom. The PMG was set at -12db. The applied voltage to the signal generator was set at 2V, and the fuel flow rate was at 40ml/min. All parameters listed above were fixed during experiments to provide a consistent environment.

The main objective of this case is to reveal the influence of external infrasound excitation on the diffusion flame dynamics. Very few researches have been studied on this aspect. In this research, some very interesting results have been found. For example, in a very limited range of frequency of excitation acoustic

wave, the half acoustic wave frequency was observed clearly in the power spectrum of CH^* chemiluminescence. The detailed observations related to the effect of the infrasound on the flame dynamics is discussed in this section. And they are analyzed based on the FFT of CH^* chemiluminescence signal.

Figure 4-4 describes the power spectrum of CH^* chemiluminescence, collected by a photomultiplier, at the frequency of 3Hz, 5Hz, 8Hz, 13Hz, 14Hz, 16Hz, 18Hz, 20Hz, 70Hz, 80Hz and 140Hz acoustic excitation respectively. The spectrums show varieties of characteristics. It can be noticed that the observed flickering frequency varies following the increment of frequency of the acoustic excitation. Details of results are presented below.

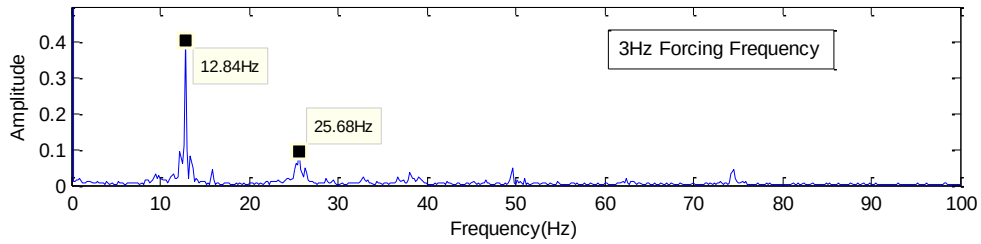

(a)

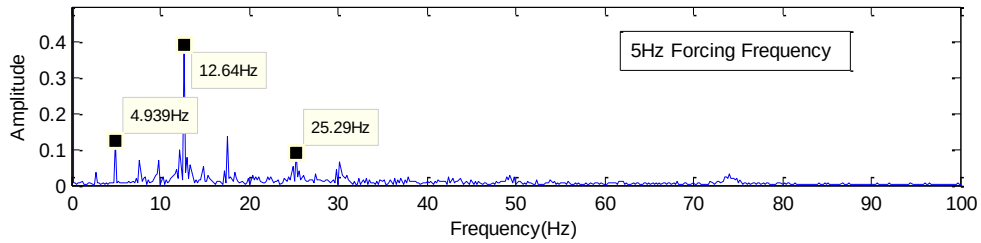

(b)

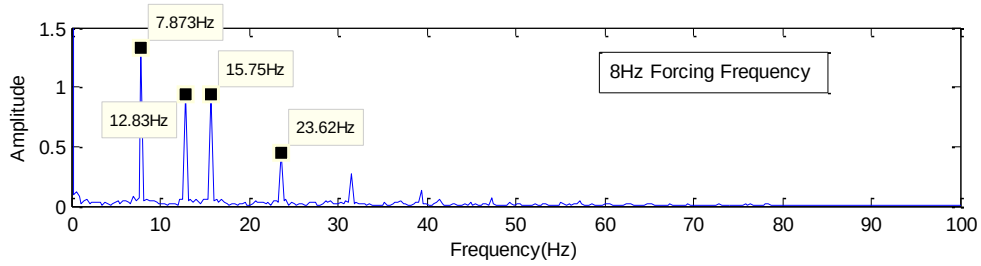

(c)

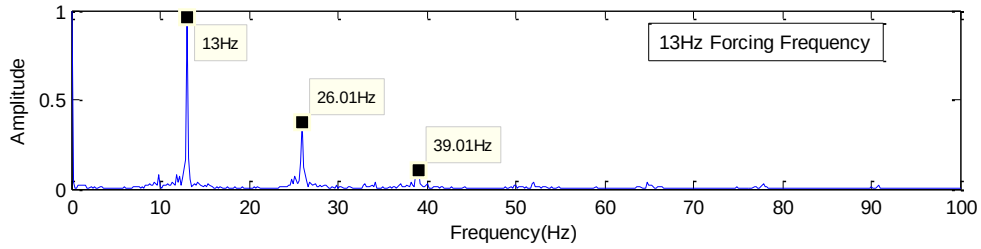
13Hz
26.01Hz
39.01Hz
13Hz Forcing Frequency
Amplitude
Frequency(Hz)

(d)

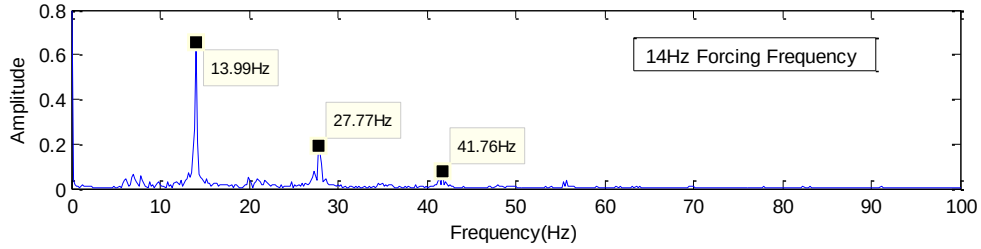
13.99Hz
27.77Hz
41.76Hz
14Hz Forcing Frequency
Amplitude
Frequency(Hz)

(e)

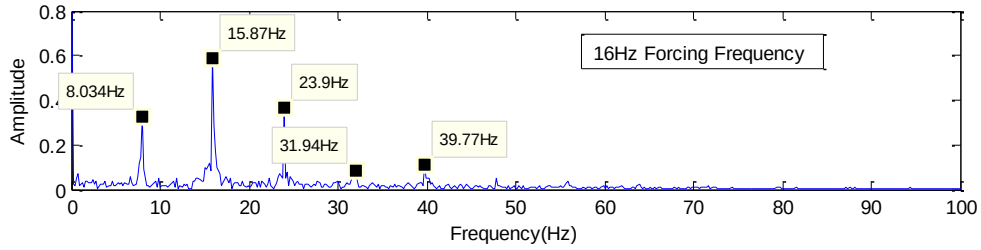
8.034Hz
15.87Hz
23.9Hz
31.94Hz
39.77Hz
16Hz Forcing Frequency
Amplitude
Frequency(Hz)

(f)

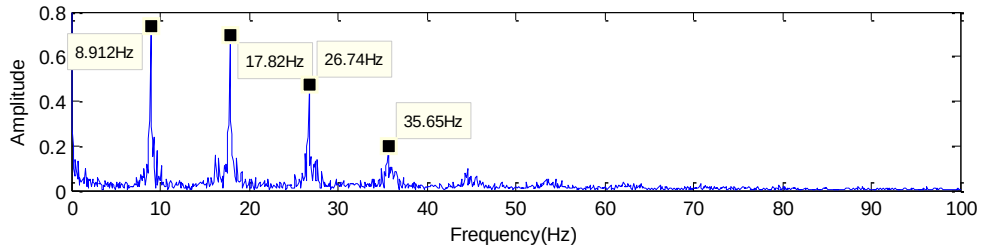
8.912Hz
17.82Hz
26.74Hz
35.65Hz
Amplitude
Frequency(Hz)

(g)

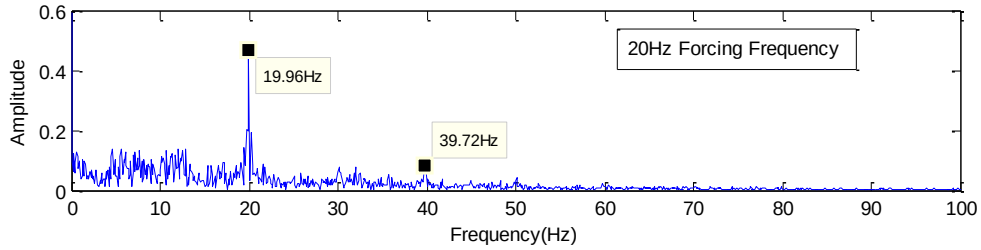
19.96Hz
39.72Hz
20Hz Forcing Frequency
Amplitude
Frequency(Hz)

(h)

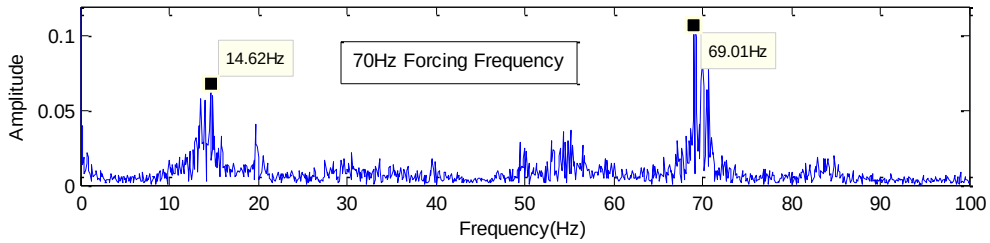

(i)

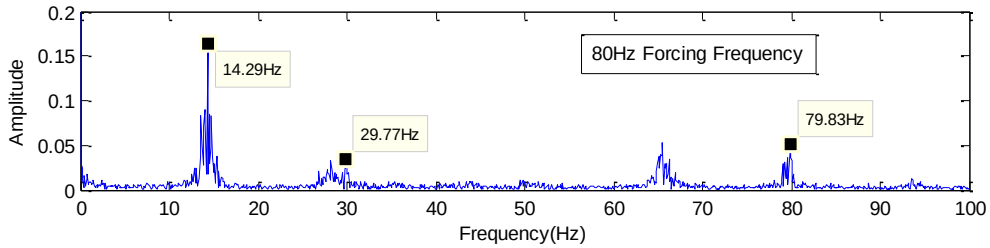

(j)

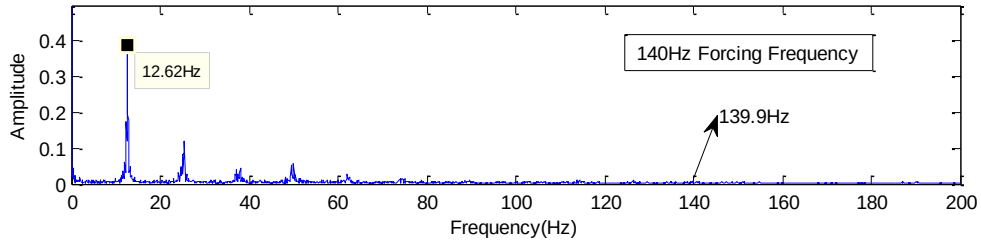

(k)

Figure 4-4: Power spectrum of $\boldsymbol{CH^*}$ with different frequency acoustic excitation (Case One)

1. For the frequency of acoustic excitation below 5 Hz (f_a<5 Hz)

   As it can be seen from Figure 4-4(a), with 3Hz acoustic excitation, the dominant frequency in the power spectrum of CH^* chemiluminescence is 12.84Hz, which is very similar to the flickering frequency under no excitation, which is 12.45Hz, as shown in Figure 4-3. Under such condition, the conclusion is that the acoustic excitation has little influence on the flame dynamics and the buoyancy-driven instability is dominant.

2. For the frequency of acoustic excitation between 5Hz and 8Hz ($5\text{Hz} \leq f_a < 8\text{Hz}$)

   Figure 4-4(b) shows the power spectrum of CH^* chemiluminescence with an acoustic excitation at 5Hz frequency, where the dominant frequency of CH^* signal is still 12.64Hz. The result is similar to the condition without

excitation, but the 5Hz frequency (4.939Hz) can be easily observed from the power spectrum. Under this condition, the acoustic excitation starts to have an impact on the flame but it is still not able to suppress the buoyancy-driven oscillation.

3. For the acoustic excitation at a frequency between 8Hz and 14Hz ($8\text{Hz} \leq f_a < 14\text{Hz}$)

   When the excitation frequency is increased to 8Hz (Figure 4-4(c) illustrates the power spectrum of CH^* chemiluminescence with 8Hz acoustic excitation and Figure 4-4(d) illustrates the power spectrum of CH^* chemiluminescence with 13Hz acoustic excitation), it was observed that the dominant frequency is the same as the excitation frequency (the dominant frequency is 7.873Hz and 13Hz respectively). The acoustic excitation has an impressive influence on the flame dynamics. The dominant frequency of CH^* signal follows the frequency of the acoustic excitation determinately. The acoustic excitation has taken over the buoyancy-driven instability and becomes the main controlling factor.

4. For the acoustic excitation at a frequency in the range of 14Hz and 20Hz ($14\text{Hz} \leq f_a < 20\text{Hz}$)

   Figure 4-4(e)-(g) shows the power spectrum of CH^* chemiluminescence with an acoustic excitation at frequency of 14Hz, 16Hz and 18Hz. It was observed that the dominant frequency of CH^* signal still follows the acoustic excitation frequency determinately (the dominant frequency is 13.99Hz, 15.87Hz and 17.82Hz respectively). Although the flickering frequency is not shown in the power spectrum, the dominant frequency is very close the typical flickering frequency (10-20Hz). Hence, under this condition, the conclusion is that the acoustic excitation has impressive influence on the flame dynamics and the acoustic excitation is the main controlling factor.

   A very interesting phenomenon which can be noticed here is that a peak frequency that is half value of the frequency of acoustic excitation

appears clearly in the power spectrum. This phenomenon is repeatable and not occasionally observed only. It has not been reported very much. Williams et al. [88] observed the half acoustic excitation frequency ($\frac{f_a}{2}$) in their experiments and found the sub-harmonic flame response is various for types of fuel and rate of fuel. It was reported that the methane flame has a much broader response function than the ethylene flame and also shows a $\frac{f_a}{4}$ response at low air flow rates. References [82][78] have reported similar phenomenon. However none of the work proposed an explanation to the phenomenon. It seems that the acoustic excitation at this frequency range has induced vortex merging at certain spatial location, which generates the half frequency mode because vortex merging is known to occur in flames [32].

5. For the excited acoustic at a frequency between 20Hz and 80Hz ($20\text{Hz} \leq \text{f}_\text{a} < 80\text{Hz}$)

   Figure 4-4(h) and (i) present the power spectrum of CH^* chemiluminescence under an acoustic excitation with the frequency 20Hz and 70Hz respectively, where the flame oscillation is still dominated by the acoustic excitation but the flame flickering frequency becomes visible (the dominant frequency is 19.96Hz and 69.01Hz respectively), especially for the case of 70Hz (Figure 4-4(i)). It can be deduced that under this condition the excitation acoustic has a less influence in the flame dynamics, and acoustic excitation is dominant but buoyancy-driven instability starts to take over.

6. When the frequency of acoustic excitation is above 80Hz($\text{f}_\text{a} \geq 80\text{Hz}$)

   When the frequency of acoustic excitation is set at 80Hz, the typical flame flickering frequency becomes dominant again though the excitation frequency still plays a role on the flame dynamics. Figure 4-4(j) and (k) illustrate the power spectrum of CH^* chemiluminescence under the acoustic excitation at frequency 80Hz and 140Hz respectively (the

dominant frequency is 14.29Hz and 12.62Hz respectively). The acoustic excitation frequency becomes vaguer in the power spectrum and the flame was observed disappeared eventually, which means that under this condition the buoyancy-driven instability becomes the main controlling factor for the flame instability again.

Table 4-1 lists the detected dominant frequencies (f_d) in the power spectrum of CH^* chemiluminescence at different acoustic excitation frequency in this test case. Figure 4-5 illustrates its tendency of change over frequency, where it was observed that the dominant peak frequencies of the flame flickering match the excitation frequency exactly from 8Hz to 70Hz, which leads to the conclusion that the acoustic excitation takes over the buoyancy-driven instability. Outside of this frequency range, the typical flame flickering frequency was observed, which concludes that the buoyancy-driven instability suppresses the acoustic excitation.

Table 4-1: Detected dominant frequencies $\boldsymbol{f_d}$ by $\boldsymbol{CH^*}$ chemiluminescence (Case One)

f_a	f_d	Detected $\frac{f_d}{2}$
No Excitation	12.48 Hz	None
3 Hz	12.84 Hz	N
5 Hz	12.84 Hz	N
8 Hz	7.87 Hz	N
13 Hz	13.00 Hz	N
14 Hz	13.99 Hz	Y
16 Hz	15.97 Hz	Y
18 Hz	17.82 Hz	Y
20 Hz	19.96 Hz	N
70 Hz	69.21 Hz	N
80 Hz	14.29 Hz	N
140 Hz	12.62 Hz	N

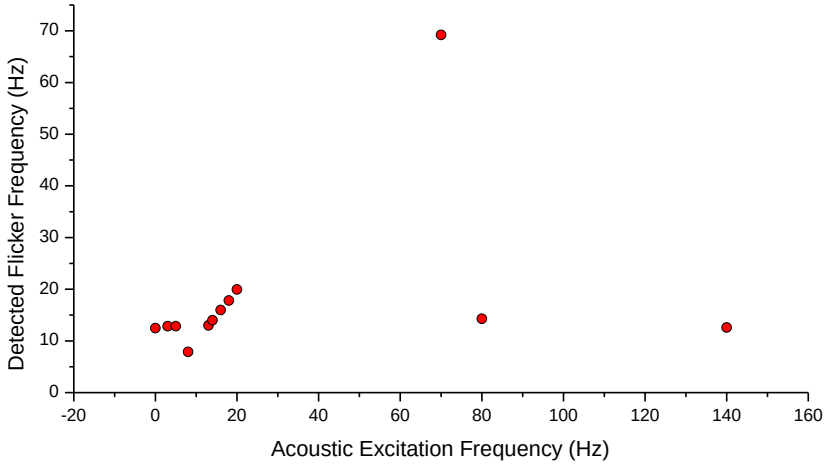

Figure 4-5: Illustration of the detected dominant frequencies f_d by CH^* chemiluminescence (Case One)

4.3.2 Test Case Two

This test case was conducted at a nozzle height of 13.5cm from the tube bottom. The PMG was set at -12db. The applied voltage to the signal generator was set at 5V (this parameter was different with that of the test case one, which was 2V), and the fuel flow rate was kept at 40ml/min. All parameters listed above were fixed during experiments to keep consistency of environment. It was observed that the flame blows out when the frequency of acoustic excitation was below 80Hz and above 210Hz, which exhibits very different results compared to the test case one (the detected frequency moves exactly the same as the excitation frequency from the acoustic forces at 8Hz to 70Hz). Moreover, it also has been observed that the flame becomes relatively stable when the frequency of acoustic excitation is at 120Hz, 130Hz, 140Hz, 150Hz and 170Hz.

As shown in Chapter 3 the calculated resonance frequency of the tube burner is 72.67Hz, which indicates that the third harmonic is 218.01Hz. These two figures are very similar to 80Hz and 210Hz. It therefore can be guessed that the flame was blows out because the excitation frequency is very close to the tube resonance frequency and its third harmonic. This conclusion needs to be further

proven.

Figure 4-6 shows the power spectrum of CH^* chemiluminescence under acoustic excitation at frequency 110Hz, 140Hz, 150Hz, 160Hz, 170Hz and 180Hz. There is always a peak frequency around 50Hz that exists in the power spectrum due to the electricity. It has been noticed that the dominant frequency is very close to the typical flame flickering frequency (10-20Hz). The frequency of the acoustic excitation frequency was also be found in these set of experiments, which can be explained by that both buoyancy-driven instability and thermoacoustic instability exists but the former contributes more than the latter in the flame dynamics.

Interestingly, the flame at the excitation frequency of 140Hz is observed to be very stable which is worth of further investigation. Figure 4-6(d) shows the power spectrum of CH^* chemiluminescence with acoustic excitation at the frequency 140Hz. It is noticed that only acoustic excitation frequency appears without other peak frequency (except for electricity signal), which can deduce that acoustic excitation suppresses buoyancy-driven instability at this excitation.

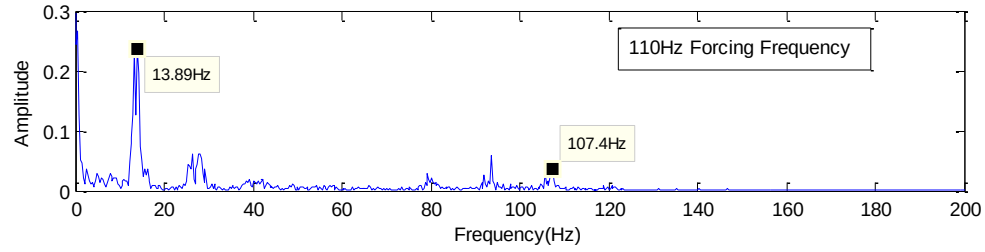

(a)

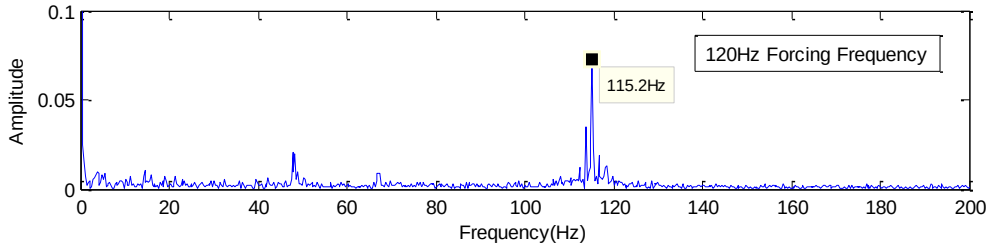

(b)

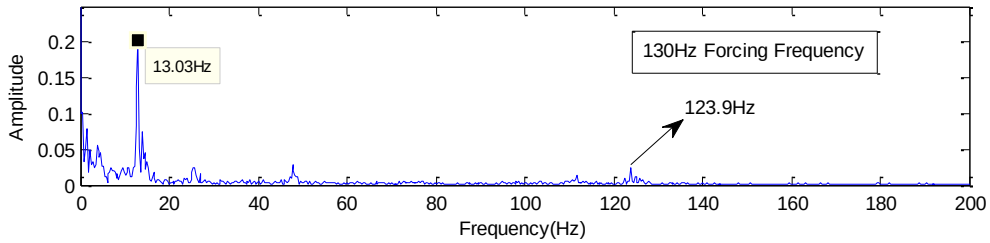
Amplitude
Frequency(Hz)
130Hz Forcing Frequency
13.03Hz
123.9Hz

(c)

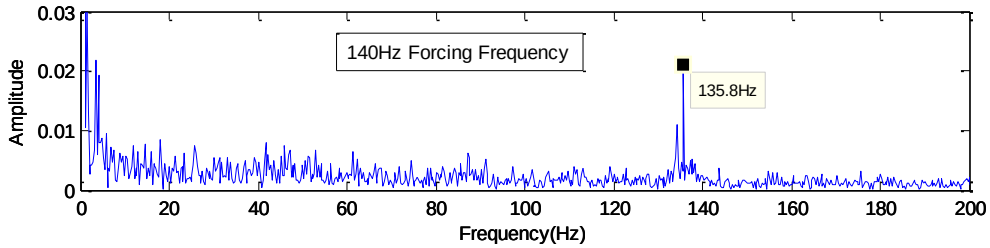
Amplitude
Frequency(Hz)
140Hz Forcing Frequency
135.8Hz

(d)

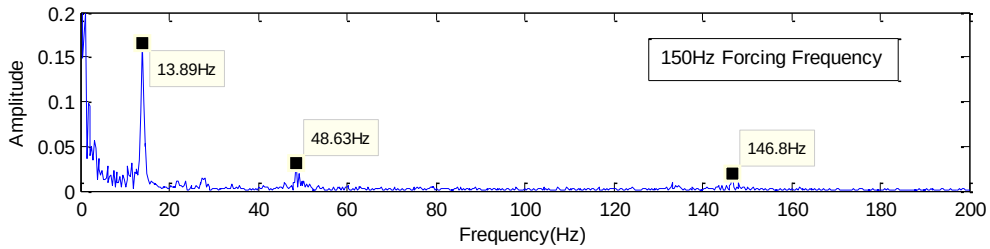
Amplitude
Frequency(Hz)
150Hz Forcing Frequency
13.89Hz
48.63Hz
146.8Hz

(e)

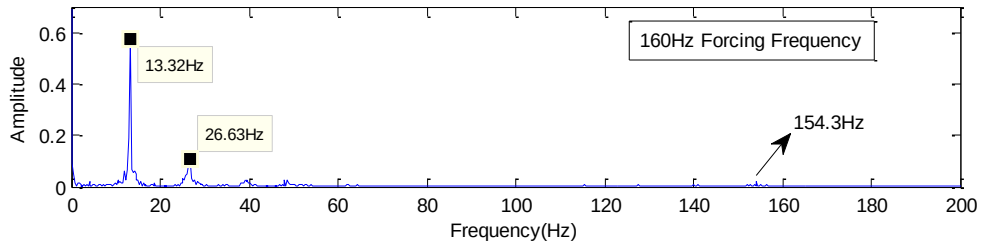
Amplitude
Frequency(Hz)
160Hz Forcing Frequency
13.32Hz
26.63Hz
154.3Hz

(f)

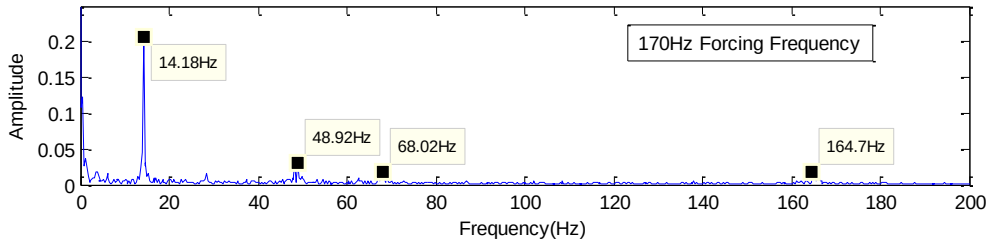
Amplitude
Frequency(Hz)
170Hz Forcing Frequency
14.18Hz
48.92Hz
68.02Hz
164.7Hz

(g)

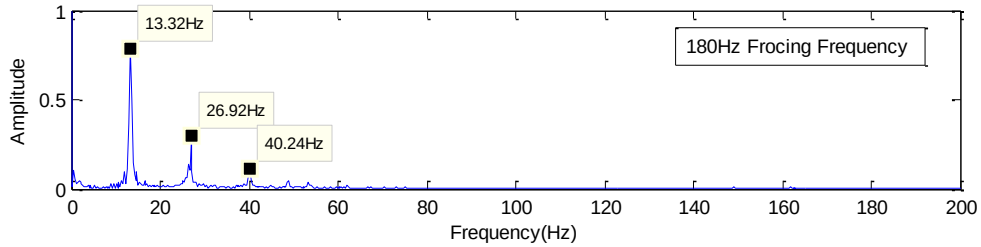

(h)

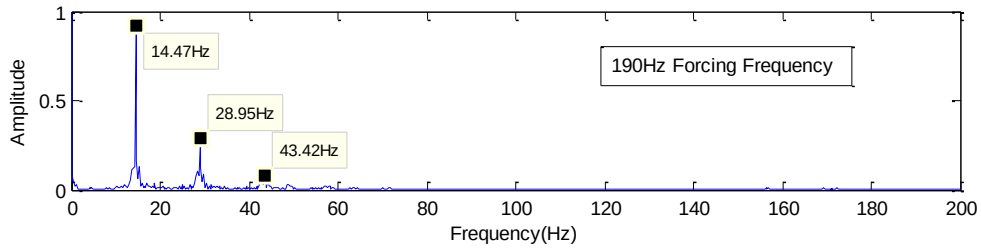

(i)

Figure 4-6: Power spectrum of $\boldsymbol{CH^*}$ with different frequency acoustic excitation (Case Two)

Table 4-2 lists the detected dominant frequencies (f_d) in the power spectrum of CH^* chemiluminescence at different acoustic excitation frequency in this test case. Figure 4-6 illustrates its tendency of change. It was observed that the peak dominant frequencies only change around the typical flickering frequency in a very limited range (12Hz-15Hz) for most frequencies (except for 120Hz and 140Hz). It therefore can be concluded that the buoyancy-driven instability takes over the acoustic excitation for all forces in this test case.

These results prove that the flame dynamic is affected by not only the frequency of the excitation acoustic but also the intensity. More importantly, it also has been observed that the flame is relatively stable under an acoustic excitation at the frequency of 140Hz, which is very important for monitoring of combustion stability and worth for further investigation.

Table 4-2: Detected dominant frequencies f_d by CH^* chemiluminescence (Case Two)

f_a	f_d
No Excitation	12.45Hz
110Hz	13.89Hz
120Hz	None
130Hz	13.03Hz
140Hz	None
150Hz	13.89Hz
160Hz	13.32Hz
170Hz	14.18Hz
180Hz	13.32Hz
190Hz	14.47Hz

4.4 Hot-wire Anemometry Measurement

Hot-wire anemometer is used in this study to measure the air flow velocity. Section 2.4.1 has presented the idea of using hot-wire anemometer to measure the air flow velocity. Figure 4-7 shows the FFT results of the data from the microphone and the hot wire anemometer. It was observed that the peak frequencies of both figures are 107.7Hz instead of 110Hz, which indicates about 2.3Hz errors. The errors could be caused by experimental equipments, such as the signal generator, loudspeaker, and power amplifier etc. During experiments, it also has been found that errors not only happen under 110Hz acoustic excitation but also under other frequencies of acoustic excitation.

Figure 4-8 illustrates some FFT results of hot-wire anemometer for air flow velocity in the tube with different acoustic excitation frequency, which was implemented at the same condition as Test Case Two.

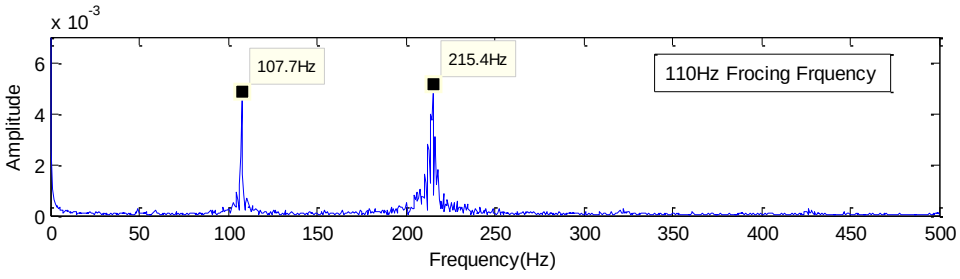

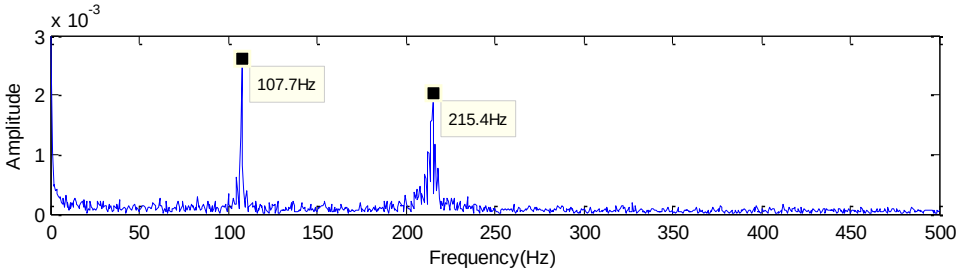

Figure 4-7: Comparison of Microphone and Hotwire results for 110Hz

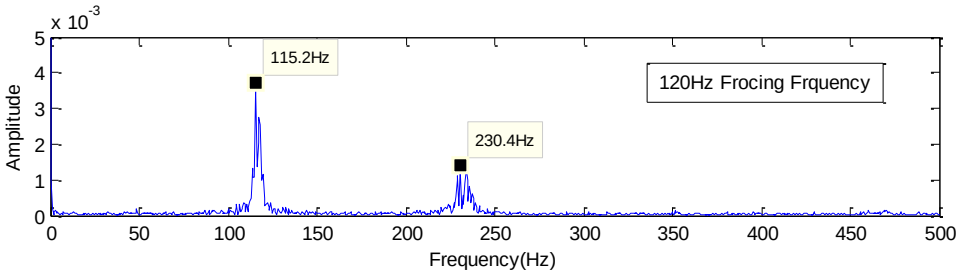

(a)

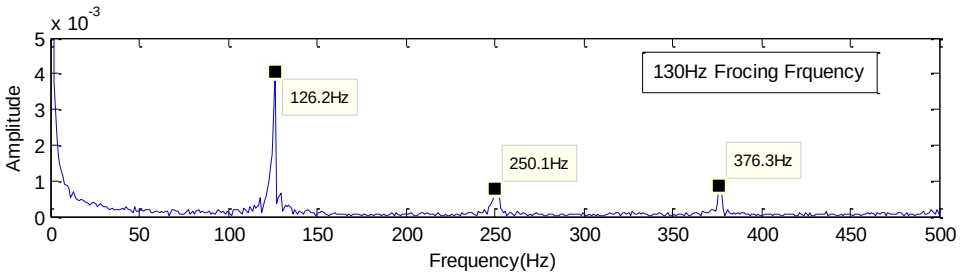

(b)

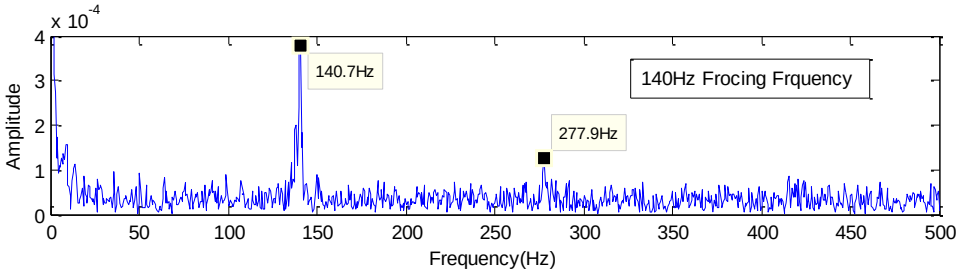

(c)

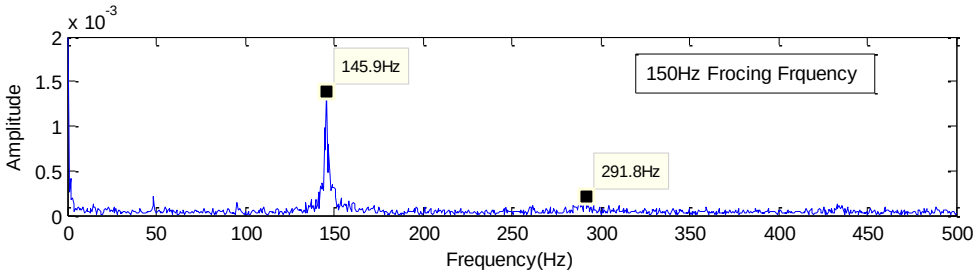

(d)

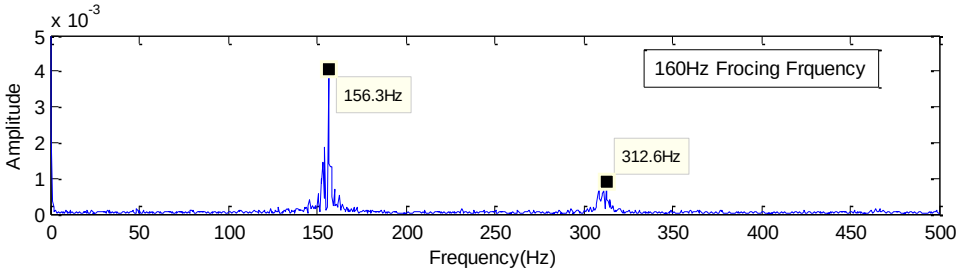

(e)

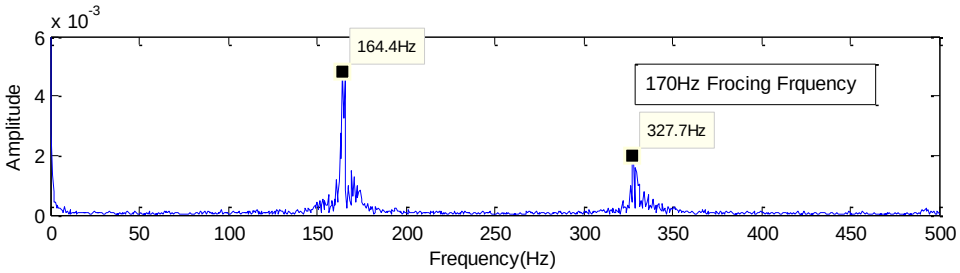

(f)

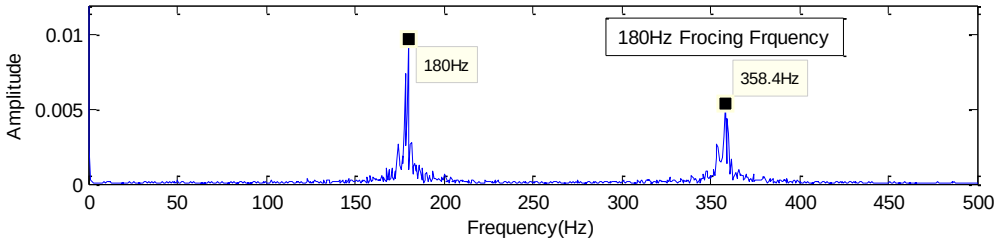

(g)

Figure 4-8: FFT for air flow velocity with different acoustic excitation.

4.4.1 Result Analyse by Amplitude Value of FFT

Table 4-3 shows the amplitude value of peak frequency in Figure 4-8. It clearly shows that the amplitude of the peak frequency at 140Hz reaches minimal. Figure 4-9 illustrates the tendency of amplitude of the peak frequency.

Table 4-3: Values of peak amplitude of different frequencies of acoustic excitation.

f_a	Peak Amplitude
110 Hz	0.005119
120 Hz	0.003732
130 Hz	0.004072
140 Hz	0.0003789
150 Hz	0.001380
160 Hz	0.004055
170 Hz	0.004790
180 Hz	0.009699

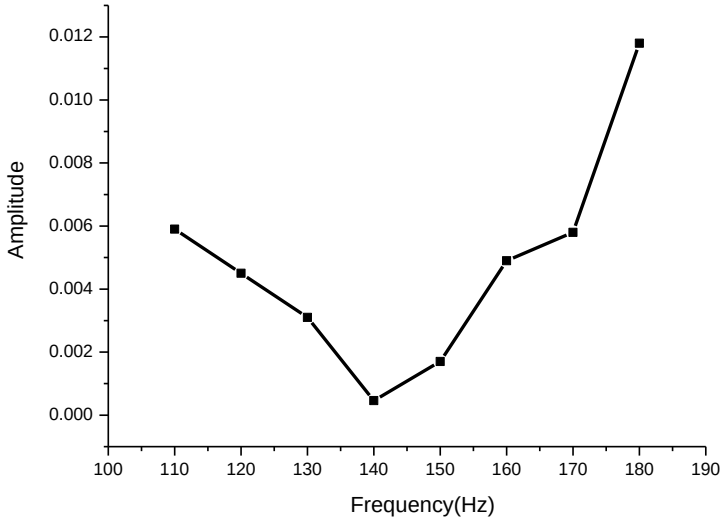

Figure 4-9: Illustration of the peak amplitudes of different frequency excitation

4.4.2 Results Analyse by SD Value

As an another criteria describing stability, the Standard Derivation (SD) values of the data sets collected by hot-wire were calculated. At the frequency of 140Hz of acoustic excitation, the SD is very small as shown in Table 4-4, which also gives the corresponding SD values for other acoustic excitation frequency between 110Hz and 180Hz. Figure 4-10 illustrates the tendency of SD values.

Table 4-4: Values of standard deviation different frequencies of acoustic excitation.

f_a	SD
110 Hz	0.0125
120 Hz	0.0076
130 Hz	0.0103
140 Hz	0.0018
150 Hz	0.0036
160 Hz	0.0060
170 Hz	0.0095
180 Hz	0.0172

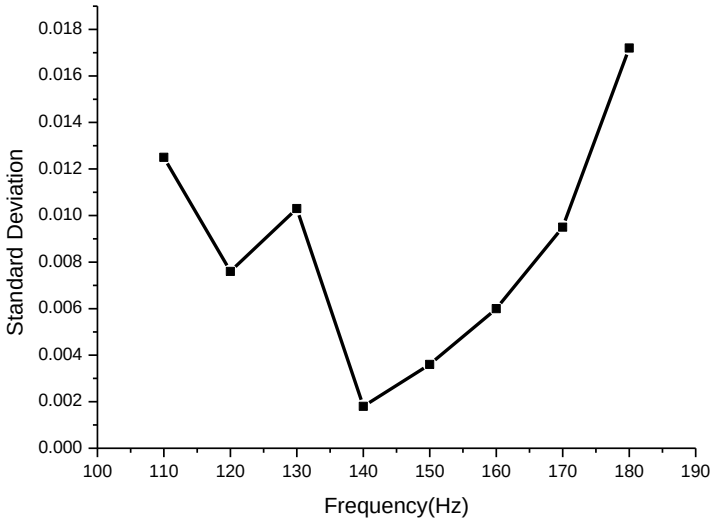

Figure 4-10: Illustration of the standard deviation different frequencies of acoustic excitation.

It can be observed from Table 4-4 that when the excitation frequency is 140Hz, the SD value reaches the minimum. This result is well suited for the result which was deduced from image processing method.

Based on different analyzing methods discussed above, a conclusion can be deduced that the flame is much more stable under an acoustic excitation with frequency 140Hz compared to other frequencies of acoustic waves.

4.5 Summary

Based on the experimental set up of this research, the photomultiplier and

hot-wire anemometer were applied to collect the CH^* chemiluminescence signal and air velocity around the flame.

The interaction between flame dynamics and acoustic excitation was investigated based on experimental data. It has been found that the frequency and intensity of acoustic excitation can considerably influence the flame dynamics.

For the experimental condition of the nozzle height 13.5cm from the tube bottom, the PMG at -12db, the applied voltage to the signal generator at 2V, and the fuel flow rate at 40ml/min, with a low intensity acoustic excitation, the acoustic excitation takes over the buoyancy-driven instability when the acoustic frequency is between 8Hz and 80Hz, otherwise the buoyancy-driven is the main control factor for the flame dynamics.

With a high intensity acoustic excitation, it is very difficult to establish a flame when the acoustic frequency is below 80Hz or above 220Hz, but interestingly relatively stable flame was observed when using 140Hz acoustic wave to excite the flame, which shows that it is feasible to improve the flame stability by applying an external acoustic source to the burner.

Chapter 5

Investigation of Flame Dynamics by Image Processing Techniques

---

Image processing is any form of signal processing for whose input is an image or a series of images, such as photographs taken by a digital camera or frames of a video. Image processing usually refers to the digital image processing. This technique becomes very popular in these years and has been used in many kinds of research field. The output of image processing can be either an image or a set of characteristics or parameters related to the image, such as the grey values, intensity or boundary of the object etc. This chapter analyzes the flame stability by applying image processing methods, which have never been studied before. Gray images are investigated from different aspects including the projected area of flame, position of the flame centre and results of which are compared to the results obtained from Chapter 4 in the end of this chapter.

5.1 Introduction

In order to obtain limited spatial information, a high resolution and high-speed digital camera was applied to acquire 2D images of the flame emissions. Gray images have been used in this research to extract flame information as much as possible.

The flame stability is analyzed by means of several image processing methods and the results are presented and discussed in the following part. The data analyzed in this section were collected under the same condition as the test case two of Chapter 4. The nozzle height was 13.5cm from the tube bottom. The PMG was set at -12db. The applied voltage to the signal generator was set at 5V, and the fuel flow rate was kept at 40ml/min.

5.2 Stability Analyse based on Synthetic Images

A software package was developed to process the flame images based on C++. Figure 5-1 shows eleven sequences of flame image in 120ms (sampled at interval of 8ms) under the condition of without excitation, at frequency of acoustic excitation 100 Hz, 110 Hz, 120 Hz, 130 Hz, 140 Hz, 150 Hz, 160 Hz, 170 Hz,180 Hz and 190 Hz respectively. Figure 5-1(a) shows the sequences flame image without acoustic excitation. From Figure 5-1 (a), it can be observed that at certain time, the flame starts to grow higher and thinner and then separate into two parts, in a very short while, and the upper part lifts and burns away. The next cycle (from the tenth image in Figure 5-1(a)) starts with a new flame growing from the bottom part of the ninth frame nearby the burner orifice. Under different frequencies of acoustic excitation, the flame manifests different dynamics. Some acoustic frequencies make the flame very unstable, but under some frequencies the flame becomes relatively stable. For example, Figure 5-1(b) shows the sequences of flame image under 100 Hz acoustic excitation, where the profile of the flame is blurred and very unstable. Figure 5-1(f) shows the sequences of flame image under 140Hz acoustic excitation, where the flame was observed to be relatively stable compared to the flames under other frequencies acoustic excitation.

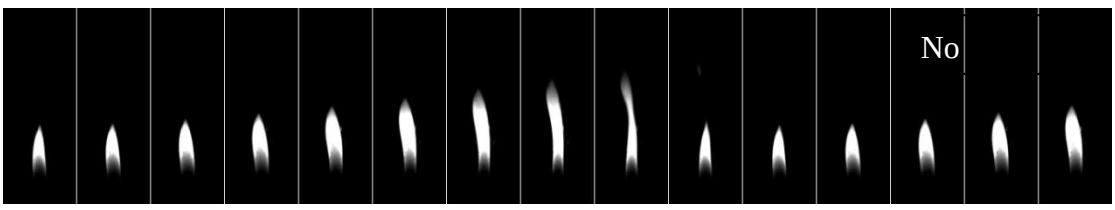

(a)

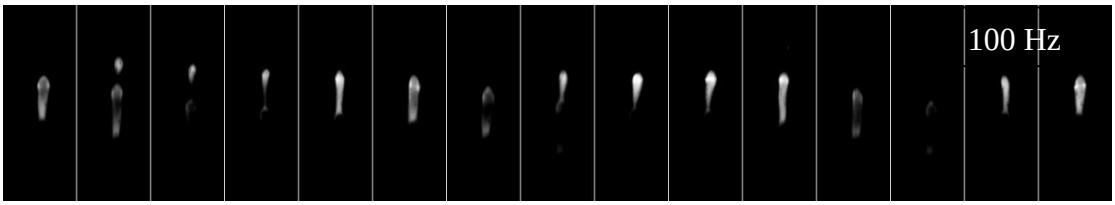

(b)

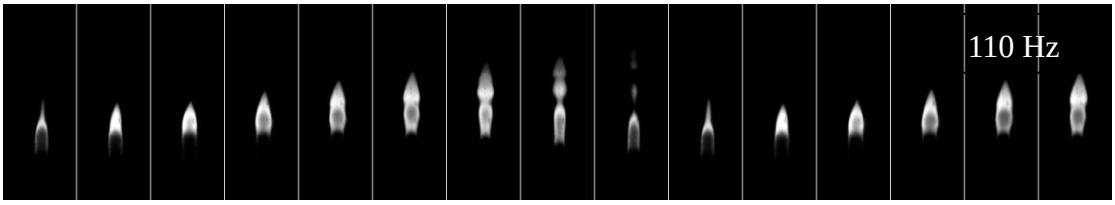

(c)

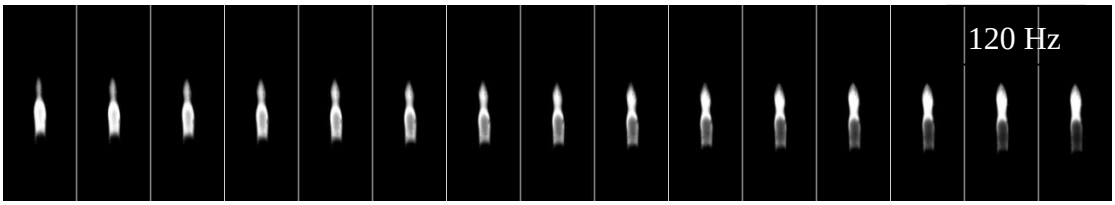

(d)

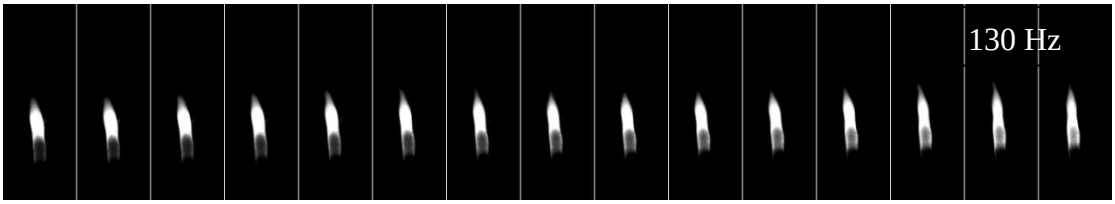

(e)

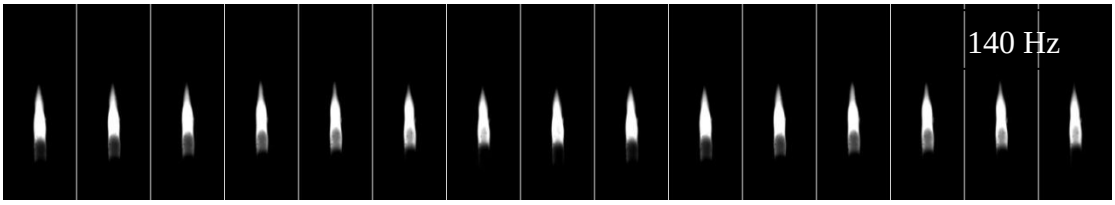

(f)

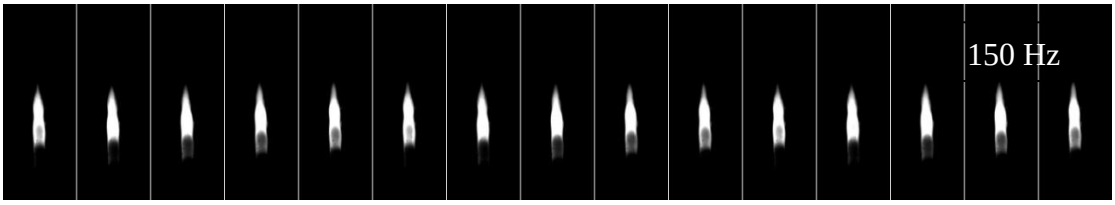

(g)

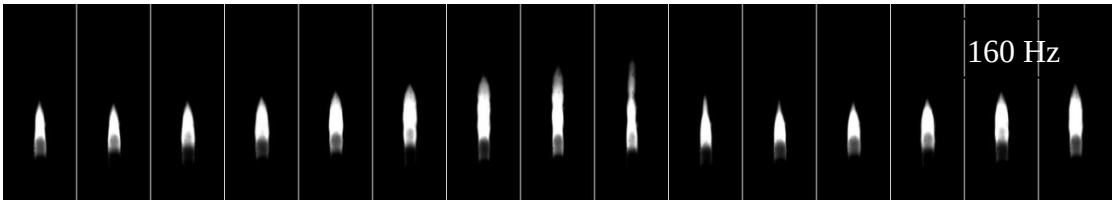

(h)

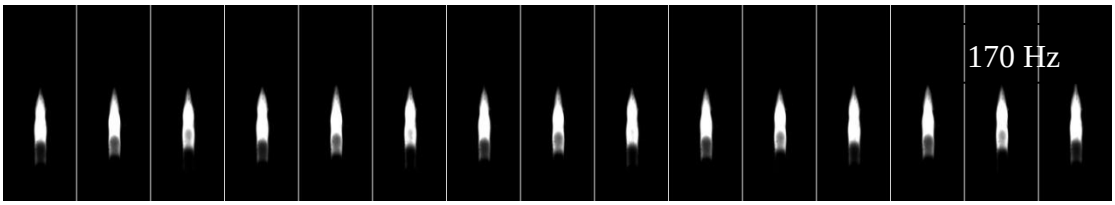

(i)

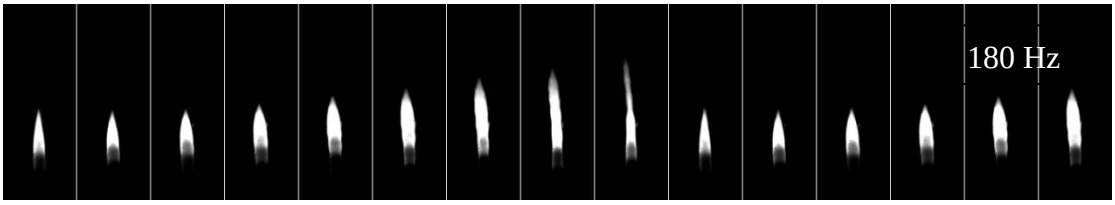

(j)

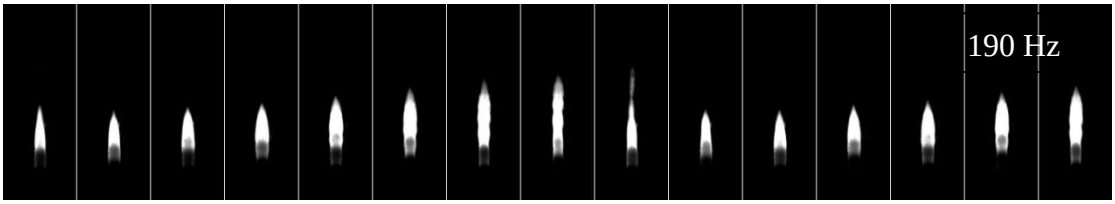

(k)

Figure 5-1: Sequences of flame image under at frequencies of acoustic excitation

As shown in Figure 5-1 (b), the flame with 100Hz acoustic excitation is very unstable and the shape of the flame is relatively irregular compared to other flame images. If the acoustic wave frequency continues to be decreased, the flame blows off immediately. Therefore, under this condition, the external acoustic wave has a big influence on the flame dynamic and acoustic effect overtakes the buoyancy instability and makes the flame very unstable. But if the acoustic wave frequency is increased to 110Hz (as shown in Figure 5-1(c)), the flame becomes relatively stable compared to Figure 5-1(b). Acoustic effect is still dominant, because the flame is not as stable as that without acoustic excitation. Keep increasing the excitation frequency, the flames become less unstable. For the flames at the forcing frequency of 140Hz, the flame is relatively stable. In Figure 5-1(f), the flame has nearly the same height and the same brightness and there is no flame lift that exists in each flame image. Therefore it can be deduced that the external acoustic excitation can change flame dynamic and make flame more stable or unstable compared to no excitation. The following part analyses this phenomenon by an image processing technique that synthesizes a sequence

of image into one image.

Figure 5-2 shows eleven corresponding synthetic flame images without excitation and under 100-190Hz of acoustic excitation. The synthetic image is generated by accumulating images into an ensemble of a sequence of image. A threshold H is essential to be defined before generating a synthetic image. Consider a pixel (x_i, y_i) in image, if the brightness level of which is larger than H, this pixel belongs to the flame and the counter adds one. Otherwise, the pixel is taken as the background. If more than 255 frames are accumulated, the gray value of the synthetic image will be normalized to 0 to 255. In order to distinguish the flame from the background of the image distinctly, the gray value was normalized from the range of 0-255 to 0-1. The value 1 (denoted by the red color) presents the gray value of 255; the value 0 (denoted by the blue color) presents the grey value of 0. It is observed in Figure 5-2 that synthetic images can be very different in terms of different frequency of acoustic excitation. The synthetic image of 140Hz has the most uniform profile of flame compared to other synthetic images. It also can be seen that the spatial variation of the flame oscillation is significant and the influence of acoustic excitation on flame dynamics is highly three dimensional.

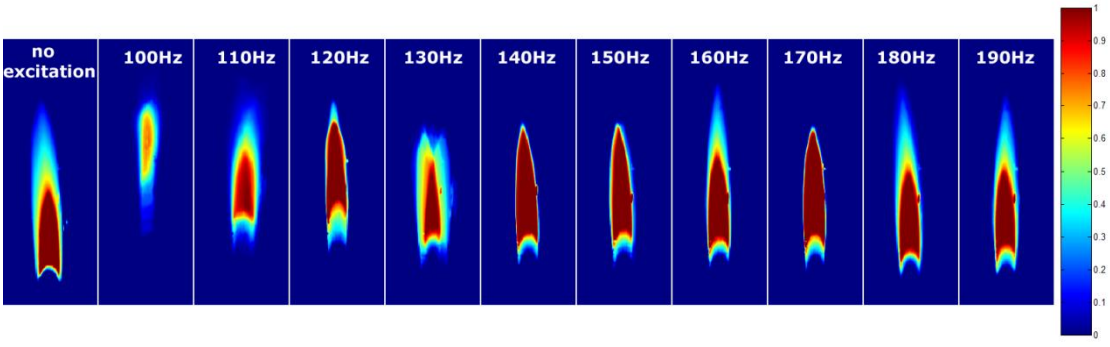

Figure 5-2: Syethetic flame image with different acoustic excitation

Define the synthetic flame area in the whole synthetic image is composed of gray value from a_1 to 255. The brighter area in the synthetic image is the gray value from $a_2 (a_1 < a_2)$ to 255. Bigger size of bright areas in the whole flame area denotes higher stability of the flame. To qualitatively measure the stability of the

flame, this research introduces a criterion p, which can be expressed by the equation (5-1).

$$p = \frac{S_1}{S_2} \quad \textbf{(5-1)}$$

where S_1 denotes the area size (number of pixels) of the brighter area and S_2 denotes the area size of the whole flame area. Obviously, the closer to 1 the value of p is, the more stable the flame is.

Based on the data collected in test case two introduced in last chapter, Table 5-1 shows the values of p under different acoustic excitation by setting $a_1 = 20, a_2 = 200$. Figure 5-3 illustrates the tendency of p over different frequency acoustic excitation.

Table 5-1: $\boldsymbol{p}$ value over different acoustic excitation

f_a	p
No Excitation	37.62%
110 Hz	21.41%
120 Hz	51.41%
130 Hz	20.41%
140 Hz	71.08%
150 Hz	55.73%
160 Hz	43.05%
170 Hz	72.04%
180 Hz	35.45%

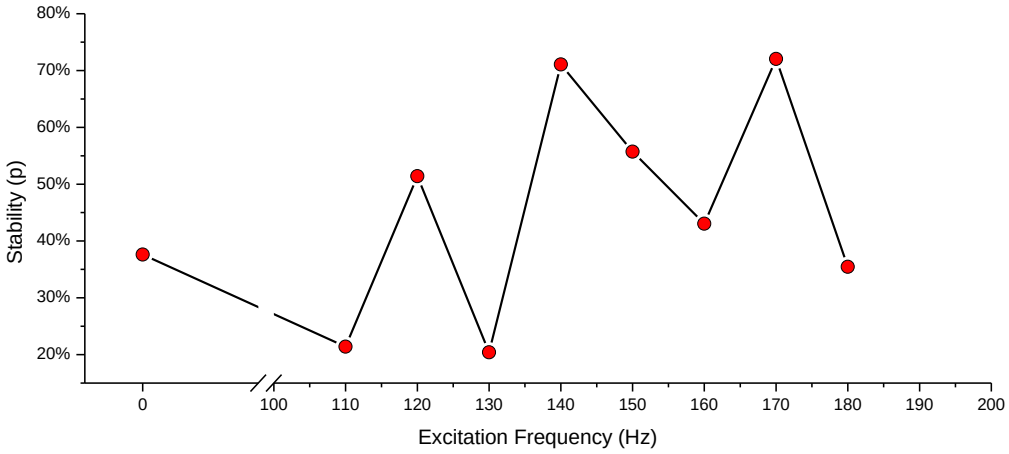

Figure 5-3: Illustration of $\boldsymbol{p}$ over different excitation frequency

From Table 5-1, it is found that for the acoustic excitation frequency of 140Hz and 170Hz, p values are remarkably bigger than other figures and much closer to 100%. So, it is presumed that in these two conditions the flame is more stable than other excitation. Furthermore, from results deduced from $CH*$ analysis and the synthetic flame image (Figure 5-2), very similar results are obtained. Therefore, to a certain extent, p value can be taken as a parameter to measure the degree of the flame stability. The closer of the flame's p value to 1, the more stable of the flame is. Flame image's p value provides a measurable parameter for flame stability which provides a controllable parameter for combustion instability control. But it is worthy to be noted that p is very dependent on the threshold selection, therefore it does not make sense to compare p values derived from different thresholds.

5.3 Stability Analyse based on the 2D Projected Area of Flame (AoF)

As it can be noticed from Figure 5-1, the 2D projected area of flame (AoF) changes dramatically and periodically by time when it is not stable, which inspires us to analyze the stability based on this parameter. This section introduces another image processing method to analyze the flame stability, which is based on the 2D projected area of flame in both time domain and frequency domain.

The projected area of flame is defined as the total number of pixels belongs to the flame in the whole image. For example, for a pixel (x_i, y_i) in image, if its brightness level is larger than the threshold H, then this pixel is classified belonging to the flame and the counter adds one. Normally, the flame can be identified distinctly when H is chosen from 20-200. There is no significant influence to the results if H varies in this range. In this experiment, H was chosen as 30. Take the case with no excitation as an example. The projected flame area by time is illustrated by Figure 5-4, where 1000 frames were

sampled with rate 1000fps (frame per second). Figure 5-4 clearly shows that the projected flame area oscillates periodically.

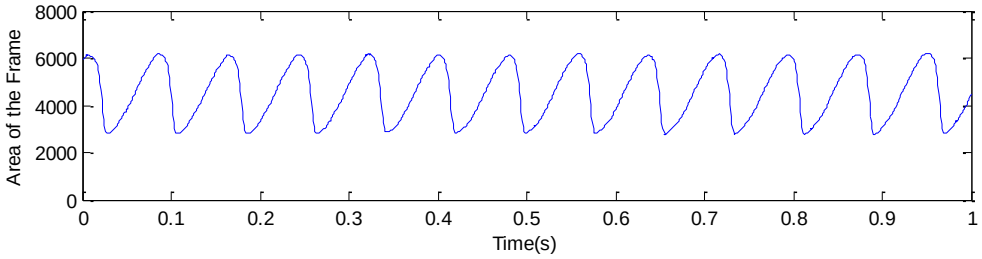

Figure 5-4: Projected area of flame by time with no excitation.

To analyze the stability of the flame under different acoustic excitations, two parameters, peak frequency in the frequency spectrum and standard deviation in time domain were calculated in this research. Figure 5-5 shows the spectrum of the projected area of flame with no excitation, where the flicker frequency $12.70Hz$ was distinctly detected.

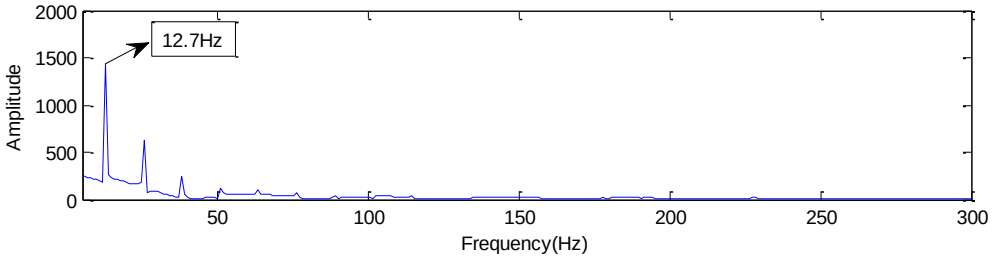

Figure 5-5: Spectrum of the projected area of flame with no excitation

Figure 5-6 to Figure 5-14 show the value of projected area of flame by time and corresponding spectrum with different excitation frequencies, where 1000 frames were sampled with rate $1000fps$.

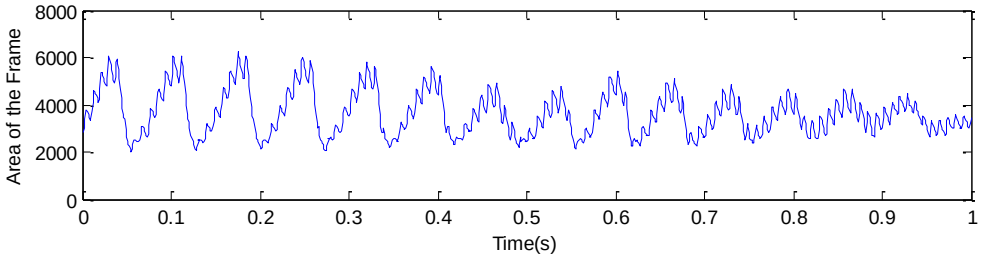

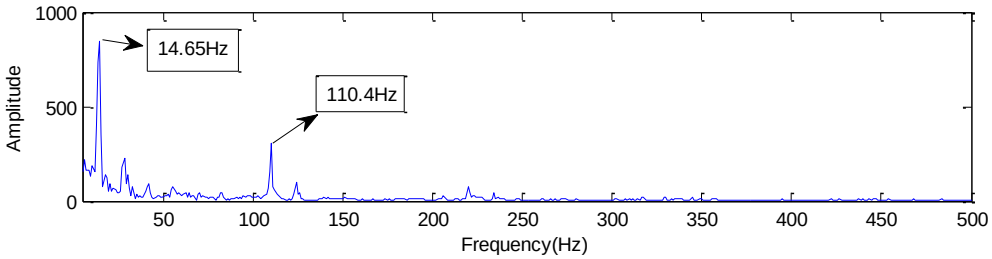

Figure 5-6: Projected area of flame by time and corresponding spectrum with excitation frequency 110Hz

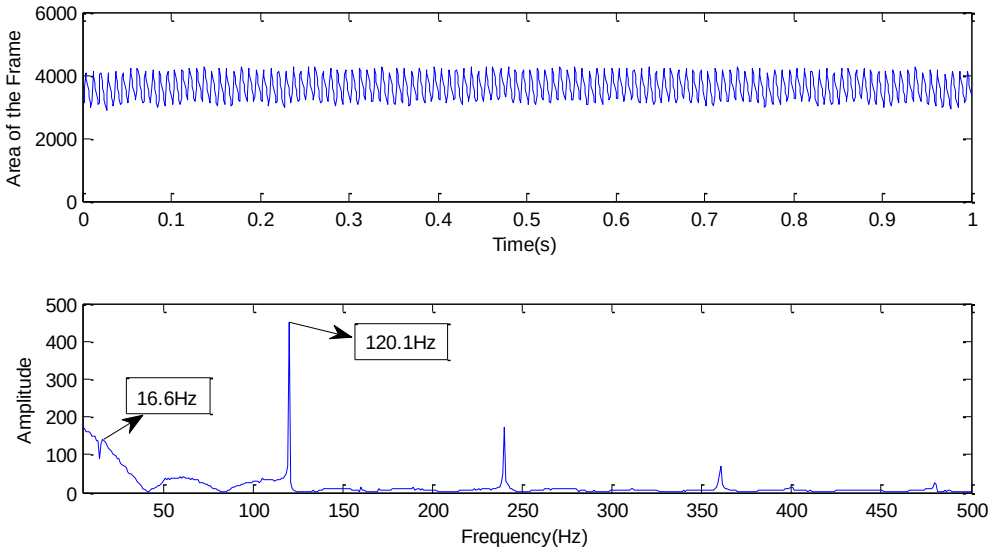

Figure 5-7: Projected area of flame by time and corresponding spectrum with excitation frequency 120Hz

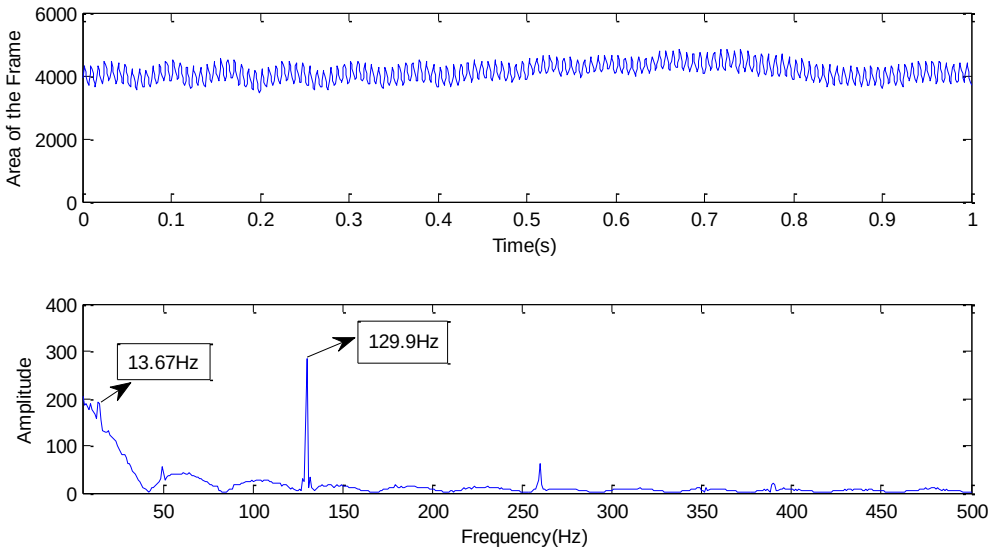

Figure 5-8: Projected area of flame by time and corresponding spectrum with excitation frequency 130Hz

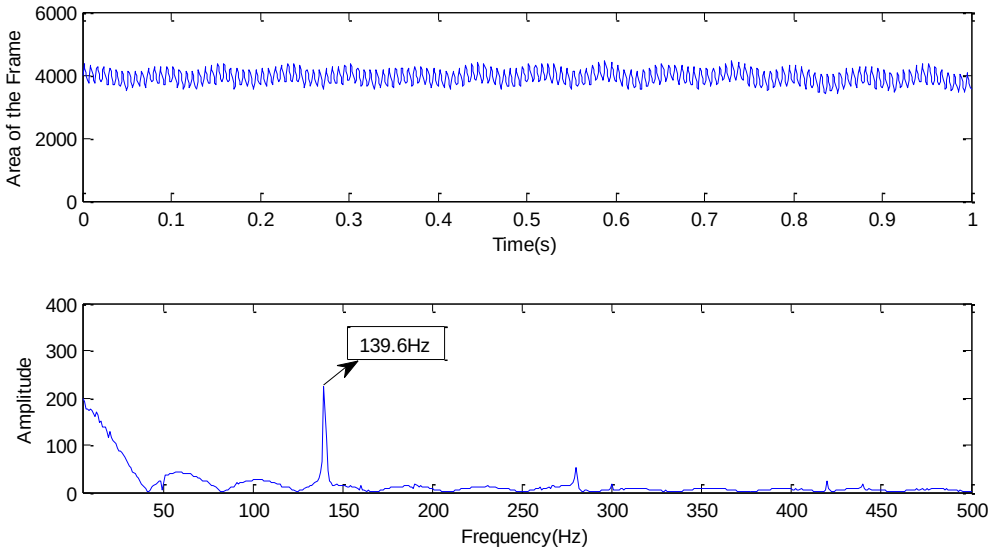

Figure 5-9: Projected area of flame by time and corresponding spectrum with excitation frequency 140Hz

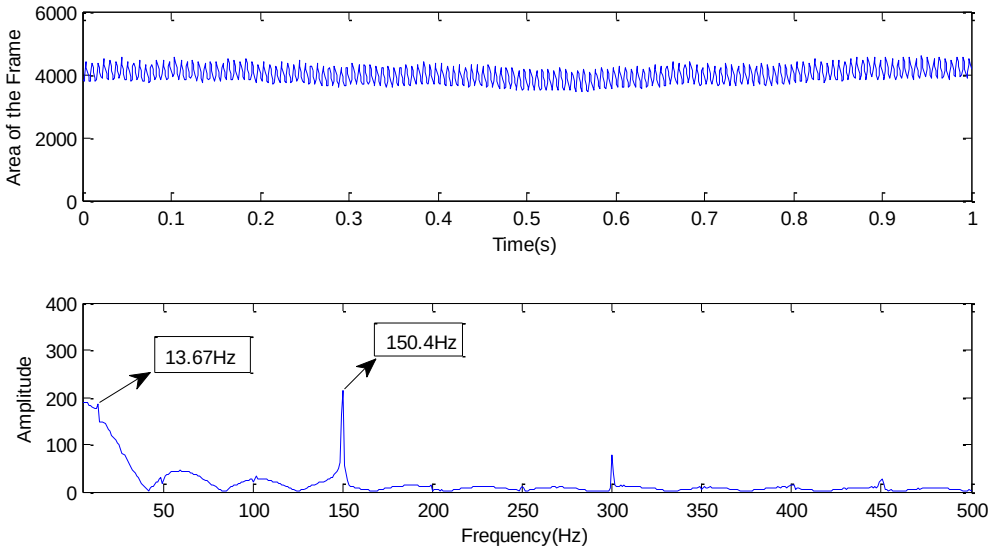

Figure 5-10: Projected area of flame by time and corresponding spectrum with excitation frequency 150Hz

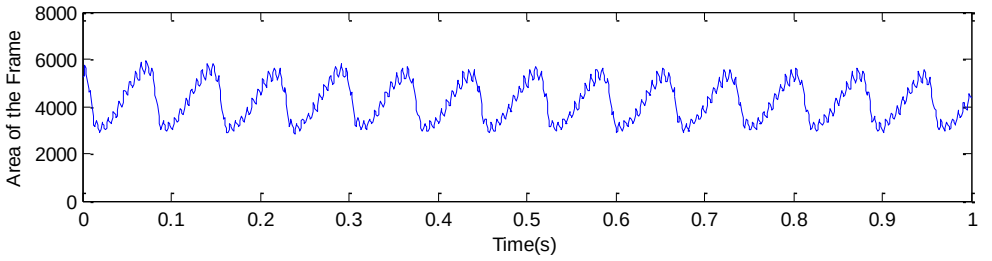

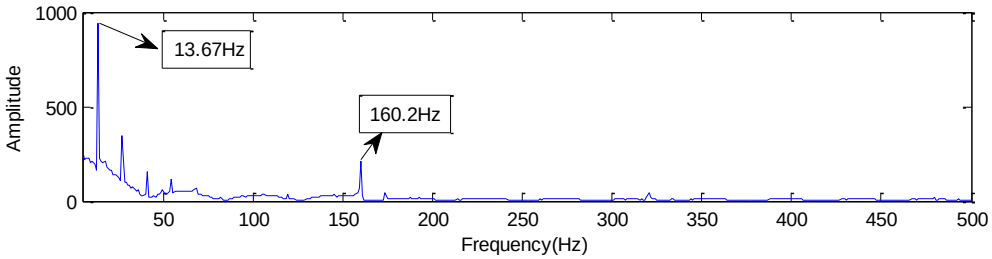

Figure 5-11: Projected area of flame by time and corresponding spectrum with excitation frequency 160Hz

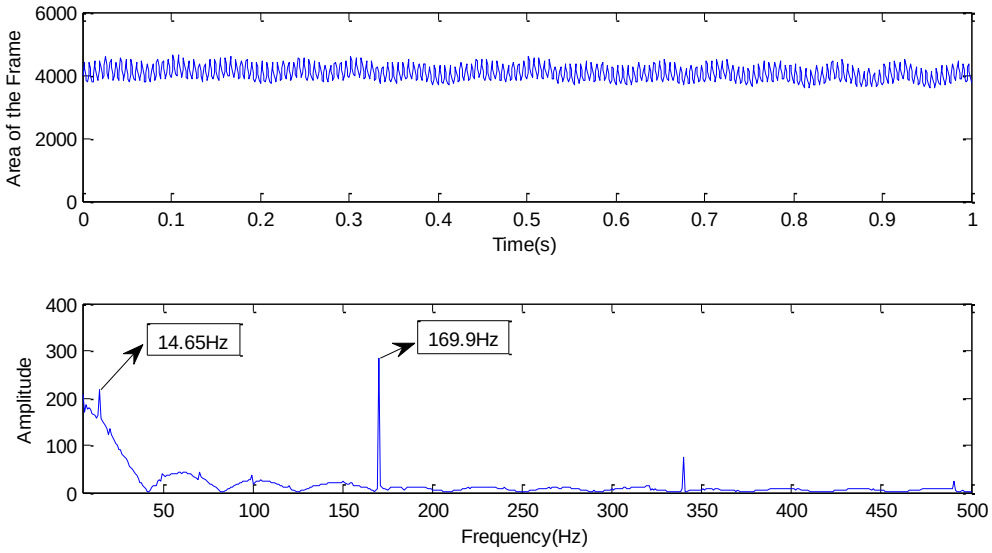

Figure 5-12: Projected area of flame by time and corresponding spectrum with excitation frequency 170Hz

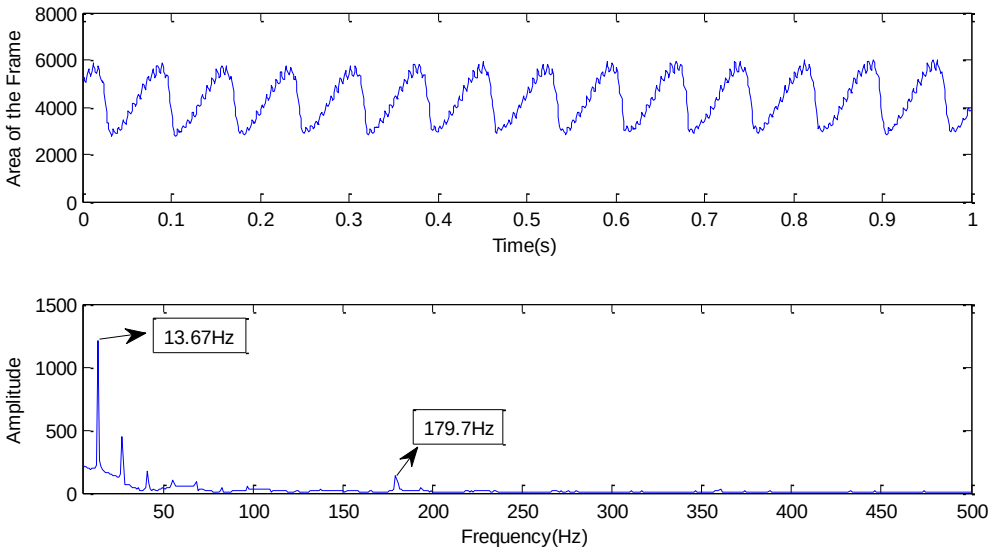

Figure 5-13: Projected area of flame by time and corresponding spectrum with excitation frequency 180Hz

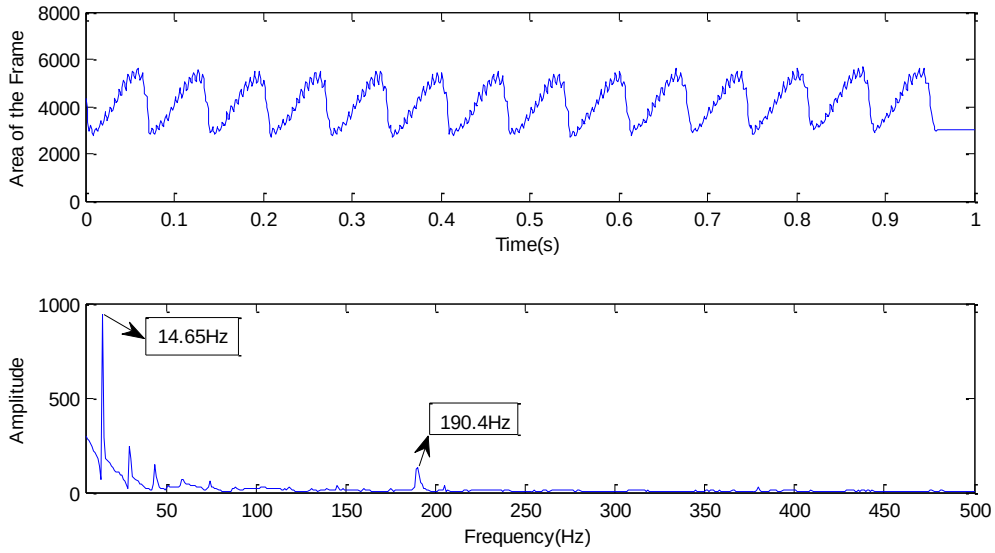

Figure 5-14: Projected area of flame by time and corresponding spectrum with excitation frequency 190Hz

From Figure 5-6 to Figure 5-14, we can find that all excitation frequencies can be detected accurately by the spectrums of the 2D projected area of the flame. The flicker frequency can be detected in some groups of data, but not in other groups. If the flame is very stable, the flicker frequency should not be reflected in spectrum at all. Hence, the stability of the flame can be judged by the appearance of the flicker frequency in spectrum. Table 5-2 shows the detected excitation frequencies and flicker frequencies under different excitation. Obviously, excitation frequencies were detected perfectly and the error is smaller than 0.2%. Flicker frequency was detected distinctly under no excitation, excitation frequency 110Hz, 160Hz, 180Hz and 190Hz, which denotes that the flames are significantly unstable under those conditions. Flicker frequency was detected but indistinctly at excitation frequency of 120Hz, 130Hz, 150Hz and 170Hz, which denotes that the flames are relatively stable under those conditions. Flicker frequency cannot be detected at excitation frequency of 140Hz, which denotes the flame is very stable under this condition.

Table 5-2: Detected frequency by the spectrum of projected area of flame

f_a	Detected Excitation Frequency	Detected Flicker Frequency	
		Value	Distinct?
No excitation	None	12.70Hz	Y
110Hz	110.40Hz	14.65Hz	Y
120Hz	120.10Hz	16.60Hz	N
130Hz	129.90Hz	13.67Hz	N
140Hz	139.60Hz	undetected	None
150Hz	150.40Hz	13.67Hz	N
160Hz	160.20Hz	13.67Hz	Y
170Hz	169.90Hz	14.65Hz	N
180Hz	179.70Hz	13.67Hz	Y
190Hz	190.40Hz	14.65Hz	Y

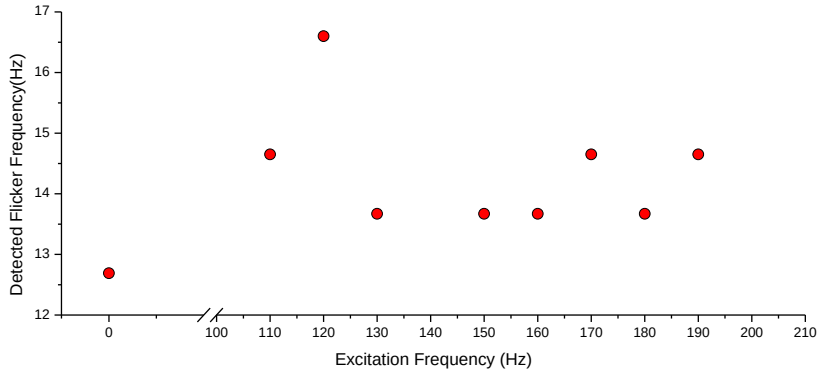

Figure 5-15: Detected flicking frequency for different excitation frequency

Table 5-3 lists the different values of SD (standard derivation) and Figure 5-16 illustrates the SD tendency of projected area of flame. It is found that the corresponding SD of the excitation frequency of $140Hz$ is smallest, which indicates the flame is the most stable in this case; different levels of stabilities can be defined, flames with $120Hz, 130Hz, 150Hz$ and $170Hz$ are relatively stable; the flames with no excitation frequency, with excitation frequency of $110Hz, 160Hz, 180Hz$ and $190Hz$ are most unstable. These conclusions are exactly the same as that generated by analyse the dominant frequencies in their frequency spectrums.

Table 5-3: Table of the SD values for different excitation frequencies based on projected area of flame.

f_a	SD
No Excitation	1176.42
110Hz	938.00
120Hz	363.33
130Hz	271.36
140Hz	217.43
150Hz	245.39
160Hz	842.50
170Hz	227.49
180Hz	965.62
190Hz	854.45

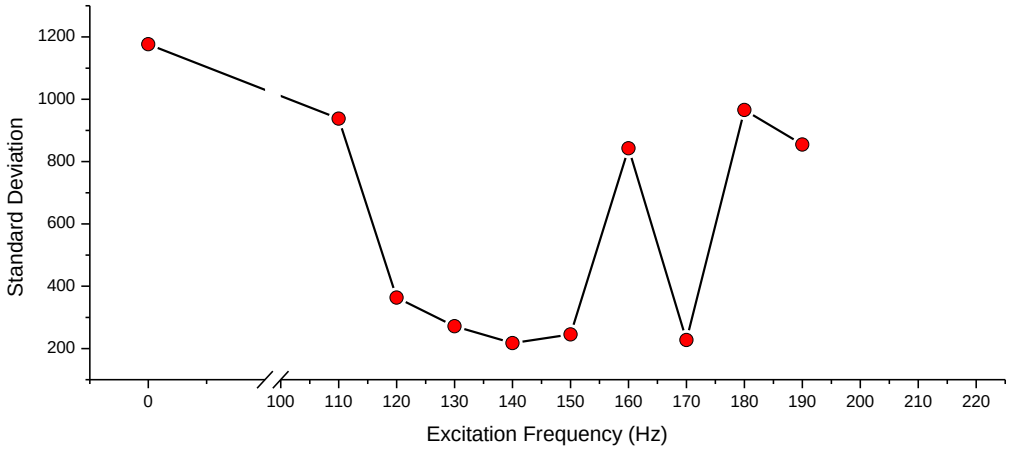

Figure 5-16: Illustration of SD values for different excitation frequencies based on AoF

Obviously, the selection of threshold H has influence to the calculation of SD values. For the collected flame images in this research, the flame profile is always visually separable with the background, which means the threshold H can be chosen within a range (20-200) that can produce very similar profile of flame. Hence the values of SD of AoF will be the same or change very slightly if H is chosen within this range. If H is chosen out of this range, the profile of the flame cannot be defined correctly, which leads to considerably change of SD values of AoF.

5.4 Stability Analyse based on the Centre of Flame (CoF)

A disadvantage to analyze stability based on projected area of flame is that the information in spatial of the flame is ignored. For example, if a flame jumps vertically but doesn't change area by time, it will be detected as stable mistakenly using projected area of flame. Of course, such a case can happen in theory but seldom in real data set. To solve this potential problem, this research proposes another method to analyze flame stability based on the centre of flame. The same as the above method, data were analyzed in both time domain and frequency domain.

For all pixels $(x_i, y_i), i = 1, \dots, m$ in image which belong to the flame, where m denotes the number of the pixels in the flame or the projected area of the flame, computing their average coordinates by:

$$\bar{x} = \frac{\sum_{i=1}^{m} x_i}{m} \quad \textbf{(5-2)}$$

$$\bar{y} = \frac{\sum_{i=1}^{m} y_i}{m} \quad \textbf{(5-3)}$$

The point at the average coordinates $(\bar{x}, \bar{y})$ is defined as the centre of the flame. The scheme to judge a pixel whether belongs to the flame or not is the same as what has been discussed in above method.

Consider the case with no excitation for an example. The centre of the flame by time is illustrated by Figure 5-17, where 1000 frames were sampled with rate $1000fps$. It is noticed that there is only five pixels shift in horizontal position (Figure 5-17 (a)) of the CoF in one second, which is relatively much smaller compared to 69 maximal pixels offset in vertical position (Figure 5-17 (b)) of the CoF. Hence, in this research we analyze flame stability only based on the vertically position of CoF. Figure 5-17 (b) also clearly shows that the vertical position of CoF oscillates periodically.

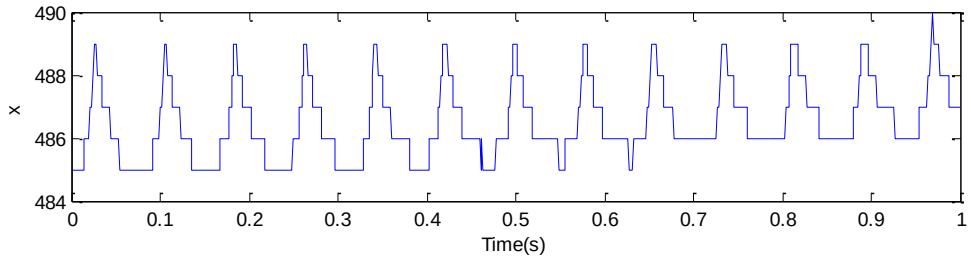

(a)

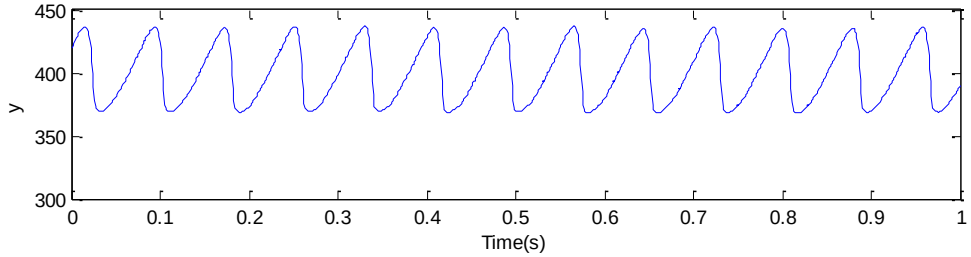

(b)

Figure 5-17: Horizontal position and vertical position of the CoF by time for no excitation.

Two parameters, standard deviation in time domain and the dominant frequency in the power spectrum of CoF, were calculated to represent the stability of the flame. Figure 5-18 shows the spectrum of the CoF with no excitation, where the flicker frequency $12.70Hz$ was distinctly detected.

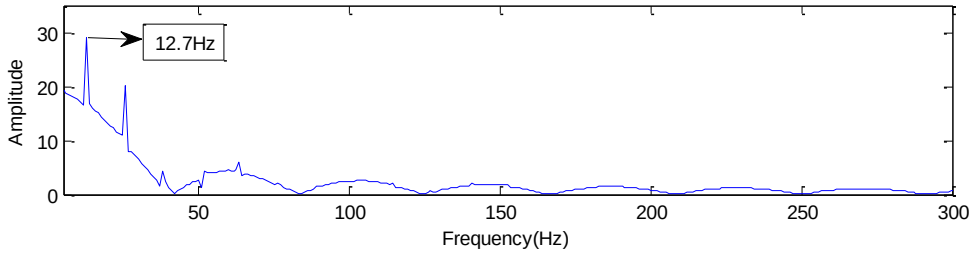

Figure 5-18: Spectrum of the CoF with no excitation.

To compare the stability of the flame, standard deviation in time domain and frequency spectrum were calculated for each group of data. Table 5-4 shows the values of SD, and Figure 5-18 illustrates the tendency of SD change over frequency. Both of them show that flame with excitation frequency $140Hz$ is most stable; the flames with $120Hz, 130Hz, 150Hz$ and $170Hz$ are relatively stable; the flames with no excitation frequency, excitation frequency $110Hz, 160Hz, 180Hz$ and $190Hz$ are very unstable.

Table 5-4: Table of the SD values for different excitation frequencies based on CoF.

f_a	SD
No Excitation	23.53
110 Hz	18.12
120 Hz	9.65
130 Hz	3.73
140 Hz	3.16
150 Hz	3.91
160 Hz	16.77
170 Hz	3.59
180 Hz	20.22
190 Hz	18.04

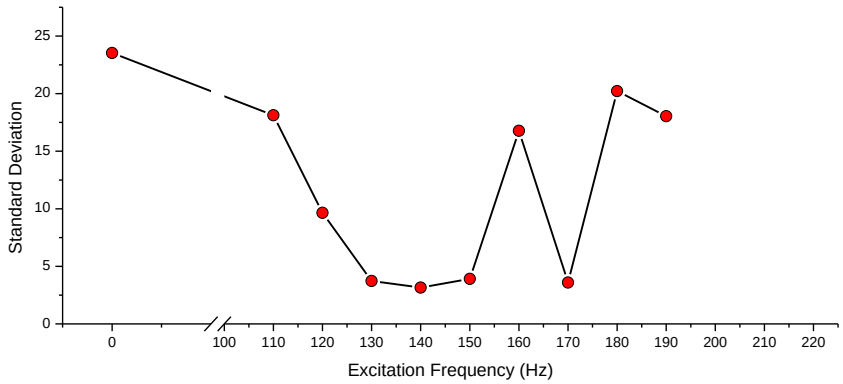

Figure 5-19: Illustration of SD values for different excitation frequencies based on CoF

As discussed in the section of 5.3, the selection of threshold H has influence on the calculation of SD values. For the collected flame images in this research, the flame profile is always visually separable from the background, which means the threshold H can be chosen within a range (20-200) that can produce very similar profile of flame. Hence the values of SD of CoF will be the same or change very slightly if H is chosen within this range. If H is chosen out of this range, the profile of the flame cannot be defined correctly, which leads to considerably change of SD values of CoF.

Figure 5-20 to Figure 5-28 show the value of CoF by time and corresponding spectrum with different excitation frequencies.

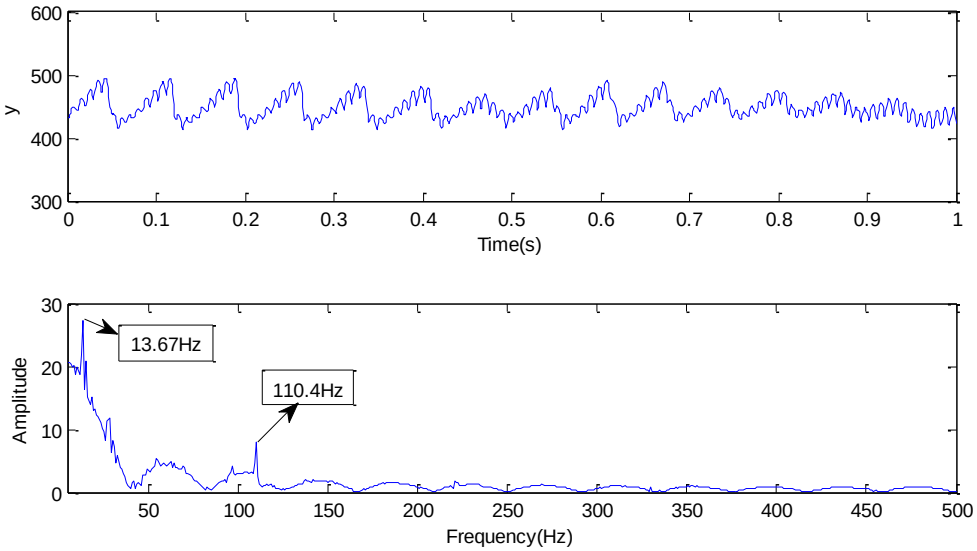

Figure 5-20: y of CoF by time and corresponding spectrum with excitation frequency 110Hz

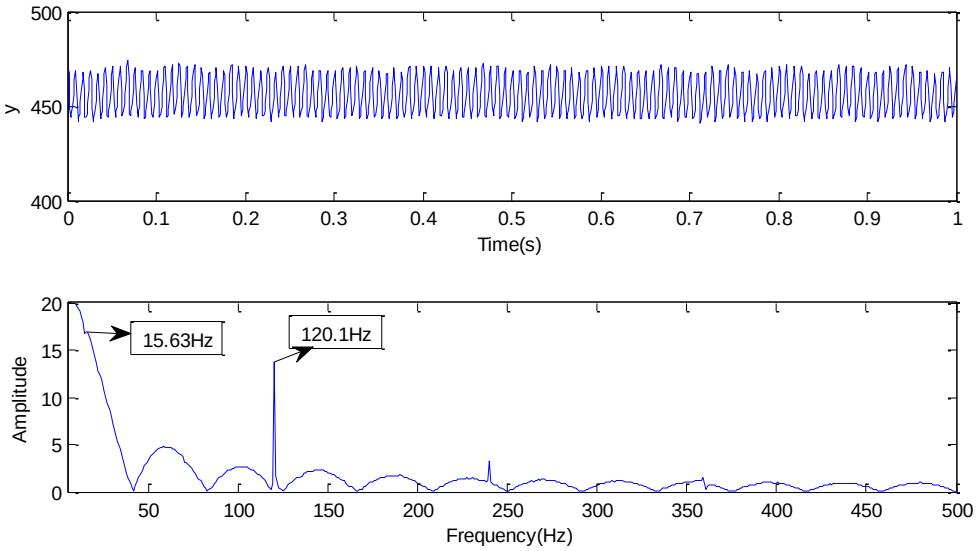

Figure 5-21: y of CoF by time and corresponding spectrum with excitation frequency 120Hz

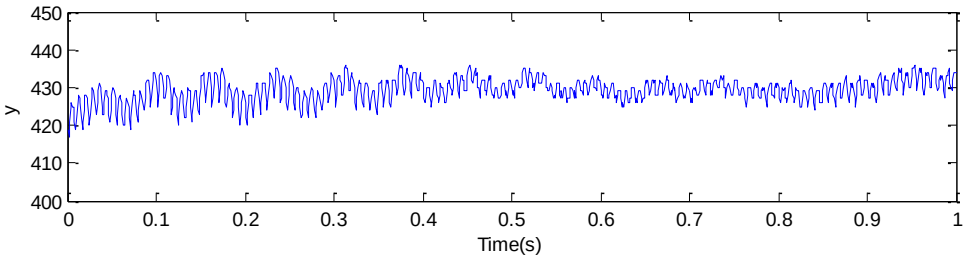

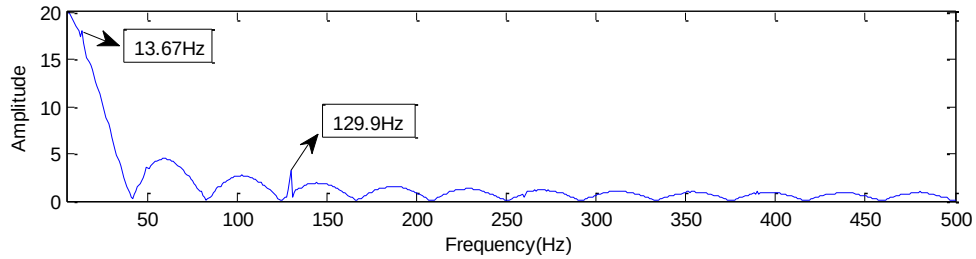

Figure 5-22: y of CoF by time and corresponding spectrum with excitation frequency 130Hz

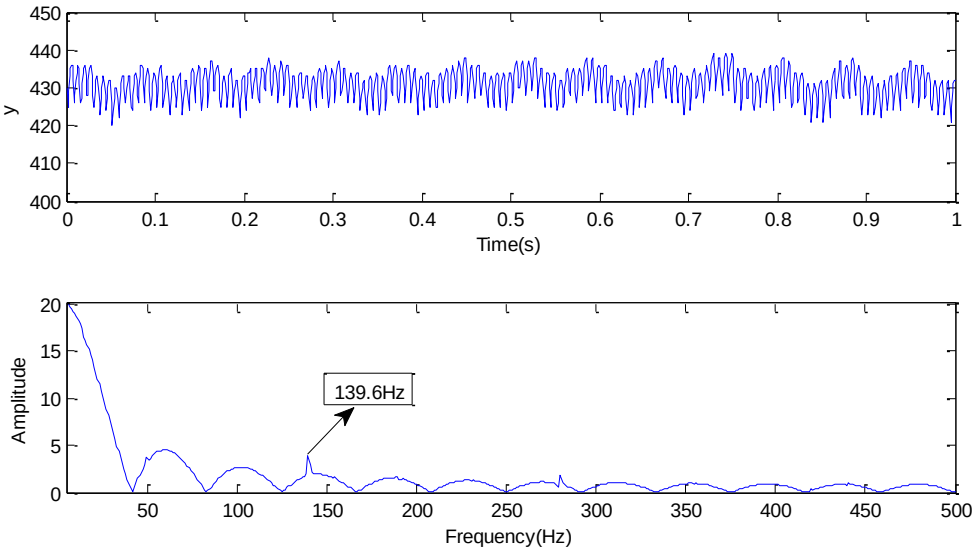

Figure 5-23: y of CoF by time and corresponding spectrum with excitation frequency 140Hz

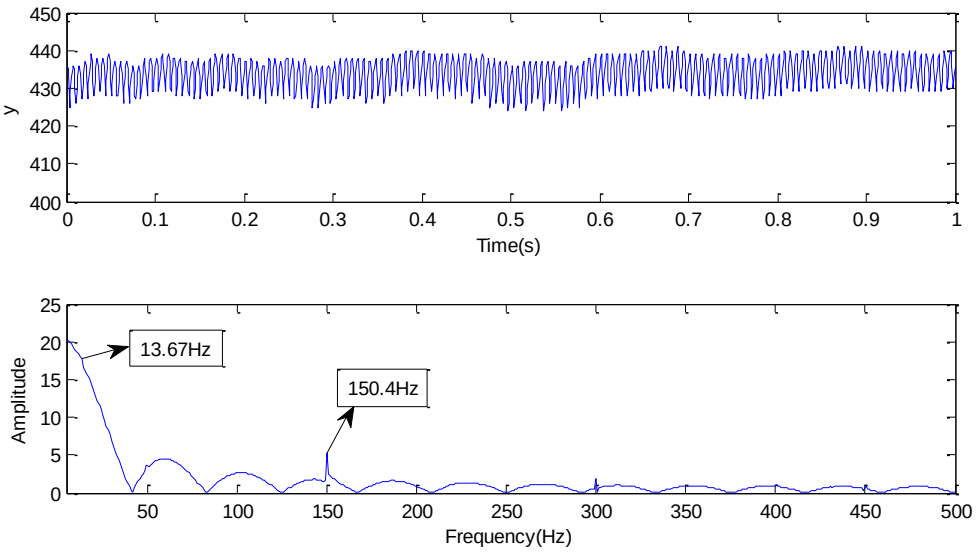

Figure 5-24: y of CoF by time and corresponding spectrum with excitation frequency 150Hz

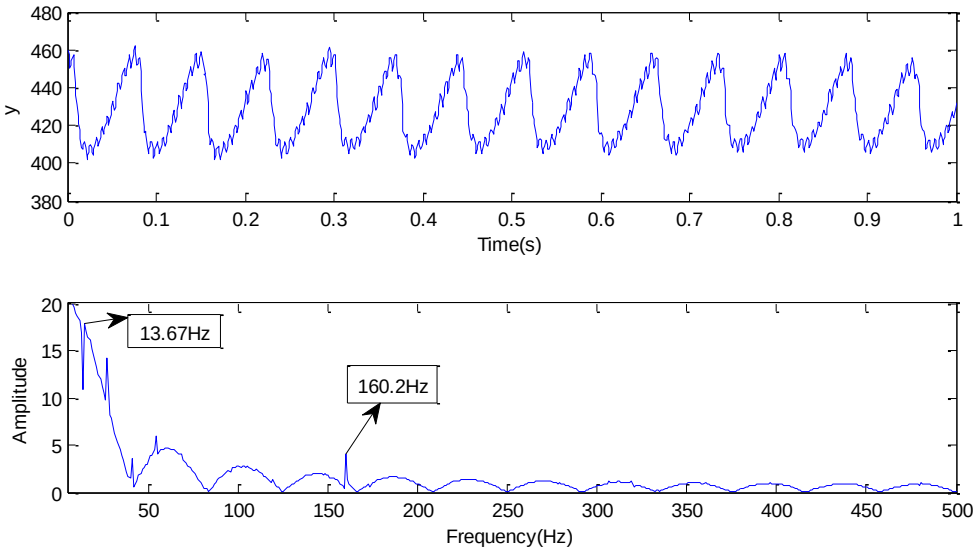

Figure 5-25: y of CoF by time and corresponding spectrum with excitation frequency 160Hz

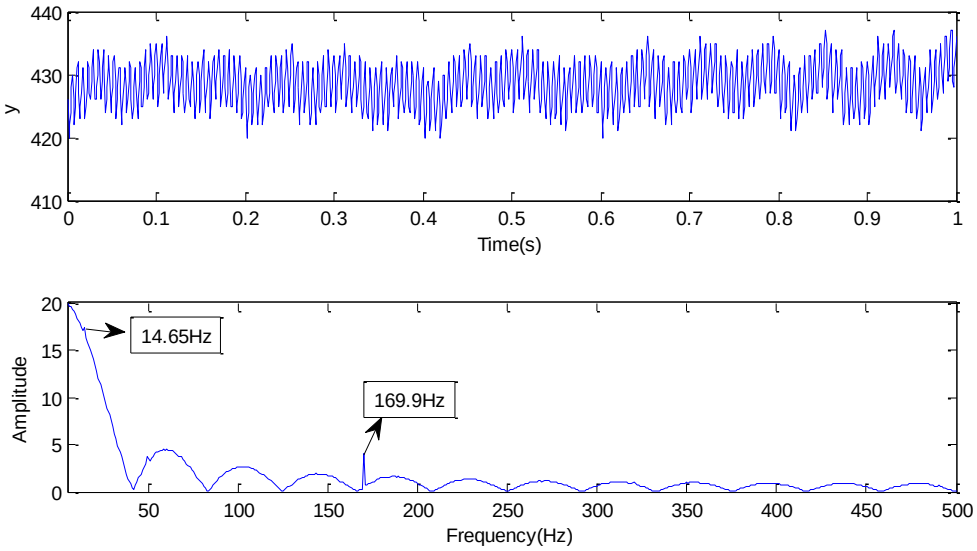

Figure 5-26: y of CoF by time and corresponding spectrum with excitation frequency 170Hz

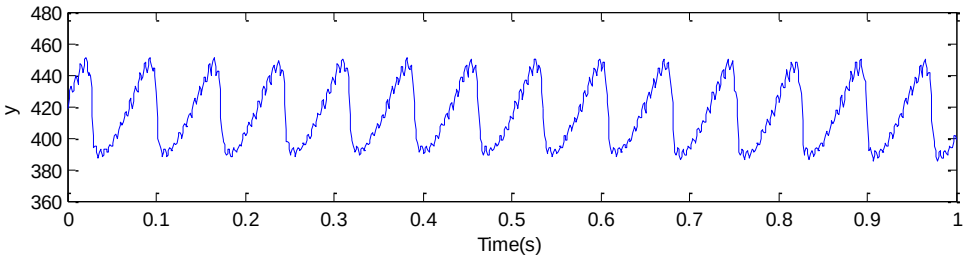

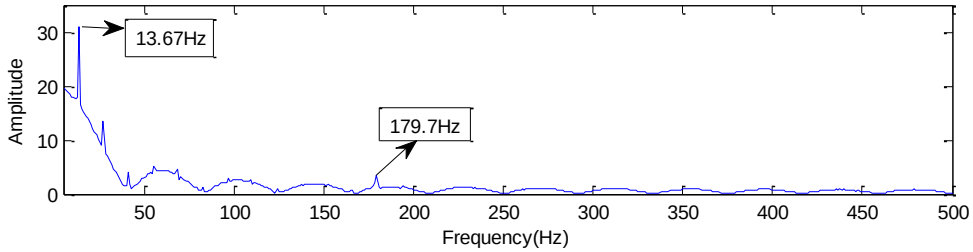

Figure 5-27: y of CoF by time and corresponding spectrum with excitation frequency 180Hz

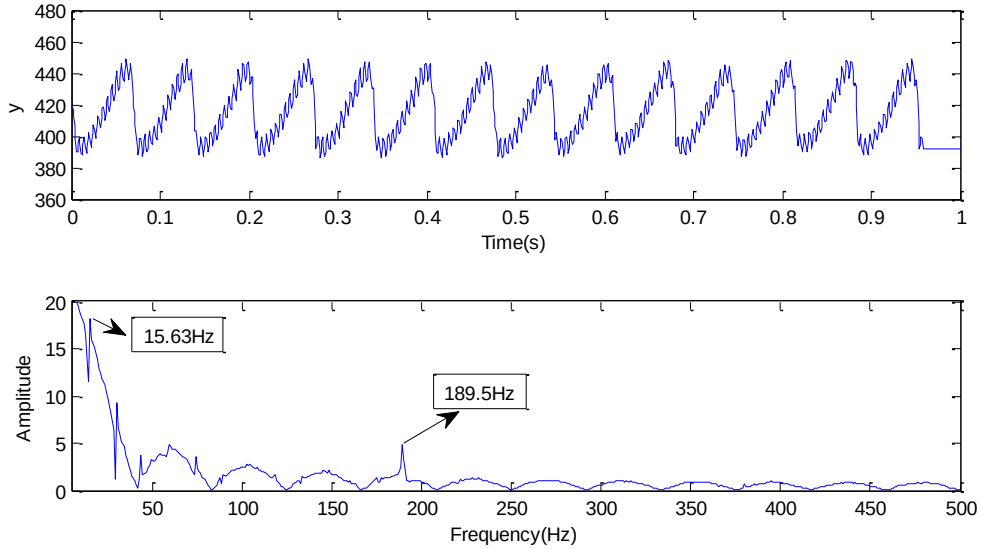

Figure 5-28: y of CoF by time and corresponding spectrum with excitation frequency 190Hz

Table 5-5 shows the detected frequencies under different excitation. Obviously, excitation frequencies were detected perfectly and the error is less than 0.34%. Flicker frequency was detected distinctly under no excitation, excitation frequency 110Hz, 160Hz, 180Hz and 190Hz, which denotes that the flames are significantly unstable under those conditions. Flicker frequency was detected but indistinctly under excitation frequency 120Hz, 130Hz, 150Hz and 170Hz, which denotes that the flames are relatively stable under those conditions. Flicker frequency cannot be detected under excitation frequency 140Hz, which denotes the flame is very stable under this condition. The conclusions are exactly the same as that generated by standard deviation in time domain.

Table 5-5: Detected excitation frequencies and flicking frequency by the spectrum of CoF

f_a	Detected Excitation Frequency	Detected Flicker Frequency	
		Value	Distinct?
No excitation	undetected	12.70Hz	Y
110Hz	110.40Hz	13.67Hz	Y
120Hz	120.10Hz	15.63Hz	N
130Hz	129.90Hz	13.67Hz	N
140Hz	139.60Hz	undetected	None
150Hz	150.40Hz	13.67Hz	N
160Hz	160.20Hz	13.67Hz	Y
170Hz	169.90Hz	14.65Hz	N
180Hz	179.70Hz	13.67Hz	Y
190Hz	189.50Hz	14.63Hz	Y

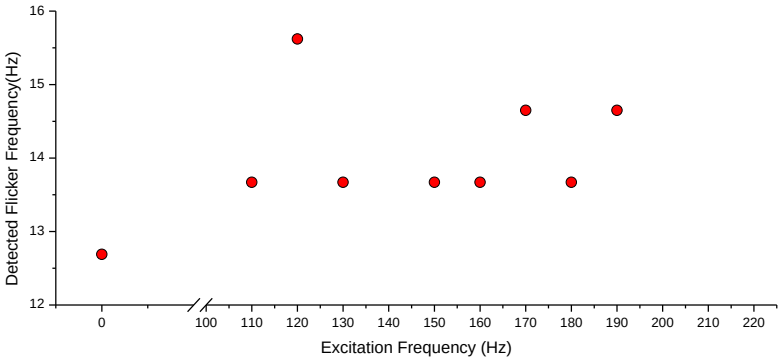

Figure 5-29: Flicking frequency by the spectrum of CoF

5.5 Flame Dynamics Analyse based on Power Spectrum of Each Pixel in Flame image

In order to get the spatial fluctuation of the investigated diffusion flame, the frequency of each pixel of the 2D flame image was calculated in this research.

5.5.1 Flame Pixel Fluctuation based on 2D Flame Images

Based on the grey value, Figure 5-30 illustrates the frequency distribution for each pixel at different frequency of acoustic forcing.

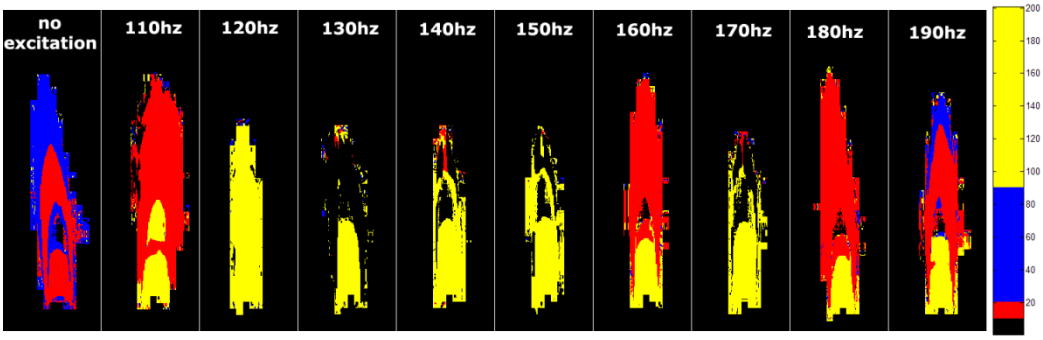

Figure 5-30: Frequency illustration of each pixel by grey image

Each detected frequency range is presented by a corresponding colour. The palette shown in the right side of Figure 5-30 allocates each frequency value to a colour with the following rules:

- The black colour denotes frequencies value lower than 10Hz which is mainly considered as background and noise.
- The red colour denotes the frequency range from 10Hz to 20Hz. This colour can highlight typical flickering frequency of the flame that is deduced by the buoyancy-driven instability.
- The blue colour denotes the frequency range for 20Hz to 90Hz, which is the harmonic of flickering frequency.
- The yellow colour denotes frequency larger than 90Hz which is the forcing frequency.

From Figure 5-30, it is observed that the yellow colour exists in every picture except for the first one, which can be explained by that the acoustic forcing always has an influence on the flame. Some forcing have stronger influence on the flame dynamics; other forcing have little influence on the flame dynamics. It is also noticed from the frequency map that the flame can be partly buoyancy dominant and partly acoustic forcing dominant. For example, the acoustic forcing dominates the fame instability at the frequency of 120Hz, 130Hz, 140Hz, 150Hz and 170Hz; the buoyancy instability dominates the flame instability at the acoustic wave frequency of 110Hz, 160Hz, 180Hz and 190Hz.

5.5.2 Flame Pixel Fluctuation based on Binary Flame Images

This section analyses the lame pixel fluctuation by converting a 2D flame image to a binary image. Converting a normal image to a binary image has been used in many applications since it is a very easy method to be processed. Binary images are digital images that have been quantized to two values, 0 and 1, representing black or background and white or object. They are very useful in digital image processing fields, because most required information can be provided by the silhouette of the object.

Binary images are typically obtained by setting a threshold to a multi-level grey image. Pixels are set to 0 if a grey level under the threshold, whilst other pixels are set to 1. This method produces a white object on a black background if 1 in the binary image denotes white colour and 0 denotes black; or black object on a white background when 1 in the binary image denotes black colour and 0 denotes white. However, it is difficult to determine or choose a appropriate threshold that can distinctly separate object and background accurately, which has been considered as a `black art' in image processing methods [28]. Histogram has been widely used in determining the threshold. It illustrates the number of times or frequency each grey level occurs in the image. If the histogram of the image is bimodal, it would be very easy to choose a threshold manually by choosing the valley between two peaks. Sometimes, an automatic procedure is required to be constructed to determine the threshold. Ideally, an image with a white object on a black background the histogram should appear as in Figure 5-31.

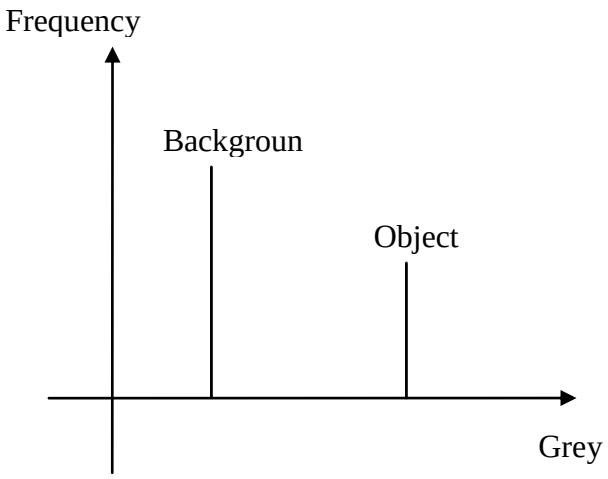

Figure 5-31: The ideal histogram of a light object on a darker plain background

However normally, measurement noise or instrumental error is inevitable during experiments, which makes the histogram of the image is much more complicated compared to the ideal histogram. The histogram obtained from experimental image is the result of convolving the 'ideal' histogram with the probability distribution of the noise.

Figure 5-32 illustrates the histogram of a real image with noise, showing the frequency of occurrence of each grey value. It can be seen that if the grey levels of the object and the background are very close, the threshold is very difficult to be determined automatically. Under this condition, repeated observations and averaging have to be applied to help determine the threshold.

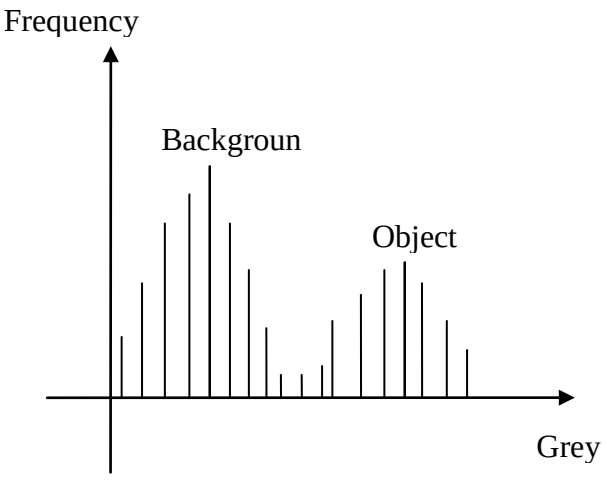

Figure 5-32: The histogram of an image showing the frequency of occurrence of each grey value

Take the 2D flame image of no acoustic excitation as an example, Figure 5-33 shows the histogram of the real flame image, showing the numbers of times of the occurrence of each grey value. It can be seen that the background component is very close to grey level of 0 and the flame (object) component is very close to grey level of 255. Hence, segmentation of background and object is not very sensitive to the selection of threshold. Or it can be said that the threshold have a large range selection from 10 to 250.

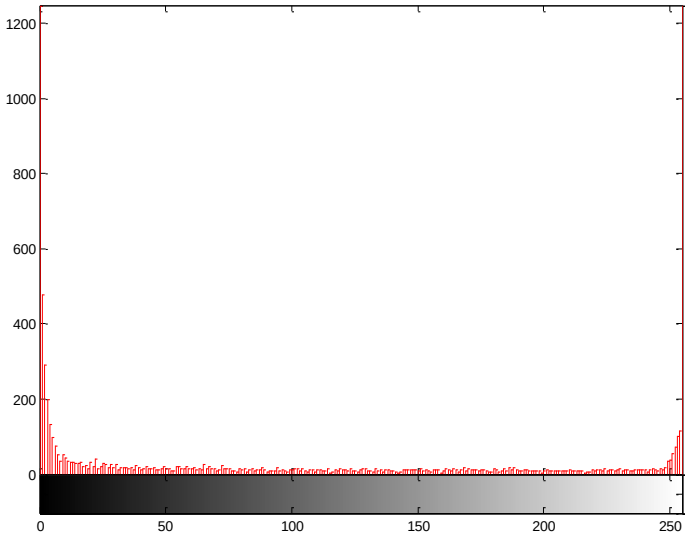

Figure 5-33: The histogram of flame with no excitation showing the numbers of times of occurrence of each grey value

Figure 5-34 shows the binary image of the flame image under no acoustic excitation with the threshold of 50. The flame is distinctly separated from the background.

Figure 5-34: The binary image of flame with no excitation

After converting each acquired flame image into binary image, the frequency distribution for each pixel of flame image is calculated. Figure 5-35 illustrates the pixel fluctuation of flame with different acoustic excitation.

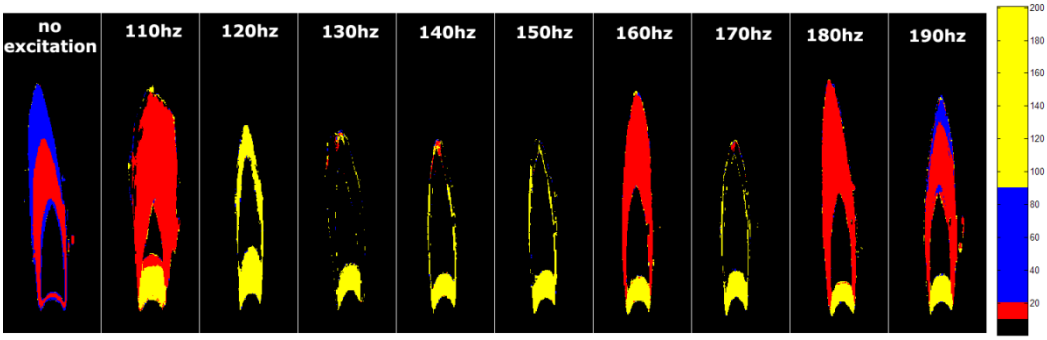

Figure 5-35: Frequency illustration of each pixel by binary image

Each detected frequency range is represented by the same colour palette as illustrated in Figure 5-30: the black colour is mainly considered as background and noise; the red colour denotes typical flickering frequency of the flame; the blue colour represents the second harmonic of flickering frequency; and the yellow colour shows the acoustic exciting frequency.

From Figure 5-35, it is observed that the same results are achieved from this method, but they were illustrated in a much clearer way. For example: the external acoustic forcing always has an influence on the flame because yellow colour exists in the bottom of every picture except for the first one; the acoustic

forcing dominates the flame instability at the frequency of 120Hz, 130Hz, 140Hz, 150Hz and 170Hz because there is very little red colour in these pictures; the buoyancy instability dominates the flame instability at the acoustic wave frequency of 110Hz, 160Hz, 180Hz and 190Hz, because the proportion of red colour is higher than yellow in these pictures. Besides these results, Figure 5-35 also delivers some other information:

- The bottom of the flame is most affected by acoustic excitation;
- The flame at the frequency of 130Hz acoustic excitation has bi-silhouette, which will be introduced in the next part;
- Under all acoustic excitations, pixels in middle part of flame do not fluctuate, because there is always flame or flame is saturated in these positions. Therefore the flame dynamics in these parts of the flame cannot be resolved with this method.
- The flame status is relative stable at the frequency of 140Hz, 150Hz and 170Hz acoustic excitation, because the length of the flame nearly keeps same value.

5.6 Interesting Phenomena

A very interesting phenomenon was found by analysing flame images. It was observed that the direction of the flame was changed dramatically at the excitation of 130Hz acoustic force. Data were collected for one second time period. The flame diverts to the left at the beginning (around the first 600ms), and then changes to the right (601ms-900ms), but it keeps in the vertical direction in the end (901ms-1000ms). Obviously, the phenomenon was not caused by wind or other noises. It must be the influence of 130Hz acoustic excitation. But the reason is uncertain and which is expected to be explained by future study.

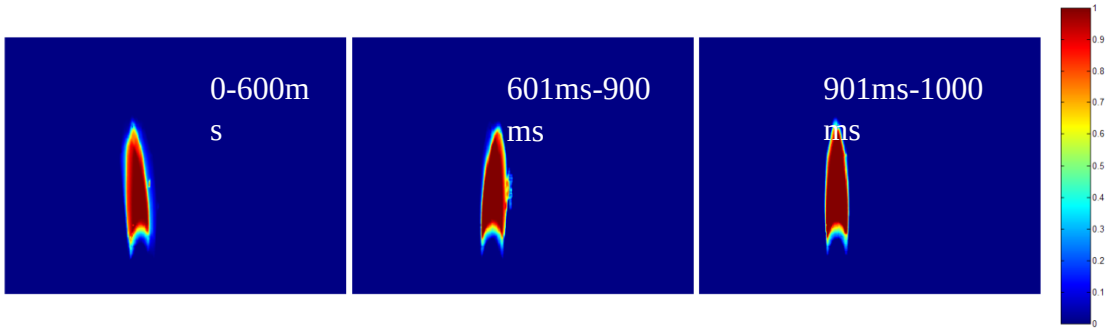

Figure 5-36: Synthetic flame image with 130Hz acoustic excitation

5.7 Cross Analysing

In order to compare the results from the methods proposed in this chapter and the previous chapter, Table 5-6 lists the detected dominant frequencies based on CH^* chemiluminescence, 2D projected area of flame image and centre of flame image. From Figure 5-37, it can be seen that the tendency of the detected dominant frequency is very similar for most of time, except for the condition with 120Hz acoustic excitation, which shows no detected dominant frequency with CH^* chemiluminescence result.

Table 5-6: Detected dominant frequency by different methods

f_a	f_d		
	Detected from AoF	Detected from CoF	Detected from CH^*
No Excitation	12.70Hz	12.70Hz	12.45Hz
110Hz	14.65Hz	13.67Hz	13.89Hz
120Hz	16.60Hz	15.63Hz	None
130Hz	13.67Hz	13.67Hz	13.03Hz
140Hz	undetected	undetected	None
150Hz	13.67Hz	13.67Hz	13.89Hz
160Hz	13.67Hz	13.67Hz	13.32Hz
170Hz	14.65Hz	14.65Hz	14.18Hz
180Hz	13.67Hz	13.67Hz	13.32Hz
190Hz	14.65Hz	15.63Hz	14.47Hz

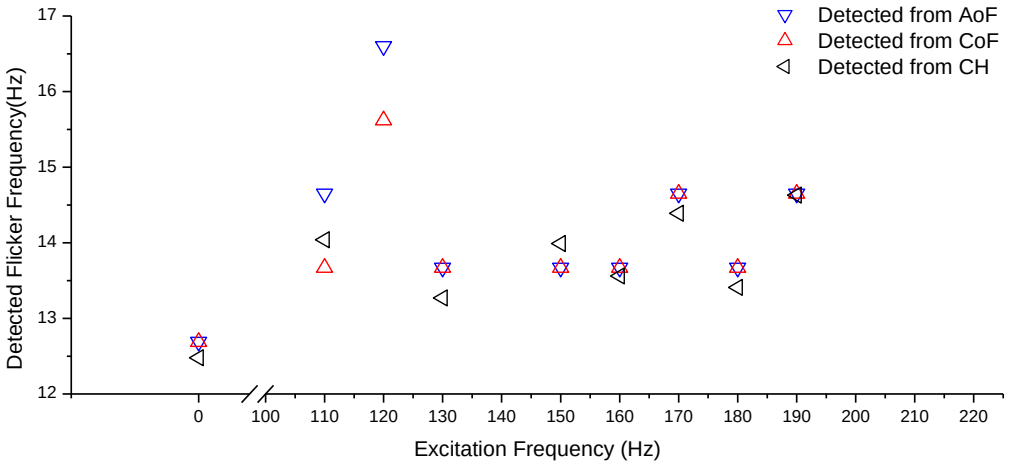

Figure 5-37: Detected dominant frequency by different methods

5.8 Summary

By applying a high speed camera to the system, 2D images of the flame have been captured and analyzed to study the interaction between flame dynamics and acoustic excitation. In order to take comparison between the two groups of result from CH^* chemiluminescence and 2D projected area of flame image, flame images were captured at the same condition as the test case two of Chapter 4.

By analyzing the flame synthetic images, 2D flame projected area and the centre position of the flame etc, the same results as last chapter have been obtained, where acoustic excitation at 120Hz, 130Hz, 140Hz, 150Hz and 170Hz makes the flame relatively stable compared to no acoustic excitation or other frequency acoustic excitation. More detailed information of the interaction has been achieved by analyzing the flame images, which is the finding of the localization fluctuation of flame and some interesting phenomenon like the bi-direction of the flame with 130Hz acoustic excitation.

Chapter 6

Discussion of Control Strategy for the Laboratory Burner based on the Gained Physical Insights

---

In this chapter, two fuzzy control strategies (controllers) are introduced for the laboratory burner based on the gained physical insights from the previous chapters. The first strategy is based on the FFT results of CH^* chemiluminescence emissions signal collected by a photomultiplier, which has been discussed in Chapter 4. The second strategy is the p method on the basis of image processing method, for data collected from a high speed camera, which has been presented in Chapter 5.

6.1 Introduction

As reviewed in Chapter 2, there are two control methods for combustion instability, passive instability control (PIC) and active instability control (AIC). This chapter designs a new AIC strategy based on the results discussed in Chapter 4 and Chapter 5. It has been observed that under external acoustic excitation, the diffusion flame in cylindrical tube presents very different properties. Some acoustic waves make the flame blows out, some acoustic waves

stable the flame and other acoustic waves do not have influence on the flame dynamics. Combined with control theory, some control strategies for the laboratory burner are designed in this chapter, which aim to monitor the combustion process working status and maintain it to work at a stable condition.

Traditionally, a typical automatic control system is composed of three components:

- Sensor(s), which measure some physical state of the system, such as: temperature, pressure, velocity, or fuel flow rate etc.
- Responder(s) or Controller(s), which may be simple electrical or mechanical systems or general purpose computers.
- Actuator(s), which affect a response to the system under the command of the responder or controller.

A typical feedback control system can be illustrated by Figure 6-1. It aims to control system behaviors closer to the given reference behaviors. Regarding to the system of this research (Figure 6-2), the “controller” in the Figure 6-1 is PC, which analyses data collected from the sensors and produces control signals to the actuator; the “actuator” is the loudspeaker and corresponding drive equipment, which takes a response to the system under the command of the PC ; the “system” is the cylindrical tube burner; “output” denotes the flame status: stable or unstable ;“sensors” are microphone, photomultiplier, hot-wire anemometry and digital camera, which measure physical states of the flame from the cylindrical tube burner.

The purpose of this chapter is to design a “controller”, whose input is the error of system output with the designed target, and output is a sequence of control commands.

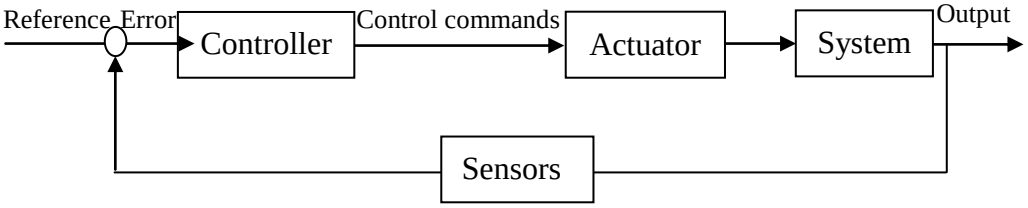

Figure 6-1: A typical feedback control system

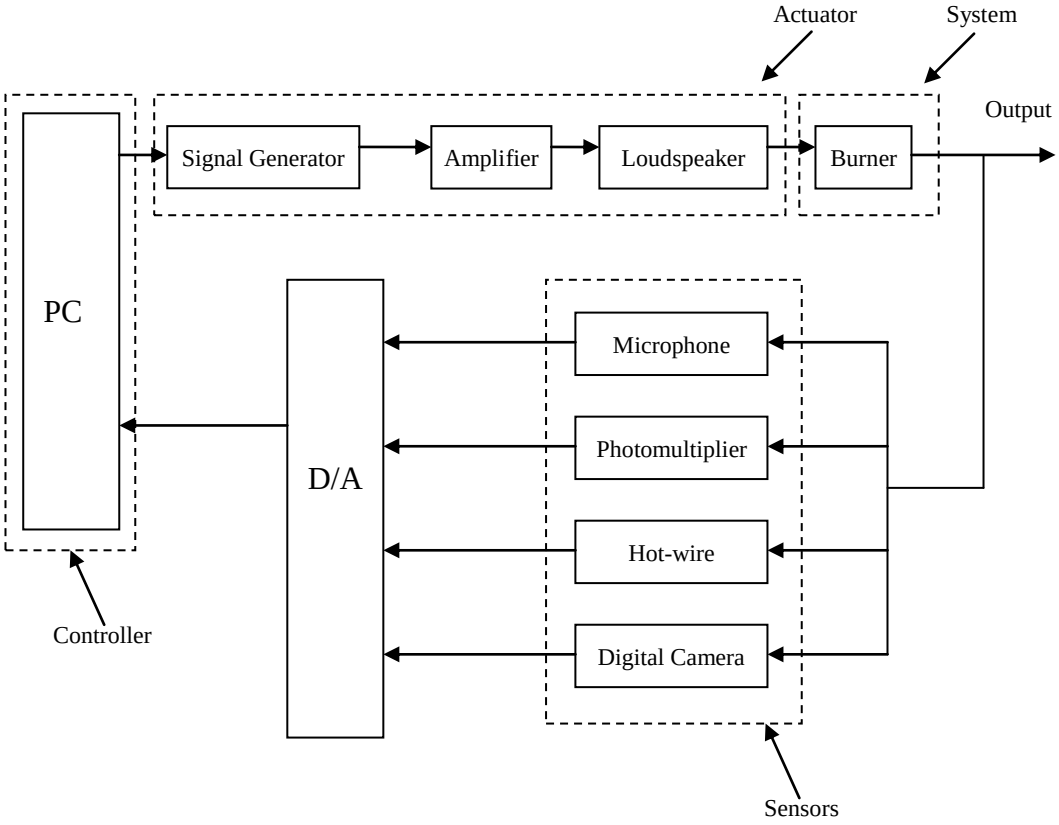

Figure 6-2: Block diagram of the control system framework

If we assume the controller C, the system P, the sensors F, the output Y, the control command U, the error E, and the reference R, the systems can be analyzed using the Laplace transform based on following relationships:

$$Y(s) = P(s)U(s) \quad \textbf{(6-1)}$$

$$U(s) = C(s)E(s) \quad \textbf{(6-2)}$$

$$E(s) = R(s) - F(s)Y(s) \quad \textbf{(6-3)}$$

Solving for $Y(s)$ in terms of $R(s)$ gives

$$Y(s) = \left(\frac{P(s)C(s)}{1+F(s)P(s)C(s)}\right)R(s) = H(s)R(s) \quad \textbf{(6-4)}$$

If we consider the closed-loop feedback as a single system, the expression $H(s)$

is referred as the transfer function of the system, which is determined by the applied controller.

The PID controller is probably the most popular feedback controller employed in industrial field. PID is an acronym for Proportional-Integral-Derivative. A PID controller has the general expression of:

$$u(t) = K_P e(t) + K_I \int e(t)dt + K_D \frac{d}{dt} e(t) \quad \textbf{(6-5)}$$

The designed behaviors or targets can be simply achieved by adjusting three parameters K_P, K_I, K_D. After Laplace Transform the PID controller transfer function can be expressed as

$$C(s) = (K_P + K_I \frac{1}{s} + K_D s) \quad \textbf{(6-6)}$$

Unfortunately, the control procedure of the system in this research has some logic conditions, for example: is the flame stable or unstable, does the power spectrum of CH^* chemiluminescence signal has dominant frequency or not; does the system is excited by an external acoustic source or not; does the dominant frequency of CH^* chemiluminescence signal is between 10-20Hz etc, which leads to the difficulty of designing a traditional PID controller. Therefore, based on these characteristics of the system another controller, fuzzy controller, is employed in this research.

Fuzzy control is a control method based on fuzzy logic. Fuzzy logic can be described as "computing with words rather than numbers", and fuzzy control can be described as "control with sentences rather than equations", which makes fuzzy control very flexible. Generally, a fuzzy controller works in three stages: an input stage, a processing stage and an output stage. The input stage maps sensor's data to the appropriate membership functions and truth values. The processing stage invokes each appropriate rule and generates a result for each rule, then combines the results of the rules. Finally, the output stage converts the combined results back into a specific control output value.

A typical fuzzy control system can be illustrated by Figure 6-3:

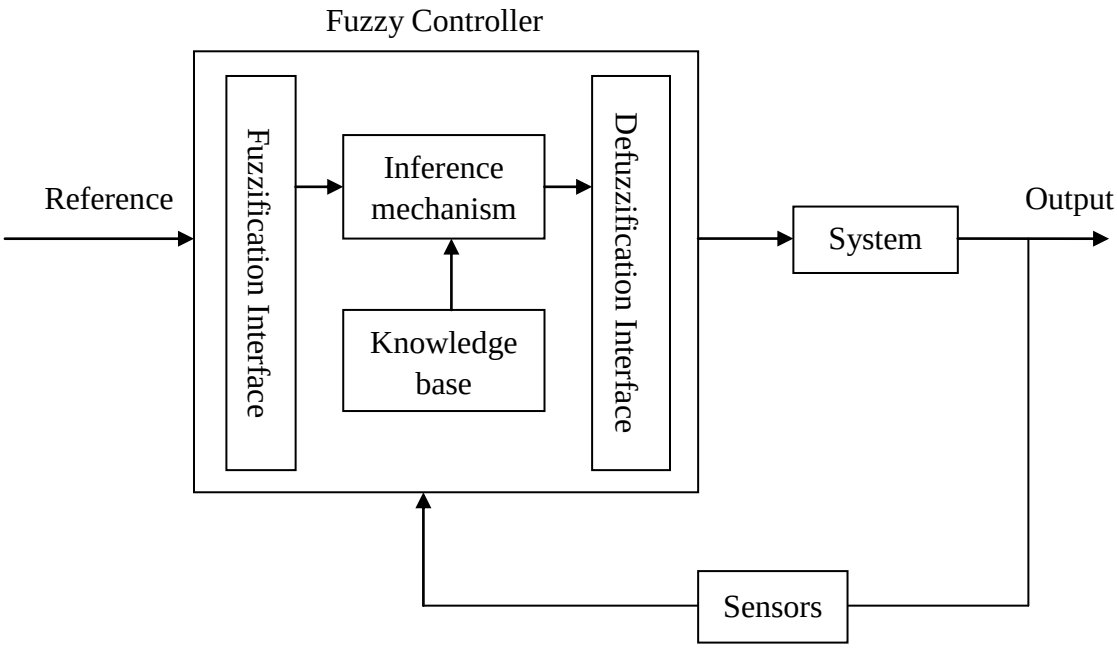

Figure 6-3: Block diagram of a fuzzy control system

There are four components in a fuzzy controller:

- The fuzzification interface: transforms the real input values to fuzzy values.
- The knowledge base: contains knowledge of the application domain and the control rules and goals.
- The inference mechanism: performs the decision-making logic.
- The defuzzification interface: transforms the fuzzy commands to the real control signals.

Design of two fuzzy logic controllers based on the current cylindrical burner is discussed in the following sections.

6.2 Control Strategy based on CH^* Chemiluminescence Data

In Chapter 4, it has been analysed that it is feasible to investigate the combustion stabilities by analysing the system CH^* chemiluminescence signal. For normal diffusion flame, the flame front regularly oscillates at a low frequency, known as

flame flickering frequency, ranging from 10-20Hz, which is caused by buoyancy. This research investigates the influence of acoustic waves on flame dynamics. It has been found that when using acoustic wave to excite the flame, at the frequency of 120Hz, 130Hz, 140Hz and 150Hz etc, the buoyancy-driven instability is suppressed by acoustic excitation, and makes the flame relatively stable. On the contrary, when use acoustic wave to excite the flame, at the other frequency of 100Hz, 110Hz, and 160Hz etc, the flame becomes very unstable and even blows out.

Based on these findings, Figure 6-4 presents the flow chart of the designed fuzzy controller. In the flow chart, f_d denotes the peak dominant frequency of the CH^* chemiluminescence signal and f_a presents the frequency of acoustic excitation for the burner.

Fuzzification is accomplished by doing FFT calculation for online collected CH^* chemiluminescence data every t seconds. Value of f_d is chosen as the control parameter to determine the degree of the flame stability. As discussed in previous chapters, diffusion flame flickering frequency is between 10-20Hz. If the calculated f_d is between 10Hz-20Hz, the controller takes it as the flame flickering frequency and concludes the flame oscillates at the flickering frequency. In order to improve the flame stability, it would be useful to apply an external acoustic signal to excite the flame if there is no acoustic excitation or change the frequency of the acoustic excited waves if the acoustic excitation already exists. Based on the test case two in Chapter 4, it has been found that it is difficult to establish a flame when the frequency of the acoustic excitation is above 220Hz or below 80Hz in this experiment. Hence the initial acoustic excitation frequency of the controller was set as 120Hz. The acoustic excitation frequency was adjusted by increasing 10Hz or decreasing 10Hz every time, which serves as the component defuzzification in the fuzzy logic controller. Value of f_d is detected for every cycle until a non-flickering frequency is achieved, which means that the buoyancy-driven instability is suppressed by acoustic excitation. From the results shown in section 4.3.2, it can be observed

that the f_a exists in the FFT result of CH^* chemiluminescence even if the flame is relatively stable (Figure 4-6), so the controller will exit control mode and the combustion system will be considered as relatively stable when $f_d = f_a$. Otherwise, when f_d is neither flickering frequency nor f_a, the system is concluded as faulty and alarmed.

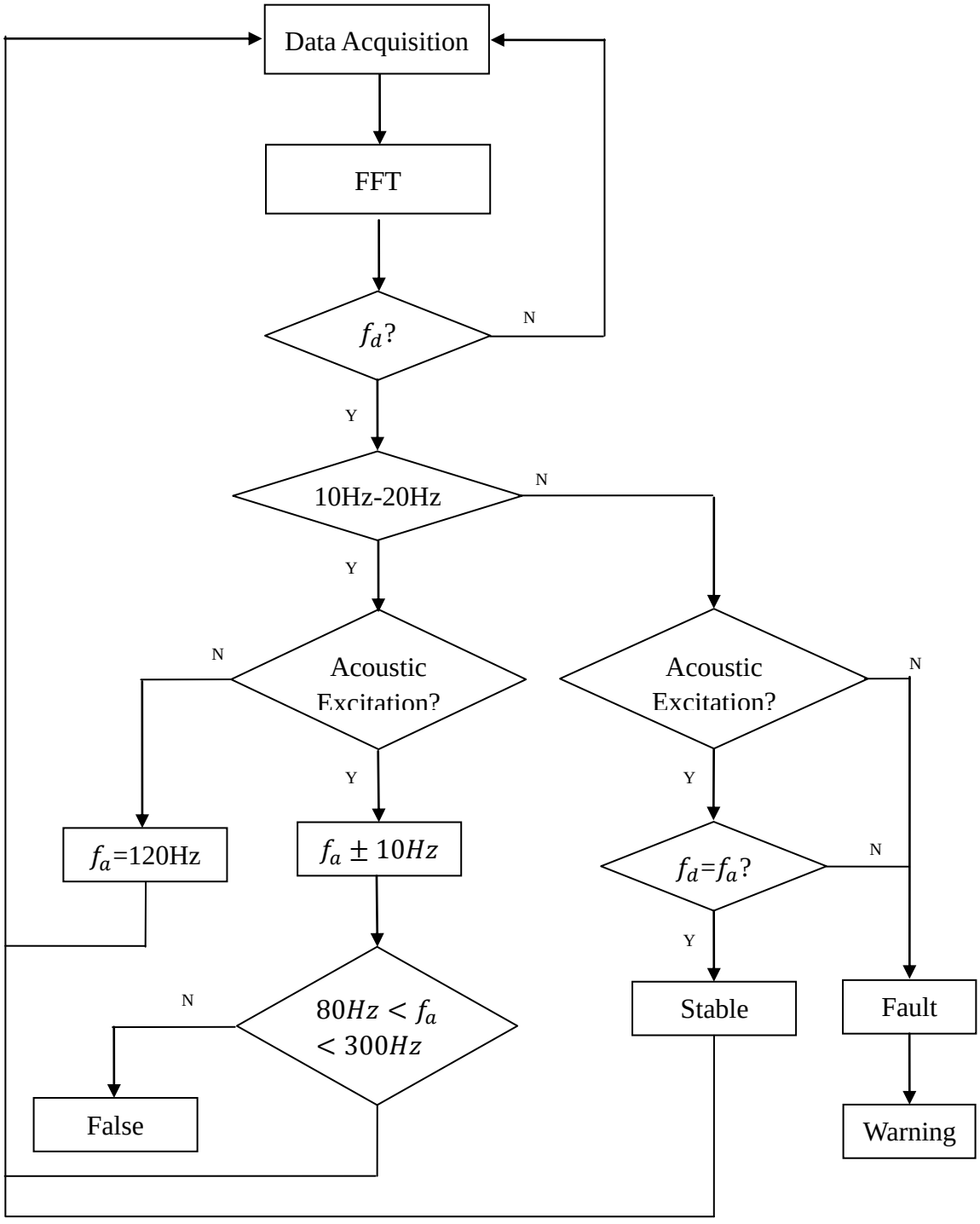

Figure 6-4: Flow char of the fuzzy controller based on f_d

6.3 Control Strategy based on Image Processing Methods

Chapter 5 analyzed the flame stability by means of image processing methods, and a criterion, p , was introduced to determine the degree of the flame stability which represents the ratio of bright area size to the whole flame area for synthetic flame images. The closer of the flame's p value to 1, the more stable of the flame is. The value of p provides a measurable parameter for flame stability, also offers a controllable parameter for combustion instability control.

A fuzzy control strategy based on the flame's p parameter is illustrated by Figure 6-5, flame images were initially pre-processed after acquisition by the high speed camera to remove noise and enhance contrast of the flame. A certain amount of flame images (every t seconds) were captured and then accumulated by the method introduced in Chapter 5 to calculate the value of p. Image pre-processing and the calculation of p serve as the fuzzification component in the controller. If value of p is larger than a pre-set threshold T_h, the flame is determined as 'stable'; if value of p is smaller than T_h, it indicates the flame is unstable. For a unstable flame, if the flame is already excited by an external acoustic source, the frequency of acoustic excitation has to be adjusted by increasing 10Hz or decreasing 10Hz, which serves as the component of defuzzification in the controller. These steps are repeated until a stable flame is established. If p is achieved without acoustic excitation, an initial acoustic wave at the frequency of 120Hz joins in towards stability of the flame.

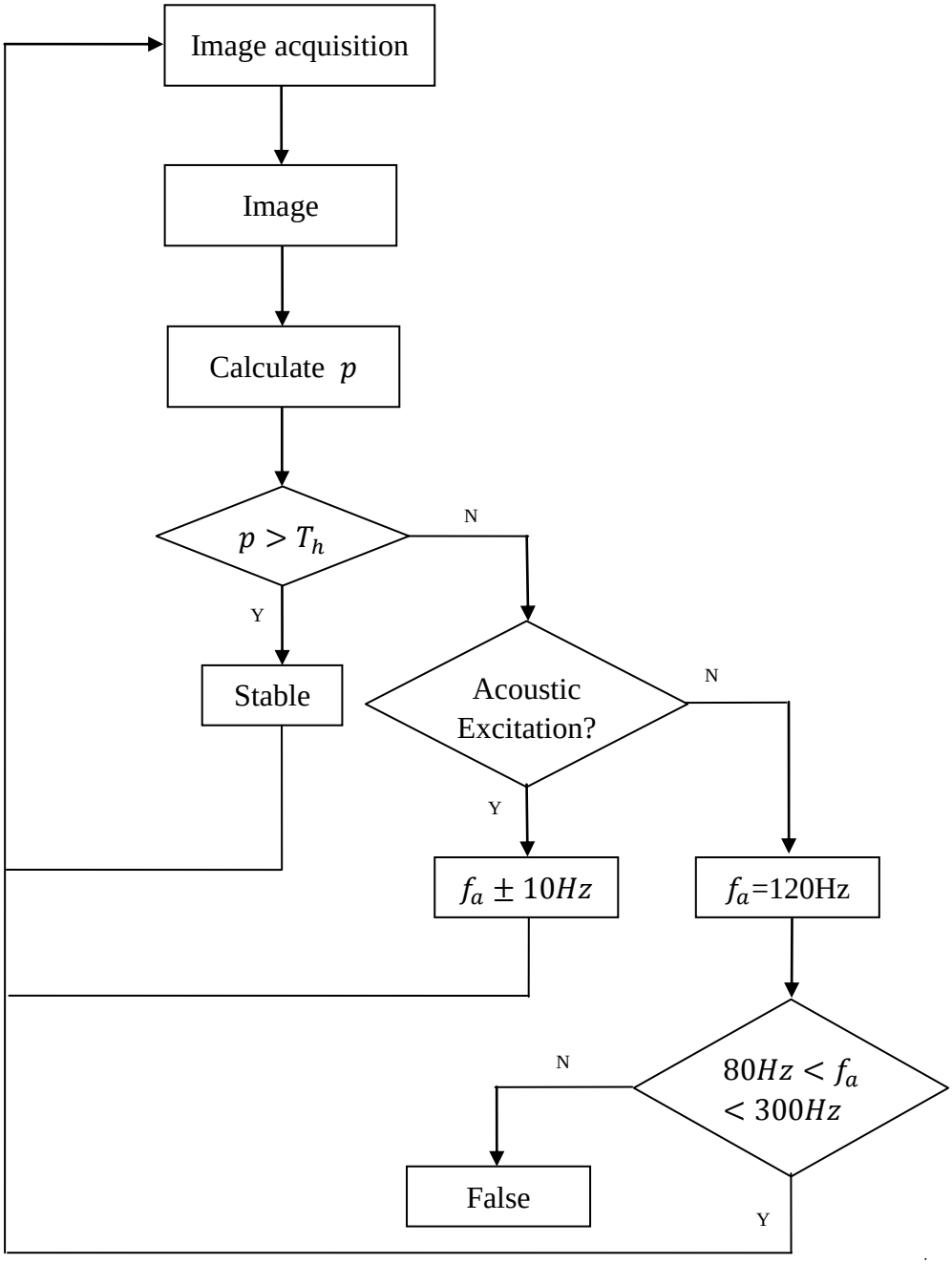

Figure 6-5: Flow char of the fuzzy controller based on $\boldsymbol{p}$ method

6.4 Summary

In this chapter, two control strategies have been designed based on CH^* Chemiluminescence data and 2D images of flame respectively. In terms of the results from previous chapters, both strategies are based on the fuzzy logic control theory because of the system's specifications.

In the first control strategy, "fuzzification" includes calculation of FFT of CH^*

chemiluminescence data and the determination of f_d. “Defuzzification” includes the transform from the stability to the change of acoustic excitation frequency. “Inference mechanism” can be described by Figure 6-4.

In the second strategy, “fuzzification” includes image pre-processing and calculation of p. “Defuzzification” includes the transform from the stability to the change of acoustic excitation frequency. “Inference mechanism” can be described by Figure 6-5.

Both “knowledge base” are learned from the results of Chapter 4 and Chapter 5.

It has to be pointed out that these control strategies are to verify the results presented in Chapter 4 and Chapter 5. It is not necessary to be applicable to the really combustor.

Chapter 7

Conclusions

In this concluding chapter, two main aspects are addressed. Firstly, the main contributions of the thesis are summarized, and secondly, some suggestions on future work are proposed.

7.1 Main Contributions

This research has been focused on investigating the acoustic excitation effect on the tube diffusion flame dynamics, setting up computer controlled diffusion flame in a cylindrical tube burner, analysing the collected observables and developing the related control strategies. Different test cases have been reported in the thesis. It was found that acoustic excitation has a very strong impact on the flame dynamics, which inspires us to explore a way to stabilize the jet diffusion flame by controlling the frequency of acoustic excitation. The main contributions of this thesis can be summarized below:

1. Interaction between acoustic wave and flame dynamics, and the competition between buoyancy-driven instability and acoustic excitation have been analyzed.
    a. Influence of infrasound effect on jet diffusion flame.

       For high intensity acoustic wave, it is difficult to establish a flame when the acoustic frequency is below 80Hz. Hence the research for

the infrasound effect on flame dynamics was carried out with low intensity acoustic wave (discussed in the test case one in Chapter 4).

With 3Hz acoustic excitation, the dominant frequency in the power spectrum of CH^* chemiluminescence is 12.84Hz, which is very similar to the typical flickering frequency under no excitation (12.48Hz). It can be concluded that 3Hz acoustic excitation has little influence on the flame dynamics and the buoyancy-driven instability is dominant. By increasing the acoustic frequency to 5Hz, the dominant frequency of CH^* chemiluminescence is still 12.84Hz, but the 5Hz frequency can be easily observed from the power spectrum, which shows the acoustic excitation starts to have an impact on the flame dynamics but it cannot suppress the buoyancy driven oscillation. When the excitation frequency is increased to 8Hz, it was observed that the dominant frequency of CH^* chemiluminescence is the exactly same as the excitation frequency. The acoustic excitation has taken over the buoyancy-driven instability completely and becomes the main controlling factor.

b. Influence of low frequency acoustic effect on jet diffusion flame.

The research of low frequency acoustic wave (between 20Hz and 80Hz) was also carried out with low intensity acoustic wave (discussed in the test case one in Chapter 4).

At acoustic excitation frequency between 20Hz and 70Hz, the flame oscillation is still dominated by the acoustic excitation but the flame flickering (buoyancy-driven instability) frequency becomes visible, especially for the case of 70Hz. When the excitation frequency is set at 80Hz, the typical flame flickering frequency becomes dominant again though the acoustic excitation frequency still plays a role on the flame dynamics.

c. Influence of higher frequency acoustic effect on jet diffusion flame.

This paragraph gives a summarised conclusion when the acoustic

excitation is over 80Hz but less than 300Hz. With low intensity acoustic wave, the effect on the flame dynamics does not exhibit much difference when varying the frequency of the acoustic wave. Hence, this investigation was conducted with higher intensity acoustic wave (discussed in the test case two in Chapter 4).

It was found that the peak dominant frequencies in the FFT results of CH^* chemiluminescence change around the flickering frequency in a very limited ranges (12Hz-15Hz) for most frequencies (except for 120Hz and 140Hz). Interestingly, the flame at 140Hz acoustic excitation frequency was observed to be very stable, which demonstrates that it is feasible to use an external acoustic excitation to stabilize the flame.

2. The high speed imaging technique discovers some specific aspects of flame dynamics. The spatial resolution offered by the technique has shown that different areas of the flame have different levels of contribution to the dominant frequency during the unstable mode. For the flame without acoustic excitation, the inner most area of the flame oscillates at the typical flickering frequency, but the most outer areas of the flame oscillate at the second-harmonic of the typical flickering frequency. Moreover the acoustic excitation and buoyancy-driven instability can be dominant at different spatial location in the flame zone. It has been observed that the most inner areas of the flame oscillate as acoustic frequency for a stable flame.
3. Based on the gained physical insights, some fuzzy control strategies were designed and stability criterions were defined in Chapter 6. The stability criterions provide mathematical controllable parameters for online combustion process monitoring and controlling.
4. A program that aims to control the output frequency of the signal generator automatically has been developed based on the platform of C++.
5. Some interesting phenomena have been observed during experiments.
    a. When the acoustic exaction frequency is in between 14Hz and 20Hz,

it was observed that a peak that is half the value of the infrasound frequency appears clearly in the power spectrum of CH^* chemiluminescence.

b. At the excitation of 130Hz, it was observed that the direction of the flame was changed dramatically. The flame diverts to the left at the beginning (around the first 600ms), and then changes to the right (601ms-900ms), but it keeps in the vertical direction in the end (901ms-1000ms).

7.2 Suggestions on Future Research

1. This research collected CH^* chemiluminescence for analysing the stability of laminar diffusion flame. As discussed in Chapter 3, there are many different chemiluminescence species in combustion emission spectrum. Even though CH^* radiation has peak intensity in the emission spectrum, there is no a clear physical picture of the various pictures governing the stability of jet diffusion flames. It is recommended that more species can be collected and compared to analyse the stability of laminar diffusion flame in future research.
2. Half value of acoustic frequency appears clearly in the power spectrum of CH^* chemiluminescence by applying infrasound as acoustic excitation. This phenomenon is highly repeatable and it is not just an occasionally observable event, which has been reported before by other researchers. However none of them proposed an explanation to this phenomenon. Further research can be conducted to find out the underlying reason for this phenomenon.
3. In this research, acoustic wave effect on flame stability was analysed for propane fuel only. It is recommended to use other fuel in future research for flame stability analyses and compare the difference influence of acoustic excitation.
4. The influence of acoustic excitation at 130Hz to the flame is very different

by comparing to that at other frequencies. The inclination of the flame changes twice in one second. The reason for this phenomenon is uncertain, which is worth to be investigated in future research.

5. The flame visualisation is based on 2D Black and White (B/W) imaging. Obviously, colour images comprise more information than the B/W images. This research also studied the pixel frequency distribution by analysing the red, green and blue (RGB) channels. It was found that RGB shows different distribution for flame pixel oscillation. It is recommended to use 2D colour flame image to analyze the flame stability in further research and compare the results acquired from red, green and blue channels, which can potentially enhance the methods proposed in this thesis.

Chapter 8

Bibliography

[1] Albas, E., Arikan, T. and Kuzkaya, C., In-process motor testing result using model based fault detection approach, *Electrical Insulation Conference and Electrical Manufacturing & Coil Winding Conference 2001 Proceedings*, 643-647(2001).

[2] Anuradha, M. A. and Ghoniem, A. F., Active control of combustion instability: theory and practice, Department of Mechanical Engineering, MIT, Cambridge, MA.

[3] Arai, M., Gravity effects on stability and flickering motion of diffusion flames, *Combustion and Flame*, 118, 293-300(1999).

[4] Auer, M. P. and Gebauer, C., Active instability control: feedback of combustion instabilities on the injection of gaseous fuel, *Transactions of the ASME*, 127, 748-754(2005).

[5] Beer, J. M. and Chigier, N. A., Combustion aerodynamics, Applied Science Publishers Ltd, London, 1972.

[6] Billoud, G. and Galland, M. A., Adaptive active control of instabilities. *Journal of Intelligent Material Systems and Structures*, 2, 457-471(1991).

[7] Billoud, G., Galland, M.A., Huynh Huu, C. and Candel, S., *Adaptive control of combustion instabilities*, *Combustion Science Technology*, 81, 257-283(1992).

[8] Blanke, M., Kinnaert, M., Lunze, J. and Staroswiecki, M., Diagnosis and

fault-tolerant control, Springer-Verlag Berlin Heidelberg New York, 2003.

[9] Brown, G. B., On vortex motion in gaseous jets and the origin of their sensitivity to sound, *Proceedings of the Physical Society*, 47(4), 703-732(1935).

[10] Brown, G. B., XIII. On sensitive flames. *Philosophical Magazine Series 7*, 13(82), 161-195(1932).

[11] Cetegen, B. M. and Dong, Y., Experiments on the instability modes of buoyant diffusion flames and effects of ambient atmosphere on the instabilities, *Experiments in Fluids*, 28(6), 546-558 (2000).

[12] Chen, L. D., Seaba, J. P., Roquemore, W. M. and Goss, L. P., Buoyant diffusion flames, Twenty-Second Symposium (International) on Combustion/The Combustion Institute, 677-684(1988).

[13] Chiang, L. H, Russell, E. L. and Braatz, R. D., Fault detection and diagnosis in industrial systems, Springer-Verlag London Berlin Heidelberg, 2001.

[14] Chigier, N., Combustion measurements, Hemisphere Publishing Corporation, 1991.

[15] Chu, A.K., Stability of acoustic streaming flows in plane channels, *Physical review. E, Statistical, nonlinear, and soft matter physics*, 68(4 Pt 2), 046305(2003).

[16] Coker, A. and Neumeier, Y., Active instability control effectiveness in a liquid fueled combustor, *Comubst. Sci. and Tech.*, 178, 1251-1261(2006).

[17] Conrad, T., Bibik, A., Shcherbik, D., Lubarsky, E., and Zinn, B. T., Feasibility of ‘‘intermittent’’ active control of combustion instabilities in liquid fueled combustors using a ‘‘smart’’ fuel injector, *Proceedings of the Combustion Institute*, 31, 2223-2230(2007).

[18] Conte, L., J. Philosophy Magazine, page HP. 235, 1958.

[19] Crocco, L. and Cheng, S. L., Theory of combustion instability in liquid propellant rocket motors", Butterworths Science Publication, AGARDOGRAPH N 8, 1956.

[20] Ducruix, S., Schuller, T., Durox, D. and Candel, S., Combustion dynamics

and instabilities: elementary coupling and driving mechanisms, *Journal of Propulsion and Power*, 19(5), 722-734(2003).

[21] Durox, D., Yuan, T. and Villermaux, E., The effect of buoyancy on flickering in diffusion flames, *Combustion Science and Technology*, 124, 277-294(1997).

[22] Eickhoff, H. and Winandy, A., Visualization of vortex formation in jet diffusion flames, *Combustion and Flame*, 60, 99-101(1985).

[23] Escobet, T. and Trave-Massuyes, L., Parameter estimation methods for fault detection and isolation, *In Proceeding of the 12th International Workshop on Principles of diagnosis*, Via Lattea, Italy, 2001.

[24] Faraday, M., *Journal of Science and the Arts*, 5, 274(1918).

[25] Farhat, S. A., Multiple signal measurement, processing and correlation studies of flame dynamics, Thesis, 2005.

[26] Farhat, S. A., Ng, W. B. and Zhang, Y., Chemiluminescent emission measurement of a diffusion flame jet in a loudspeaker induced standing wave, *Fuel*, 84(14-15), 1760-1767(2005).

[27] Farhat, S., Kleiner, D. and Zhang, Y., Jet diffusion flame characteristics in a loudspeaker-induced standing wave, *Combustion and Flame*, 142, 317-232(2005).

[28] Faugeras, O., Three-dimensional computer vision: a geometric viewpoint, M.I.T. Press, 1993.

[29] Gaydon, A. G. and Wolfhard, H. G., Flames, London Chapman and Hall, 1979.

[30] Giacomazzi, E., Cecere, D., Bocchino, G., Picchia, F. R. and Arcidiacono, N., Effects of forced acoustic waves onto jet shear layers, Italian Section of the Combustion Institute.

[31] Gotodaa, H., Ueda, T., Shepherd, I. G., Robert, K. and Cheng. Flame flickering frequency on a rotating Bunsen burner, *Chemical Engineering Science*, 62, 1753-1759 (2007).

[32] Gutmark, E., Parr, T. P., Parr, D. M. and Schadow, K. C., Stabilization of

combustion by controlling the turbulent shear flow structure, *7th Symposium on Turbulent Shear Flows*, Paper No. 23-1, 1989.

[33] Hertzberg, J.R., Conditions for a split diffusion flame, *Combust and Flame*, 109, 314-322(1997).

[34] Himmelblau, D.M., Fault detection and diagnosis in chemical and petrochemical processes, Elsevier Scientific Publishing Company, 1978.

[35] Hong, B. and Ray, A., Robust feedback control of combustion instability, Proceedings of the American Control Conference, Philadelphia, Pennsylvania - June 1998.

[36] http://en.wikipedia.org/wiki/Fft.

[37] http://en.wikipedia.org/wiki/Microphone#Electret_condenser_microphone.

[38] http://en.wikipedia.org/wiki/Photomultiplier.

[39] http://en.wikipedia.org/wiki/Vibration#Types_of_vibration.

[40] http://hyperphysics.phy-astr.gsu.edu/hbase/hframe.html.

[41] http://www.aoe.vt.edu/~simpson/aoe4154/hotwirelab.pdf

[42] http://www.kittiwake.com/Default.aspx/ProductSection/107/ProductSubSection/120/Product/277.

[43] http://www.nixonflowmeters.co.uk/pages/nt_industrial.html.

[44] http://www.openxtra.co.uk/environment-monitor/probe/temperature

[45] Huang, Y., Yan, Y., Lu, G. and Reed, A., On-line flicker measurement of gaseous flames by image processing and spectral analysis, *Meas. Sci. Technol.*, 726-733(1999).

[46] Janos, J., Fault Detection and Diagnosis in Engineering Systems.

[47] Jones, J. C., Combustion science: principles and practice, Millennium Books, 1993.

[48] Kadowaki, S., Numerical analysis on instability of cylindrical flames, *Combust. Sci. and Tech.*, 107, 181-193(1995).

[49] Katta, V. R. and Roquemore, W. M., Role of inner and outer structures in transitional jet diffusion flame, *Combustion and Flame*, 92(3), Pages 274-278(1993).

[50] Kohse-Hoinghaus, K. and Jeffries, J. B., Applied combustion diagnostics, Taylor & Francis, 2002.

[51] Krasheninnikov, Yu. S. and Mironov, A.K., Effect of the streamwise component of the vorticity formed in a turbulent jet source on the acoustic characteristics of the jet, *Fluid Dynamics*, 38(5), 698-711(2003).

[52] Lang, W., Active control of combustion instability, *Combustion and Flame*, 70, 281-289(1987).

[53] Lebedev, L.L. and Pavel'ev, A.A., Effect of the nozzle edge shape on the acoustic sensitivity of a jet, *Fluid Dynamics*, 37, 21(2002).

[54] Lee, K.M., A visual study on flame behavior in tone-excited non-premixed jet flames, *Fuel*, 81, 2249-2255(2002).

[55] Lieuwen, T., Analysis of acoustic wave interactions with turbulent premixed flames. *Proc, Combust. Inst.*, 29, 1817(2003).

[56] Lieuwen, T., Modeling premixed combustion–acoustic wave interactions: a review, *Journal of Propulsion and Power*, 19(5), 765-781(2003).

[57] Lingens, A., Reeker1, M. and Schreiber, M., Instability of buoyant diffusion flames, *Experiments in Fluids*, 20(4), 241-248(1996).

[58] Lingens, A., Neemann, K., Meyer, J. and Schreiber, S., Instability of diffusion flames, *Twenty-Sixth Symposiums (International) on Combustion/The Combustion Institute*, 1053-1061(1996).

[59] Liu, G. P. and Daley, S., Output-model based predictive control of unstable combustion systems using neural networks, *Control Engineering Practice,* 7, 591-600(1999).

[60] Marble, F. E. and Cox, D. W. J., Servo-stabilization of low frequency oscillations in liquid rocket motors, *Journal of Appl. Math. Phys*, 6, 1(1955).

[61] Matalon, M., Intrinsic flame instabilities in premixed and non-premixed combustion, Annual Review of Fluid Mechanics, *Invited Review Article*, 39, 163-191(2007).

[62] Ng, W. B, Salem, A. F. and Zhang, Y., Three-dimensional visualization of diffusion flame shapes under acoustic excitation using stereoscopic imaging

and reconstruction technique, *Journal of Visualization*, 6(4), 329-336(2003).

[63] Noiray, N., Durox, D., Schuller, T. and Candel, S., Dynamic phase converter for passive control of combustion instabilities, *Proceedings of the Combustion Institute*, 32, 3163-3170(2009).

[64] Nolle, A.W., Sinuous instability of a planar air jet: propagation parameters and acoustic excitation, *The Journal of the Acoustical Society of America*, 103(6), 3690-705(1998).

[65] Nori, V. N. and Seitzman, J. M., CH^* Chemiluminescence modeling for combustion diagnostics, *Proceedings of the Combustion Institute*, 32, 895-903(2009).

[66] Oppenheim, A. K., Shock wave and flame interactions, Discussion of paper by G. Rudinger, Combustion and Propulsion, Third AGARD Colloquium, Palermo, Sicily, March 17-21, 1958, Pergamon Press, New York, pp. 180-182(1958).

[67] Papadopoulos, T., Pitchard, M., Green, C. and Zhang, Y., Flame patterns of acoustic wave and flame interaction in a cylindrical Tube, *Journal of Visualization*, 4(2), 179-184(2001).

[68] Passino, K. M., Fuzzy Control, Addison Wesley Longman, Inc, 1997.

[69] Pun, W., Palm, S.L. and Culick, F.E.C., Combustion dynamics of an acoustically forced flame, *Combustion Science Technology*, 175, 499(2003).

[70] Ramsdem, E., Hall effect speed sensors offer reliable operation in severe Environments, PCIM.

[71] Rayleigh, J. W. S., The theory of sound, volume 2. New York: Dover, 1945.

[72] Rijke, P. Ann., *Phys*., Lpz 107, 339(1959).

[73] Rue, D. M., Wagner, J. C., Grange, L.,Zelepouga, S., Inventor, Method and apparatus for measuring the heating value of a signal or multi-component fuel gas, United States Patent US 6,977,179 B2, 2005 Dec.20.

[74] Saito, M., Sato, M. and Nishimura, A., Soot suppression by acoustic oscillated combustion, *Fuel*, 77, 973(1998).

[75] Sato, H., Amagai, K. and Arai, M., Diffusion flames and their flickering

motions related with Froude numbers under various gravity levels, *Combustion and Flame*, 123(1-2), 107-118(2000).

[76] Sato, H., Amagai, K. and Arai, M., Flickering frequencies of diffusion flames observed under various gravity fields, *Proceedings of the Combustion Institute*, 28, 1981-1987(2000).

[77] Shanbhogue, S. J., Seelhorst, M., and Lieuwen, T., Vortex phase-jitter in acoustically excited bluff body flames, *International Journal of Spray and Combustion Dynamics*, 1(3), 365-387(2009).

[78] Stocker, D. P., Sheu, J. C. and Chen, L. D., in: Proceedings of the 1993 Fall Meeting of the Western States Section of the Combustion Institute, Paper 93-065.

[79] Suzuki, M., Atarashi, T. and Masuda, W., Behavior and structure of internal fuel-Jet in diffusion flame under transverse acoustic excitation, *Combust. Sci. and Tech.*, 179, 2581-2597(2007).

[80] Tarakanov, S. V., Khoruzhnikova, T. D. and Chivilikhin, S. A., Excitation of gas acoustic oscillations in laminar combustion of a mixture within a tube, Combustion, *Explosion, and Shock Waves*, 25(5), 561-564(1989).

[81] Temkin, S., Selective damping of resonant acoustic waves in tubes, *Journal of Sound and Vibration*, 36(3), 389-398(1974).

[82] Thuillard, *Fire Safety J*. 37, 371–380(2002).

[83] Tsien, H. S., Servo-stabilization of combustion in rocket motors, *American Rocket Society Journal*, 22, 256-263(1952).

[84] Tyndal, J. and Sound. D., Appleton & Company, New York, 1897.

[85] Van Dyke, M., An album of fluid motion, The Parabolic Press, Stanford, California, IV edition, 1988.

[86] Watton, J., Condition monitoring and fault diagnosis in fluid power systems, Ellis Horwood Series in Mechanical Engineering, 1992.

[87] Welle, E.J., Roberts, W.L., Decroix, M.E., Carter, C.D. and Donbar J.M., Simultaneous particle-imaging velocimetry and OH planar laser-induced fluorescence measurements in an unsteady counterflow propane/air diffusion

flame. *Proc. Combust. Instit.*, 28, 2021(2000).

[88] Williams, T. C. and Shaddix, C. R., The response of buoyant laminar diffusion flames to low-frequency forcing, *Combustion and Flame*, 151, 676–684(2007).

[89] Xu, L. and Yan, Y., An improved algorithm for the measurement of flame flicker frequency, Instrumentation and Measurement Technology Conference, 18-20 May 2004.

[90] Yoshida, H., Koda, M., Ooishi, Y., Kobayashi, K.P. and Saito, M., Supermixing combustion enhanced by resonance between micro-shear layer and acoustic excitation, *International Journal of Heat Fluid Flow*, 22, 372(2001).

[91] Yuan, J. and Ju, Y., Pulsating and hydrodynamic instabilities at large Lewis numbers, *Combustion and Flame*, 144, 386-397(2006).